Department of Mathematics and Statistics

Analytical Study of Fluid Flows with Slip Boundary

Suharsono S.

This thesis is presented for the Degree of

Doctor of Philosophy

of

Curtin University

May 2012

Declaration

To the best of my knowledge and belief, this thesis contains no material previously published by any other person except where due acknowledgement has been made.

This thesis contains no material which has been accepted for the award of any other degree or diploma in any university.

Signature:

Date: 1 May 2012

Acknowledgments

I am extremely grateful to my supervisor, Professor Yong Hong Wu, for his guidance and support during my study. I also thank my co-supervisor, Dr. GuangLu Zhow, for his encouragement and Professor Kok Lay Teo for his helpful advice.

I am very grateful to Indonesian Government for the financial support during the period of my study.

Finally, I sincerely thank all the students and staff in the Department of Mathematics and Statistics for their encouragement during my study at Curtin.

Abstract

One of the important scientific research focuses worldwide has been on the study of behavior of materials at micro and nano-scales. Continuing theoretical and technological development in this area has led to the development of many biological and engineering devices and systems which involve fluid flow through micro-channels, referred to microflows. Typical examples include fuel cells, drug delivery systems and energy conversion devices.

As the functional characteristics of micro-systems depend, to a large degree, on the behavior of fluid flow in the micro-channels, it is extremely important to study microflows. In recent years, many investigations were carried out to study various flow problems of Newtonian and non-Newtonian fluids under the steady state condition. However exact solutions to many flow problems of Newtonian fluids in micro-channels under the unsteady condition have not been developed and investigated. Hence, in this project, we study the unsteady flow of incompressible Newtonian fluids through rectangular and elliptic micro-channels with boundary slip.

For the unsteady flow through micro-channels of rectangular cross-section, the governing equations are constructed and formulated in the rectangular coordinate system. Then by using Fourier series expansion and separation of variables, the governing partial differential equation for the velocity field is successfully reduced to two simpler families of boundary value problems which are then solved analytically. From the derived exact solution of the velocity field, the transient flow rate and the stress field in the fluid are subsequently derived. An investigation is then conducted to study the behaviour of microflows in

rectangular channels. Various interesting results, showing the influence of boundary slip and cross-section geometry (width to depth ratio) on the flow behaviour and efficiency, have been obtained and presented in the thesis.

For the unsteady flow through micro-channels of elliptic cross section, the complete set of governing equations, including the partial differential equation and the boundary conditions, are formulated in elliptic cylindrical coordinates. Then by using Fourier series expansion and separation of variables, the partial differential equation for the velocity field is successfully reduced to two families of Mathieu type equations which are then solved analytically subject to the symmetric condition and the slip boundary condition. Exact solutions for the transient flow rate and the stress field in the fluid are then derived subsequently. The solutions are expressed in terms of the Mathieu functions and the modified Mathieu functions, which are in series form and are determined by computing their characteristic numbers and the coefficients of the series. A numerical investigation is then conducted to demonstrate the flow behavior of fluids in elliptic micro-channels.

List of Publications Related to This Thesis

1. Suharsono, Y. H. Wu, B. Wiwatanapataphee, Mathematical Analysis of fluid flow through channels with slip boundary, International Conference of Mathematical Applications in Engineering (ICMAE'10), Kuala Lumpur, Malaysia, 3^{rd} – 4^{th} August 2010.

2. Suharsono, Y. H. Wu, B. Wiwatanapataphee, Mathematical Analysis of fluid flow through rectangular micro-channel with slip boundary under constant pressure gradient, International Conference on Mathematics and Its Applications, The 6^{th} SEAMS-GMU, Yogyakarta, Indonesia, July 12 – 15, 2011.

3. B. Wiwatanapataphee, Y. H. Wu, Suharsono, Transient flows of Newtonian fluids through rectangular micro-channels with slip boundary, in preparation.

Contents

List of Figures

Nomenclature

Ce_{2n}, Se_{2n} Ce_{2n+1}, Se_{2n+1}	modified Mathieu function
Da	the Darcy number
F_n, G_n, W_n U_n, V_n f_n, u_n, v_n	functions as defined in chapter 3 and chapter 4
K	permeability
Kn	Knudsen number
Kn^*	modified Knudsen number
Po	Poiseuille number
Q^*, Q Q_0, Q_n	flow rates
ce_{2n}, se_{2n} ce_{2n+1}, se_{2n+1}	Mathieu functions
$\mathbf{d} = (d_{ij})$	rate of deformation tensor
$\frac{dp}{dz}$	pressure gradient
$f \operatorname{Re}_{\sqrt{A}}$	Reynold number Fanning friction factor product
ℓ	slip parameter
ℓ_1	slip parameter of the surface of the inner annulus
ℓ_2	slip parameter of the surface of the outer annulus
$\mathbf{n} = (n_1, n_2, n_3)$	normal vector

p	fluid pressure
$\mathbf{t} = (t_1, t_2, t_3)$	unit vector in the tangential direction
$\mathbf{u} = (u, v, w)$	velocity vector
v_{st}	velocity component of the solid surface in the tangential direction
v_t	velocity component of the fluid in the tangential direction
∇	gradient operator
∇^2	Laplace operator
Φ_m	eigenfunctions
Γ	boundary
ε_{ij}	strain tensor
λ	molecular mean free path
μ_e	effective viscosity
μ	viscosity
μ_1, μ_n	blood viscosity
$\upsilon_m, \overline{\upsilon}_m$ $\gamma_{nm}, \overline{\gamma}_{nm}$	eigenvalues
$\dot{\gamma}$	shear rate
ρ	fluid density
σ_{ij}	stress tensor
σ_n	normal stress

Chapter 1
Introduction

1.1 Background

Fluid flow in micro-channels has emerged as an important research area. This has been motivated by its various applications such as medical and biomedical use, computer chips, and chemical separation. The advent of Micro-Electro-Mechanical Systems (MEMS) has opened up a new research area where non-continuum behaviour is important. MEMS are one of the major advancements of industrial technologies in the past decades. Micron-size mechanical and biochemical devices become more familiar both in commercial applications and in scientific research. Micro-channels are the fundamental part of microfluidic systems. In addition to connecting different devices, micro-channels have also been used in biochemical reaction chambers, physical particle separation, inkjet print heads, infrared detectors, diode lasers, miniature gas chromatographs, or as well as heat exchangers for cooling computer chips [13].

Many investigations have been carried out to study various flow problems of Newtonian and non-Newtonian fluids in micro-channels with Navier slip boundary conditions over the recent years [7, 9, 10, 16, 17, 27, 33, 34, 35, 36]. Some attempts have also been made to emerge alternative formulae for the determination of the slip length [4, 30, 35]. Although exact and numerical solutions to various flow problems of Newtonian fluids under the no-slip assumption have been obtained [2, 3, 24, 39], very few exact solutions for the slip case are available. Recently, some steady state slip solutions for the flows through a pipe, a channel and an annulus have been derived [4, 20, 27, 35].

Advancement from the research community in sciences at microscale and nanoscale led to the development of many biological and engineering devices and systems [12]. Most of these devices and systems involve fluid flow through micro-channels, referred to as microflows [1, 5, 11, 12]. Typical examples include fuel cell devices, drug delivery systems [32], biological sensing and energy conversion devices [15]. As the behaviour of fluid flow in these systems determines the functional characteristics of the systems, the study of microflows is attracting more and more attention from the science and engineering communities in order to derive a better understanding of the mechanism of microflows and develop better models [19].

To describe the slip characteristics of fluids on the solid surface, Navier introduced a more general boundary condition. This condition attracts significant attention of the science and engineering communities for the study of flows in micro-scale. Recent advancement in the manufacture of micro devices enable experimental investigation of fluid flows in micro-scale, and many experimental results have provided evidence to support the Navier slip condition [22, 23, 31]. Some attempts have also been made to use nanotechnologies for the surface treatment of micro-channels so as to achieve large slip for maximizing the transport efficiency of fluids through micro-channels.

Many experimental results were shown to support the no-slip boundary conditions. However, it has been established that the interaction of fluids with the solid surface of micro-channels is very different from that in large systems, due to the large ratio of surface area with volume for the microsystems. The flow of fluids in microsystems is granular and slip can occur [2, 24, 31, 35, 36]. Hence, the no-slip condition is not acceptable for fluid flows in micro-channels although it is applicable to fluid flow in large systems [35]

There are many analytical results for the steady state flow of Newtonian fluid. Duan and Muzychka [36, 37] examined the solution for slip flows through rectangular ducts and elliptical ducts. The velocity distribution satisfies the slip boundary condition at the walls.

Duan and Muzychka [36] investigated slip flows in elliptic micro-channels. An analytical solution of Poiseuille number was obtained using the method of separation of variables in elliptic cylindrical coordinates. A simple model was developed for predicting the Poiseuille number for the slip flow in elliptic micro-channels. They also investigated the slip flow in non-circular micro-channels. A simple model was developed for predicting the friction factor Reynolds product for the slip flow in noncircular micro-channels.

Wu et al. [35] examined transient flows of Newtonian fluids through microtubes, and B. Wiwatanapataphee et al. [4] studied transient flows through micro-annuals with slip boundary. They assumed that the fluid flow is driven by the pressure field with a pressure gradient which can be expressed by a Fourier series but their work is limited to the cases where the pressure gradient varies with time only. Based on the solutions, they analysed the influence of the slip parameter on the velocity and the flow rate as well as the stress field in the fluid.

1.2 Objectives

Although a significant advancement in the study of velocity profile of slip flows in rectangular and elliptical micro-channels have been made, there are still many problems which require further investigation.

This research mainly studies the exact solutions for the unsteady flows in rectangular and elliptical micro-channels with slip boundary. The main objective

of this research is develop and investigate the analytical solutions for fluid flows in rectangular micro-channels and elliptical micro-channels with slip boundary. The specific objectives are as follows.

(1) Construct a complete set of equations for fluid flows in micro-channels of rectangular cross-section with slip boundary. This includes construction of the governing field equation and the slip boundary conditions.

(2) Derive analytical solutions for the slip flows in rectangular micro-channels, including exact solution for the velocity field, the flow rate and the stress field.

(3) Investigate the velocity profile and the behaviour of fluid flows in micro-channels of rectangular cross-section as well as the influence of slip parameter.

(4) Formulate the governing equations for unsteady slip flows in elliptic micro-channels, including transforming the governing partial differential equations and boundary conditions to elliptic cylindrical coordinates.

(5) Develop analytical solutions for unsteady slip flows in micro-channels of elliptic cross-section.

(6) Investigate the flow behaviour of fluids in elliptic micro-channels and investigate the influence of the slip parameter on the flow behaviour.

1.3 Outline of the Thesis

This thesis develops various theoretical results for transient flows of Newtonian fluids through micro-channels with slip boundary conditions. The thesis is organized as follows:

Chapter 1 introduces the background of the research, and presents the objectives of the research.

Chapter 2 reviews previous research results relevant to the field of study, including review of fundamental field equations, boundary conditions, methods of solutions, and some relevant solutions.

Chapter 3 develops analytical solutions for the unsteady slip flow in rectangular micro-channels, including the exact solutions for the velocity field, the flow rate and the stress field. Flow behaviour for two special cases, corresponding to constant and wave form pressure gradient respectively, are investigated. The influence of the slip parameter on the flow behaviour is also investigated.

Chapter 4 develops analytical solutions for the unsteady slip flow in elliptical micro-channels. The work is restricted to investigation for wave form pressure gradient only as the result for constant pressure gradient has been found earlier.

Chapter 5 concludes the research project and discuss some problems for further research.

Chapter 2
Literature Review

2.1 An Overview

Fluid dynamics are concerned with the motion of liquids and gases. At macroscopic studies, fluids and gases are assumed to be continuous in structure. All the variables are considered to be continuous functions of the spatial coordinates and time. The equations governing the fluid flow include the continuity equations and the Navier-Stokes equations. They can be used to model the movement of air in the atmosphere, ocean currents, water flow in pipes, and many other fluid flow phenomena.

The general equations for fluid flows are time-dependent and consist of a continuity equation for conservation of mass, three conservation of momentum equations and a conservation of energy equation. Usually, these equations, in real world applications, cannot be solved in a closed form. However, in some special cases, the equations can be simplified and analytical solutions may be obtained.

Over the past decades, various studies have been carried out to investigate steady and unsteady flows through micro-channels under slip or no-slip boundary conditions. Wu et al. [35] considered the transient flow of an incompressible Newtonian fluid through a circular micro-tube with the z-axis being in the axial direction. They formulated the field equations governing the flow including the

continuity equation and the Navier–Stokes equations, then derived an exact solution for the transient velocity field, the flow rate and the stress field by using Fourier series expansion.

A method similar to that in [35] is then applied to derive an exact solution for the transient flow of a Newtonian fluid through a micro-annulu with a slip boundary involving two parameters respectively for the inner surface and the outer surface. Analytical results are derived for the transient flow in a circular annual of inner radius a and outer radius R with the z-axis being in the axial direction. However the results are limited to the fully developed flow and to the case in which the slip length does not change along the flow direction.

Duan and Muzychka [36] studied the steady slip flow in elliptic micro-channels. They examined the momentum equations and considered the various force balances between the friction and pressure forces for a long micro-channel by using the method of scale analysis. In the elliptic cross-section, they compare the scale between friction and inertial forces. The solution has been found by using the method of separation of variables and the method of Fourier expansion in elliptic cylindrical coordinates.

In [52], Ebert and Sparrow analysed the velocity and pressure drop characteristics of the moderately rarefied gas flow in rectangular and annular ducts. The density level is such that a velocity slip may occur on the duct walls. In general, it is found that the effect of slip is to flatten the velocity distribution for a continuum flow; furthermore, the axial pressure gradient is diminished under the slip flow condition. The effect of compressibility on the axial pressure drop was also investigated. It was found that compressibility increases the pressure drop primarily through an increase in viscous shear rather than through an increase in momentum flux.

Duan and Muzychka [37] studied the slip flow in non-circular micro-channels. They examined the solution for steady slip flow in rectangular ducts. The solution for rectangular ducts was derived by using the method of eigenfunction expansions and following Ebert and Sparrow [52]. A simple model was developed for predicting the friction factor Reynolds product for slip flows in non-circular micro-channels. This developed model may be used to predict mass flow rate and pressure distribution of slip flows and could be extended to the early transition regime by employing the second order slip boundary conditions.

In this chapter, we will give a comprehensive review on the fundamental theories for fluid dynamics, the basic methods for the solution of fluid dynamics problems and some analytical results relevant to this project. In section 2.2, the fundamental field equations are presented. In section 2.3, two types of boundary conditions are given, including the no-slip boundary condition and the slip boundary condition. In section 2.4, some methods for finding exact solutions under no-slip boundary conditions are reviewed. In section 2.5, some methods for finding exact solutions under slip boundary conditions are given. In section 2.6, a brief introduction of numerical studies in the field is given.

2.2 Fundamental Field Equation

The basic variables in continuum mechanics include velocity vector **v**, density ρ, deformation rate **d,** and stress tensor σ. These variables are related by a set of equations derived from the principles of continuum mechanics, including the continuity equation, the stress equations of motion, the geometric equations, and the constitutive equations.

2.2.1 Stress Equations of Motion

To determine the stress field, one needs to construct a set of differential equations with stress components as unknown functions [107].

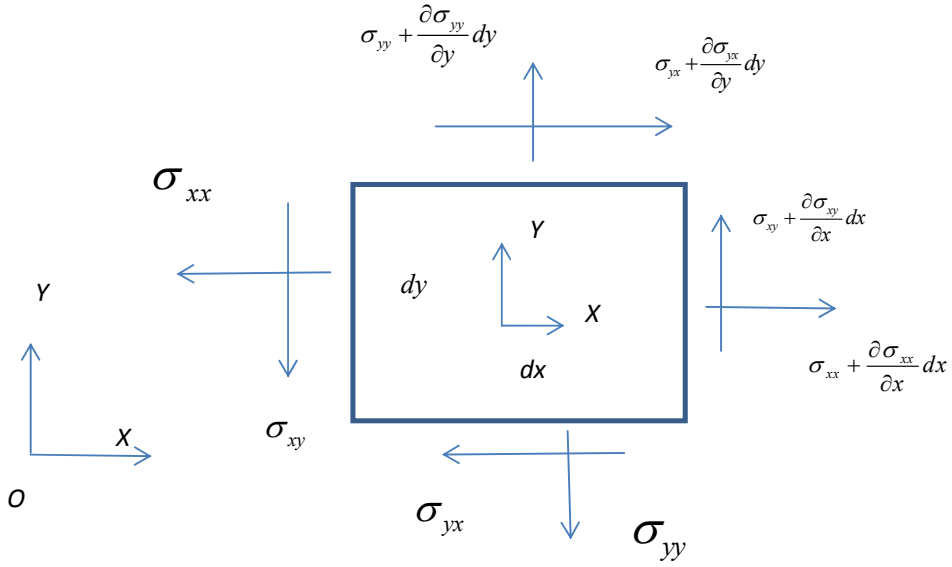

Figure 2.1: Free body diagram showing the forces acting on a differential element

Consider a differential element as shown in figure 2.1. Assume that the material is continuous and the stresses are continuous in space, then the stress acting in the surfaces of the differential element (to a first order approximation) are as shown in figure 2.1.

From Newton's second law, the stress and acceleration of the differential element must satisfy:

$$-\sigma_{xx}dy+\left(\sigma_{xx}+\frac{\partial\sigma_{xx}}{\partial x}dx\right)dy+\left(\sigma_{yx}+\frac{\partial\sigma_{yx}}{\partial y}dy\right)dx-\sigma_{yx}dx+\rho Xdxdy = \rho dxdya_x \tag{2.1}$$

$$\left(\sigma_{yy}+\frac{\partial\sigma_{yy}}{\partial y}dy\right)dx-\sigma_{yy}dx+\left(\sigma_{xy}+\frac{\partial\sigma_{xy}}{\partial x}dx\right)dy-\sigma_{xy}dy=\rho dxdya_y, \tag{2.2}$$

where $a=\frac{Dv}{Dt}=\frac{\partial v}{\partial t}+v\frac{\partial v}{\partial x}$.

After simplification, we have

$$\begin{aligned}\frac{\partial\sigma_{xx}}{\partial x}+\frac{\partial\sigma_{yx}}{\partial y}+\rho X&=\rho a_x\\ \frac{\partial\sigma_{xy}}{\partial x}+\frac{\partial\sigma_{yy}}{\partial y}+\rho Y&=\rho a_y\end{aligned}, \tag{2.3}$$

Using index notation, we can write the above equations as

$$\frac{\partial\sigma_{ji}}{\partial x_j}+\rho X_i=\rho a_i, \tag{2.4}$$

where i, j = 1, 2 for two dimensional problems. For three dimensional problems, equations (2.5) are still applicable with i, j= 1, 2, 3, which can be written in unbridged form by

$$\begin{aligned}\frac{\partial\sigma_{xx}}{\partial x}+\frac{\partial\sigma_{yx}}{\partial y}+\frac{\partial\sigma_{zx}}{\partial z}+\rho X&=\rho a_x,\\ \frac{\partial\sigma_{xy}}{\partial x}+\frac{\partial\sigma_{yx}}{\partial y}+\frac{\partial\sigma_{zy}}{\partial z}+\rho Y&=\rho a_y,\\ \frac{\partial\sigma_{xz}}{\partial x}+\frac{\partial\sigma_{yz}}{\partial y}+\frac{\partial\sigma_{zz}}{\partial z}+\rho Z&=\rho a_z,\end{aligned} \tag{2.5}$$

2.2.2 Geometric Equations

When an object is subject to external forces, stresses will develop within the material of the object. The stresses will cause the material to deform including change in size and shape of the object. To measure the deformation, we consider a differential element of material within a continuum as shown in figure 2.2. In general, under the action of an applied force system, the element will be displaced and deformed as shown in figure 2.2 [107].

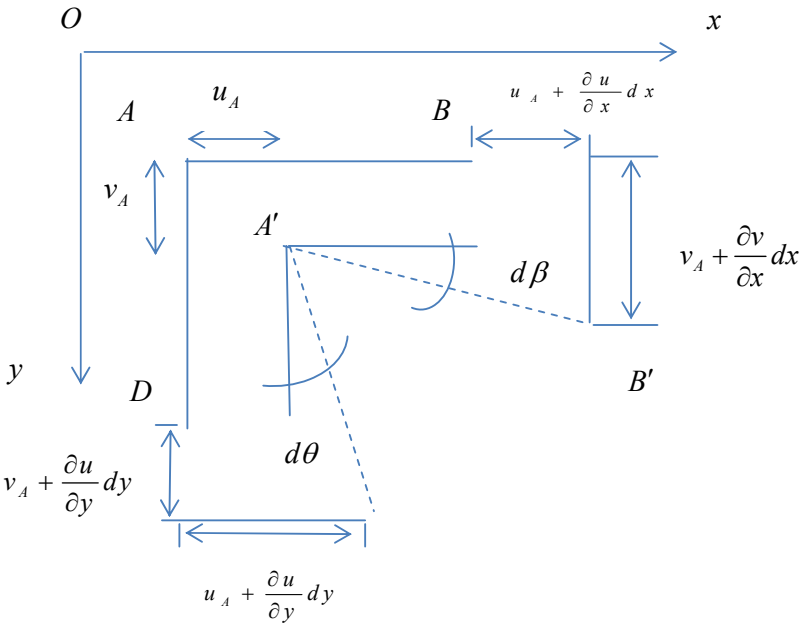

Figure 2.2: Diagram for the derivation of strain-displacement relations

Suppose the displacement of the point A, located initially at (x,y) is (u_A, v_A) with

$$u_A = u(x,y,t)\,,\ v_A = v(x,y,t)\,. \tag{2.6}$$

From the continuum assumption, the displacement of point *B* is (u_B, v_B) and its first order Taylor approximation is

$$\begin{aligned} u_B &= u(x+dx, y, t) = u(x, y, t) + \frac{\partial u}{\partial x} dx = u_A + \frac{\partial u}{\partial x} dx, \\ v_B &= v_A + \frac{\partial v}{\partial x} dx, \end{aligned} \tag{2.7}$$

and the displacement of point *D* is (u_D, v_D) with

$$\begin{aligned} u_D &= u(x, y+dy, t) = u(x, y, t) + \frac{\partial u}{\partial y} dy = u_A + \frac{\partial u}{\partial y} dy, \\ v_D &= v_A + \frac{\partial v}{\partial y} dy. \end{aligned} \tag{2.8}$$

As $d\beta$ is small, the stretch of the line AB is

$$\Delta(dx) = u_B - u_A = \frac{\partial u}{\partial x} dx \,. \tag{2.9}$$

Remark:

$d\beta$ and $d\theta$ are small change of angles in *x* and *y* direction respectively.

Definition *Normal Strain in the x- direction*

The change in the length of *AB* divided by its original length, representing the change in length for per unit length in the *x*-direction, is known as normal strain in the *x*-direction and can be determined by

$$\varepsilon_{xx} = \frac{\frac{\partial u}{\partial x} dx}{dx} = \frac{\partial u}{\partial x}. \tag{2.10}$$

Similarly, the normal strain in the *y*- direction measures the change in length for per unit length in the *y*-direction and can be determined by

$$\varepsilon_{yy} = \frac{\partial v}{\partial y} \ . \tag{2.11}$$

The change of shape can be measured by the change of angle from the original right angle at point *A*, that is,

$$\gamma_{xy} = d\theta + d\beta = \frac{\partial u}{\partial y} + \frac{\partial v}{\partial x} = 2\varepsilon_{xy}, \tag{2.12}$$

which is called the angular or shear strain.

The strain displacement relation (2.10) – (2.12) are called geometric equations and can be expressed in index notation by

$$\varepsilon_{ij} = \frac{1}{2}\left(\frac{\partial u_i}{\partial x_j} + \frac{\partial u_j}{\partial x_i} \right). \tag{2.13}$$

Note that the above equations are also applicable to the 3-dimensional case for which *i, j*= 1, 2, 3.

2.2.3 Continuity Equation

Based on the mass conservation principle, namely mass cannot be created or destroyed, one has another fundamental equation, namely the continuity equation.

Consider a closed surface *S*, fixed in space, enclosing a fixed volume Ω. Let *dS* be a differential surface element (on *S*) with area *dS* and an outward unit normal vector **n**, and let the velocity of the fluid on the element be ***v***, then the velocity component in the outward normal direction is $v_n = \boldsymbol{v} \cdot \mathbf{n}$.

In a unit time, the fluid originally on the surface element dS will move a distance $dl = \boldsymbol{v} \cdot \mathbf{n}$ and thus the volume of the fluid flowing out of Ω through dS per unit time is

$$dQ = \rho v_n dS = \rho \boldsymbol{v} \cdot \mathbf{n}\, dS. \tag{2.14}$$

Integrating dQ over the entire surface leads to a total mass efflux

$$Q = \iint_S \rho \boldsymbol{v} \cdot \mathbf{n}\, dS. \tag{2.15}$$

As material can be neither created nor destroyed, the mass efflux out of Ω can only be achieved at the expense of a decrease in density within Ω. The rate of decrease of mass within Ω due to the change in density is given by

$$\iiint_\Omega \lim_{\Delta t \to 0} \frac{\rho(t) - \rho(t + \Delta t)}{\Delta t} d\Omega = -\iiint_\Omega \frac{\partial \rho}{\partial t} d\Omega. \tag{2.16}$$

From (2.15) and (2.16), by equating the mass rate of flow out of Ω and the rate of decrease of mass within Ω, we have

$$-\iiint_\Omega \frac{\partial \rho}{\partial t} d\Omega = \iint_S \rho \boldsymbol{v} \cdot \mathbf{n}\, dS. \tag{2.17}$$

Using the divergence theorem, we have from (2.17) that

$$\iiint_\Omega \left[\frac{\partial \rho}{\partial t} + \operatorname{div}(\rho v) \right] d\Omega = 0. \tag{2.18}$$

Finally, since Ω may be chosen arbitrarily, by assuming the integrand is continuous, we derive

$$\frac{\partial \rho}{\partial t} + \operatorname{div}(\rho \mathrm{v}) = 0, \tag{2.19}$$

which is the equation of conservation of mass expressed in differential form. The equation above is also known as the equation of mass balance or equation of continuity.

For incompressible materials, $\partial\rho/\partial t = 0$ and thus the continuity equation becomes

$$\text{div } \boldsymbol{v} = 0. \tag{2.20}$$

In the *x,y,z* coordinate, the continuity equation is

$$\frac{\partial v_1}{\partial x} + \frac{\partial v_2}{\partial y} + \frac{\partial v_3}{\partial z} = 0\,. \tag{2.21}$$

In the cylindrical polar coordinate (r, θ, z), the continuity equation is

$$\frac{1}{r}\frac{\partial}{\partial r}\left(r u_r\right) + \frac{1}{r}\frac{\partial u_\theta}{\partial \theta} + \frac{\partial u_z}{\partial z} = 0\,. \tag{2.22}$$

2.2.4 Constitutive Equations

Fluids are classified into Newtonian fluids and non-Newtonian fluids. A Newtonian fluid is a viscous fluid for which the shear stress is linearly proportional to the rate of deformation. For an isotropic, Newtonian fluid, the stress-strain relationship is specified by the equations

$$\sigma_{ij} = -p\delta_{ij} + \lambda d_{kk}\delta_{ij} + 2\mu d_{ij}\,, \tag{2.23}$$

where $d_{ij} = \frac{1}{2}\left(v_{i,j} + v_{j,i}\right)$ is the rate of deformation tensor and $\mathbf{v} = \left(v_1, v_2, v_3\right)$ denotes the velocity vector, μ is the coefficient of viscosity, and p is the fluid pressure.

For incompressible fluids, $d_{kk} = 0$ and thus

$$\sigma_{ij} = -p\delta_{ij} + 2\mu d_{ij}, \tag{2.24}$$

which, in the rectangular *xyz* coordinate system, can be written as

$$\begin{aligned} &\sigma_{xx} = -p + 2\mu\frac{\partial u}{\partial x}, \sigma_{yy} = -p + 2\mu\frac{\partial v}{\partial y}, \sigma_{zz} = -p + 2\mu\frac{\partial w}{\partial z}, \\ &\sigma_{xy} = \mu\left(\frac{\partial u}{\partial y} + \frac{\partial v}{\partial x}\right), \sigma_{yz} = \mu\left(\frac{\partial v}{\partial z} + \frac{\partial w}{\partial y}\right), \sigma_{zx} = \mu\left(\frac{\partial w}{\partial x} + \frac{\partial u}{\partial z}\right). \end{aligned} \tag{2.25}$$

For non-Newtonian fluids, the viscosity μ is not a constant. Various non-Newtonian models have been proposed including the Carreau model, the Walburn-Scneck model, the Power Law model, the Casson model and the generalised power law model.

For the Carreau model [108], the effective viscosity is

$$\mu = \mu_\infty + \left(\mu_0 - \mu_\infty\right)\left[1 + \left(\lambda\dot{\gamma}\right)^2\right]^{(n-1)/2},$$

where [108],

$$\mu_0 = 0.56P, \mu_\infty = 0.0345P, \lambda = 3.313s, \text{ and } n=0.3568.$$

For the Walburn-Schneck model [108], the effective viscosity is

$$\mu = C_1 e^{C_2 H}\left[e^{C^4\left(TPMA/H^2\right)}\right]\left(\dot{\gamma}\right)^{-C_3 H},$$

where [108],

$$C_1 = 0.00797, C_2 = 0.0608, C_3 = 0.00499,$$
$$C_4 = 14.585l\ \mathrm{g}^{-1}, H = 40\% \text{ and } TPMA = 25.9gl^{-1}.$$

For the Power Law model [108], the effective viscosity is $\mu = \mu_0 \left(\dot{\gamma}\right)^{(n-1)}$ where [108], $\mu_0 = 0.035,$ and n=0.6 .

For the Casson model [108], the effective viscosity is

$$\mu = \left[\left(\eta^2 J_2\right)^{1/4} + 2^{-1/2}\tau_y^{1/2}\right]^2 J_2^{-1/2},$$

where $|\dot{\gamma}| = 2\sqrt{J_2}$, $\tau_y = 0.1\left(0.625H\right)^3$, $\eta = \eta_0\left(1-H\right)^{-2.5}$, $\eta_0 = 0.012$ and H=0.37

For the Generalised Power Law model [108], the effective viscosity is

$$\mu = \lambda\left|\dot{\gamma}\right|^{(n-1)},$$

where

$$\lambda\left(\dot{\gamma}\right) = \mu_\infty + \Delta\mu \exp\left[-\left(1+\frac{|\dot{\gamma}|}{a}\right)\exp\left(\frac{-b}{|\dot{\gamma}|}\right)\right],$$
$$\eta\left(\dot{\gamma}\right) = n_\infty - \Delta n \exp\left[-\left(1+\frac{|\dot{\gamma}|}{a}\right)\exp\left(\frac{-d}{|\dot{\gamma}|}\right)\right],$$

and $\mu_\infty = 0.035$, $n_\infty = 1.0, \Delta\mu = 0.25,$ $\Delta n = 0.45$, $a = 50$, $b = 3$, $c = 50$, and $d = 4$.

2.2.5 Navier Stokes Equations for Incompressible Newtonian Fluids

Substituting the constitutive equations (2.24) into the stress equations of motion (2.4), we obtain

$$\rho\frac{Dv_i}{Dt} = \rho X_i - \frac{\partial p}{\partial x_j}\delta_{ij} + \mu\left(\frac{\partial^2 v_i}{\partial x_j \partial x_j} + \frac{\partial^2 v_j}{\partial x_i \partial x_j}\right). \qquad (2.26)$$

Using the continuity equation (2.20), we have

$$\frac{Dv_i}{Dt} = X_i - \frac{1}{\rho}\frac{\partial p}{\partial x_i} + \frac{\mu}{\rho}\nabla^2 v_i , \tag{2.27}$$

which are the so called Navier-Stokes equations for incompressible Newtonian fluids.

The Navier- Stokes equations, written out in unbridged form, are

$$\begin{aligned}
\frac{Du}{Dt} &= X - \frac{1}{\rho}\frac{\partial p}{\partial x} + \frac{\mu}{\rho}\nabla^2 u, \\
\frac{Dv}{Dt} &= Y - \frac{1}{\rho}\frac{\partial p}{\partial y} + \frac{\mu}{\rho}\nabla^2 v, \\
\frac{Dw}{Dt} &= Z - \frac{1}{\rho}\frac{\partial p}{\partial z} + \frac{\mu}{\rho}\nabla^2 w .
\end{aligned} \tag{2.28}$$

In the rectangular coordinate (*x, y, z*) system, (2.28) becomes

$$\rho\left(\frac{\partial v_x}{\partial t} + v_x\frac{\partial v_x}{\partial x} + v_y\frac{\partial v_x}{\partial y} + v_z\frac{\partial v_x}{\partial z}\right) = -\frac{\partial p}{\partial x} + \mu\left(\frac{\partial^2 v_x}{\partial x^2} + \frac{\partial^2 v_x}{\partial y^2} + \frac{\partial^2 v_x}{\partial z^2}\right) + \rho g_x , \tag{2.29}$$

$$\rho\left(\frac{\partial v_y}{\partial t} + v_x\frac{\partial v_y}{\partial x} + v_y\frac{\partial v_y}{\partial y} + v_z\frac{\partial v_y}{\partial z}\right) = -\frac{\partial p}{\partial y} + \mu\left(\frac{\partial^2 v_y}{\partial x^2} + \frac{\partial^2 v_y}{\partial y^2} + \frac{\partial^2 v_y}{\partial z^2}\right) + \rho g_y , \tag{2.30}$$

$$\rho\left(\frac{\partial v_z}{\partial t} + v_x\frac{\partial v_z}{\partial x} + v_y\frac{\partial v_z}{\partial y} + v_z\frac{\partial v_z}{\partial z}\right) = -\frac{\partial p}{\partial z} + \mu\left(\frac{\partial^2 v_z}{\partial x^2} + \frac{\partial^2 v_z}{\partial y^2} + \frac{\partial^2 v_z}{\partial z^2}\right) + \rho g_z , \tag{2.31}$$

In the cylindrical polar coordinate (r, θ, z) system, the Navier Stokes equations are

$$\rho\left(\frac{\partial v_r}{\partial t}+v_r\frac{\partial v_r}{\partial r}+\frac{v_\theta}{r}\frac{\partial v_r}{\partial \theta}+v_z\frac{\partial v_r}{\partial z}-\frac{v_\theta^2}{r}\right)= \\ -\frac{\partial p}{\partial r}+\mu\left[\frac{\partial}{\partial r}\left(\frac{1}{r}\frac{\partial}{\partial r}\left(rv_r\right)\right)+\frac{1}{r^2}\frac{\partial^2 v_r}{\partial \theta^2}+\frac{\partial^2 v_r}{\partial z^2}-\frac{2}{r^2}\frac{\partial v_\theta}{\partial \theta}\right]+\rho g_r, \tag{2.32}$$

$$\rho\left(\frac{\partial v_\theta}{\partial t}+v_r\frac{\partial v_\theta}{\partial r}+\frac{v_\theta}{r}\frac{\partial v_\theta}{\partial \theta}+v_z\frac{\partial v_\theta}{\partial z}-\frac{v_r v_\theta}{r}\right)= \\ -\frac{1}{r}\frac{\partial p}{\partial \theta}+\mu\left[\frac{\partial}{\partial r}\left(\frac{1}{r}\frac{\partial}{\partial r}\left(rv_\theta\right)\right)+\frac{1}{r^2}\frac{\partial^2 v_\theta}{\partial \theta^2}+\frac{\partial^2 v_\theta}{\partial z^2}+\frac{2}{r^2}\frac{\partial v_r}{\partial \theta}\right]+\rho g_\theta, \tag{2.33}$$

$$\rho\left(\frac{\partial v_z}{\partial t}+v_r\frac{\partial v_z}{\partial r}+\frac{v_\theta}{r}\frac{\partial v_z}{\partial \theta}+v_z\frac{\partial v_z}{\partial z}\right)= \\ -\frac{\partial p}{\partial z}+\mu\left[\frac{1}{r}\frac{\partial}{\partial r}\left(r\frac{\partial v_z}{\partial r}\right)+\frac{1}{r^2}\frac{\partial^2 v_z}{\partial \theta^2}+\frac{\partial^2 v_z}{\partial z^2}\right]+\rho g_z. \tag{2.34}$$

2.3 Boundary conditions

Two different types of boundary conditions have been used in fluid mechanics, namely the no-slip and slip boundary conditions. The no-slip boundary condition in fluid mechanics states that the velocity of a liquid at the solid wall equals the velocity of the wall (Koplik and Banavar, 1998). In other words, the fluid at a solid surface has no relative velocity to it (Zhu and Granick, 2002). When a viscous fluid flows over a solid surface, there is no relative motion between the fluid and the solid on the interface (Richardson, 1973).

The slip and the no-slip boundary conditions can be explained physically here. In [72], the authors consider gas molecules as they strike and reflect from a solid wall. If the wall is perfectly smooth, the particles reflect at exactly the same angle θ as light rays from a mirror would. This is termed as specular reflection. The

molecules conserve their tangential momentum and thus exert no shear on the wall; i.e., perfect slip flow at the wall. Specular reflection is unrealistic on a molecular scale, where even the most highly polished wall appears rough. It is more probable that the impinging particles view the wall as extremely rough and reflect at some random angle uncorrelated with their entry angle. This is termed as diffuse reflection. Equilibrium across a plane y adjacent to the wall requires that the lack of reflected tangential momentum be balanced by a finite slip velocity u_w to provide the shear transmitted to the wall. For perfectly diffuse reflection, this balance leads to the expression

$$u_w \approx \lambda \left(\frac{du}{dy} \right)_w \tag{2.35}$$

where λ denotes the mean free path of the gas and the subscript w stands for wall. If we assume that only a fraction f of the molecules are reflected diffusely, the slip velocity becomes (Kennard ,1938)

$$u_w \approx \left(\frac{2}{f} - 1 \right) \lambda \left(\frac{du}{dy} \right)_w . \tag{2.36}$$

The slip is not important at high Reynold numbers and possibly at low Reynold numbers. At high Reynolds numbers, the flow near the wall is turbulent where the no-slip happens, i.e., $u_w \approx 0$. On the other hand, it is possible to have significant slip at high Mach numbers and low Reynolds numbers, where the boundary layer is laminar [72].

Under normal situation, the no-slip condition provides a realistic restriction on solutions of the Navier-Stokes equation, except for rarefied gases. Under certain low density condition, it is still possible to presume these as continua with Newtonian properties but a slip condition has to be assumed. Confidence in the relevance of this boundary condition stems from both direct experimental

evidence and the success achieved by theories which incorporate this assumption [87].

Let us inquire the origin of the no-slip condition. Kinetic theory and thermodynamic arguments can be called upon to give an explanation of the no-slip condition for the gas, where the molecules of gas are required to remain chemically adsorbed onto a solid surface for a sufficiently long time to attain a thermal equilibrium. A similar explanation in molecular terms is possible for liquids. It can be stated that intermolecular forces between the liquid and a solid wall cause a ligament in the no-slip condition [87].

An alternative explanation of the origin of the no-slip condition relies on the fact that all solid surfaces are, in practice, rough on microscopic scale (Pearson & Petrie, 1968). They consider the boundary conditions which are applied at solid surface in the observation of a polymer melt does, which show a slip velocity, while a no-slip condition seems to be relevant for moderate values of the shear rate at the solid boundary. Richardson (1973) elaborated the original physical ideas of Pearson & Petrie (1968) and the flow of an incompressible Newtonian fluid over a particular family of models for a rough wall was examined in detail.

The no slip boundary condition has been used over the last decades, that is, the fluid velocity relative to the solid is assumed to be zero on the fluid solid interface [58]. However, evidence of slip of a fluid on a solid surface has been reported [57]. Recent experiments in micrometer scale and molecular dynamic simulations have shown that the flow of fluids in microsystem is granular and slip can occur on the fluid-solid interface [53, 54, 59, 63, 65]. Therefore for the study of microflows, it is important to take into account the boundary slip of fluids on the fluid solid interfaces.

On the other hand, the no-slip condition is not acceptable for fluid flows in microchannels under certain conditions such as those investigated in [61, 62] . Many experimental results have provided evidence to support the Navier slip boundary

condition [55, 57, 64], namely the fluid velocity tangential to the solid surface, relative to the solid surface, is proportional to the shear stress on the fluid-solid surface. The proportionality is called the slip length [56, 64]. Some attempts have also been made to derive alternative formula for the determination of the slip length [4, 60]. In this condition, we have the linear slip boundary conditions and the nonlinear slip boundary conditions.

In [35], to completely define the problem, the authors use the linear Navier slip boundary condition. That is, on the solid-fluid interface $r = R$, the axial fluid velocity, relative to the solid surface, is proportional to the shear stress on the interface. Assume that the rigid micro-tube moves with an axial velocity $\overline{v}_t(t)$, then the Navier slip condition can be written as

$$u(R,t) - \overline{v}_t(t) = -\ell \frac{\sigma_{rz}(R,t)}{\mu}, \tag{2.37}$$

where μ is the fluid viscosity, R is radial outer surface and ℓ is the so-called slip length, the negative sign on the right-hand side of the above equation is to reflect that the shear stress on the interface is always in the opposite direction of the axial fluid velocity, as any tangential momentum of a fluid particle relative to the solid surface will always be restricted by a resistance force acting on the opposite direction of the relative movement; $\sigma_{rz}(R,t)$ is the shear stress on the interface between the fluid and the wall of the micro-tube. For $\ell = 0$, the above condition reduces to the no-slip boundary condition, while for $\ell \to \infty$, the above equation gives a surface traction condition for a perfectly smooth surface, i.e. $\sigma_{rz}(R,t) = 0$. For the problem considered in [35], the authors assume that the micro-tube is fixed spatially, i.e. $\overline{v}_t(t) = 0$. Thus by noting that $\sigma_{rz}(R,t) = \mu \frac{\partial u}{\partial r}$, it results

$$u(R,t) = -\ell \frac{\partial u(R,t)}{\partial r}. \tag{2.38}$$

In [4], with slightly different boundary conditions, by adding inner surface with radius *a*, the Navier slip boundary conditions are written in the form of

$$u(a,t) = \pm \ell_1 \frac{\partial u(a,t)}{\partial r},\ u(R,t) = \pm \ell_2 \frac{\partial u(R,t)}{\partial r}, \tag{2.39}$$

where ℓ_1 and ℓ_2 denote the slip parameters of the inner surface and the outer surface, respectively. It is assumed that the slip parameters do not change along the flow.

Wiwatanapataphe et al. [4] have given argument concerning the signs for the terms on the right-hand sides of the above equation, while in the other literature, all the four possible cases are considered and the physically feasible cases are determined based on the solution derived.

In [37], the authors examined the solution for the steady slip flow in a rectangular duct. With similar reason, the velocity distribution must satisfy the linear slip boundary condition on the wall. The local slip velocity is proportional to the local velocity gradient normal to the wall. Due to symmetry, the boundary conditions are

$$\begin{aligned}
u &= -\lambda \frac{2-\sigma}{\sigma} \frac{\partial u}{\partial y} \quad \text{on} \quad y = b, 0 \le x < a, \\
u &= -\lambda \frac{2-\sigma}{\sigma} \frac{\partial u}{\partial x} \quad \text{on} \quad x = a, 0 \le y < b, \\
\frac{\partial u}{\partial y} &= 0 \quad \text{on} \quad y = 0, 0 \le x \le a, \\
\frac{\partial u}{\partial x} &= 0 \quad \text{on} \quad x = 0, 0 \le y \le b,
\end{aligned} \tag{2.40}$$

where λ is the molecular mean free path. The constant σ denotes the tangential momentum accommodation coefficient, which is usually between 0.87 and 1 (Rohsenow , 1961). The most usual conditions correspond to $\sigma \approx 1$; therefore, σ may be assumed to have a value of unity. The same procedure is valid even if $\sigma \neq 1$ by defining a modified Knudsen number as

$$Kn^* = Kn(2-\sigma)\big/\sigma, \tag{2.41}$$

where Kn is an original Knudsen number. This boundary condition will be used in conjunction with finding analytical solution of transient slip flows in rectangular micro-channels, which will be described in chapter 3.

In [36], the local slip velocity is proportional to the local velocity gradient normal to the wall. In elliptic cylindrical coordinates, the boundary conditions, for a one quarter basic cell, are

$$\begin{aligned}
&\frac{1}{\sqrt{g_2}}\frac{\partial u}{\partial \psi} = 0 \quad \text{on } \psi = 0, \\
&\frac{1}{\sqrt{g_2}}\frac{\partial u}{\partial \psi} = 0 \quad \text{on } \psi = \tfrac{\pi}{2}, \\
&\frac{1}{\sqrt{g_2}}\frac{\partial u}{\partial \eta} = 0 \quad \text{on } \eta = 0, \\
&u = -\frac{\lambda\dfrac{2-\sigma}{\sigma}}{\sqrt{g_1}}\frac{\partial u}{\partial \eta} \quad \text{on } \eta = \eta_0,
\end{aligned} \tag{2.42}$$

$$g_1 = g_2 = c^2\left(\cosh^2\eta - \cos^2\psi\right),$$

where λ is the molecular mean free path, and the constant σ denotes the tangential momentum accommodation coefficient which has values typically being between 0.87 and 1. Although the nature of the tangential momentum accommodation coefficients is still an active research problem, almost all evidence indicates that for most gas-solid interactions the coefficients are approximately 1. The same procedure is valid even if $\sigma \neq 1$, defining a modified Knudsen number as $Kn^* = Kn(2-\sigma)/\sigma$.

The parameter η_0 is related to the major and minor axes through

$$\eta_0 = \ell n \frac{1 - b/a}{\sqrt{1 - (b/a)^2}} \ . \tag{2.43}$$

The half focal length of ellipses *c* is defined by

$$c = \frac{a}{\cosh \eta_0} = \frac{b}{\sinh \eta_0} . \tag{2.44}$$

This boundary condition will be utilized in conjunction with finding analytical solutions for the transient slip flow in elliptical micro-channels, which will be described in chapter 4.

In [20] the standard no-slip boundary condition is replaced by the nonlinear Navier boundary condition, where the slip velocity is assumed to be proportional to the tangential viscous stress and the degree of slip is measured by a non-constant slip length. For an incompressible Newtonian fluid the viscous portion of the stress tensor is given by $S = 2\mu \mathbf{d}$ where μ is the viscosity and **d** is the rate of deformation tensor. On a solid surface, the tangential component of the velocity is assumed to satisfy the Navier boundary condition

$$v^* = 2\ell^* \mathbf{d} \ , \tag{2.45}$$

where ℓ^* is the slip length with the same sign as **d**, since it is always assumed that the tangential component of the velocity **v*** is positive in the direction of flow. For the nonlinear Navier boundary condition, it is assumed that the slip length ℓ^* depends on the tangential viscous stress on the solid surface through the following relation

$$\ell^* = \alpha^* \left(1 - 2\beta^* \mathbf{d}\right)^{-\frac{1}{2}} \ , \tag{2.46}$$

where

$$\beta^* = \left[2\mathbf{d}_{critical}\right]^{-1} . \tag{2.47}$$

In some critical (maximum) shear rate with the same sign as **d**, the value is such that the inverse square root does not become negative. It should be noted here that when $\beta^* = 0$ we have $\ell^* = \alpha^*$, that is α^* corresponds to the constant slip length of the boundary condition.

As an example, consider the steady flow of an incompressible Newtonian fluid through an infinite pipe with radius *R* along the z-direction. The nonlinear Navier boundary condition for the case where $\alpha > 0$ and $\beta > 0$ on the inner surface of the pipe is

$$r = 1, v_z = -\alpha \left[1 + \beta \frac{dv_z}{dr} \right]^{-\frac{1}{2}} \frac{dv_z}{dr}, \tag{2.48}$$

where $\alpha = \frac{\alpha^*}{R}$ and $\beta = 4\mu\beta^* / AR$.

2.4 Existing Exact Solutions for No-Slip Boundary Conditions

Not every non-linear partial differential equation can be solved analytically. Some of them are difficult to solve. In the case that the equation cannot be solved analytically, there are methods available to solve the problem numerically. On the other hand, a direct search for exact solutions is now much more viable. In this section, we will introduce some popular methods which have been employed to derive exact solutions for Navier-Stokes equations and review some previous results.

The fundamental governing equations for fluid mechanics are the Navier-Stokes equations. This inherently nonlinear set of partial differential equations has no general solution, and only a small number of exact solutions have been found.

Exact solutions of Navier-Stokes equations are very important. As pointed out in [46], the following are two reasons:

1. The solutions represent fundamental fluid dynamic flows. Hence, due to the uniform validity of exact solutions, the basic phenomena described by the Navier- Stokes equations can be more closely studied.
2. The exact solutions can be used for checking the accuracies of approximate methods, such as numerical, asymptotic, or empirical. The complete numerical integration of the Navier-Stokes equations can be made more feasible due to current advancement in computer technology. However, the accuracy of the results can only be convinced through a rigorous error analysis.

Now, let us define an exact solution of the Navier-Stokes equations. Let $q(x, t)$ be the velocity vector, a function of space x and time t. Let $p(x, t)$ be the pressure. The density ρ and the kinematic viscosity υ are constants. Conservative body forces may be absorbed into the pressure term. Although ρ can be eliminated by taking the curl of the Navier-Stokes Equations, the constant υ (or, in non-dimensional form, the Reynolds number) is a basic parameter. An exact solution is defined as the functions satisfying the Navier-Stokes equations and the continuity equation for all x, t. Obviously, all closed-form solutions of these equations are exact solutions.

Direct numerical solutions of the partial differential equations are not exact solutions, no matter how accurate, because the value of υ has to be assigned for each solution. On the other hand, similarity solutions, where υ is implicit in the similarity transforms, and where universal curves can be obtained once and for all, are exact solutions. The definition of infinite-series solutions obtained from expansion or separation of variables is excluded from this discussion. The reason is that the series could not be exact unless summed to infinity. The degenerate

potential-flow solutions, although satisfying the Navier-Stokes equations, are also not an exact solution (Wang, 1991).

The existing exact solutions have been published in a wide variety of journals. Most of the exact solutions are obtained by a variety of methods and address specific fluid-dynamic problems. In some cases, it is difficult for a researcher in fluid mechanics to know, for a certain problem, whether an exact solution exists or not. A notable example is the oblique stagnation flow on a plate, which was solved independently three times within a span of 47 years [Wang, 1991].

Generally, after the fluid dynamic model is simplified by some assumptions, the equations can be solved subject to some boundary conditions. For flows in micro-channels, many methods have been applied such as the direct methods, the Fourier Series Solution methods, the Variation methods, the Laplace Transform Technique and the Series Solution method.

2.4.1 Laplace Transform Technique

In [79], Das and Arakeri give a procedure to obtain analytical solutions for the unsteady laminar flow in an infinitely long pipe with circular cross section, and in an infinitely long two dimensional channel, created by an arbitrary but given volume flow rate.

The governing equation in [79] is derived by the assumption that the flow is incompressible and bidirectional in an infinitely long circular pipe with zero swirl, i.e,, $v_\theta = 0,\quad v_r = 0$ and $v_z = u = u(r,t)$. The condition of incompressibility implies that any pressure change is felt instantaneously everywhere. After substituting

these into the Navier Stokes equation (2.32), the governing equation of motion in the *x*-direction is

$$\frac{\partial u}{\partial t} = -\frac{1}{\rho}\frac{\partial P}{\partial x} + \upsilon\left(\frac{\partial^2 u}{\partial r^2} + \frac{1}{r}\frac{\partial u}{\partial r}\right). \tag{2.49}$$

The boundary condition is no-slip boundary condition and initial condition is also needed for the velocity, $u(r,0)$, which depends on the problem under consideration. The solution of these equations is possible if the pressure, as a function of time, is known. In this case, however, the pressure is unknown and is determined indirectly by the volume rate, which is given. The velocity is related to the volume rate by

$$\int_0^R 2\pi r u(r,t)dr = u_p(t)\pi R^2 = Q(t), \tag{2.50}$$

where u_p is the velocity averaged over the cross section; it can be considered as the velocity of a piston which would give the flow rate Q.

Additional conditions required are $\frac{\partial P}{\partial r} = 0$, as required by the radial momentum equation in the absence of any body force. The boundary conditions are

$$u(R,t) = 0 \quad \text{and} \quad \frac{\partial u(0,t)}{\partial r} = 0. \tag{2.51}$$

The analytical solution of equation (2.49) is found in [79] by using the Laplace transform technique.

The Laplace transform of Eqs.(2.49), (2.50) and (2.51) are shown to be

$$\frac{d^2\overline{u}(r,s)}{dr^2} + \frac{1}{r}\frac{d\overline{u}(r,s)}{dr} - \frac{s}{\upsilon}\overline{u}(r,s) = \frac{1}{\mu}\frac{d\overline{P}(x,s)}{dx} + \frac{1}{\upsilon}u(r,0), \tag{2.52}$$

$$\bar{u}(R,s)=0\ , \tag{2.53}$$

$$\left.\frac{d\bar{u}}{dr}\right|_{r=0}=0\ , \tag{2.54}$$

$$\int_0^g 2\pi r\bar{u}dr=\bar{u}_p(s)\pi R^2\ , \tag{2.55}$$

where $\bar{u}$ and $\bar{P}$ are Laplace transform of u and P, i.e.,

$$\bar{u}(r,s)=\int_0^\infty e^{-st}u(r,t)dt,\quad \bar{P}(r,s)=\int_0^\infty e^{-st}P(r,t)dt\ . \tag{2.56}$$

The equation (2.52) is a second order inhomogeneous ordinary differential equation with solution of the form

$$\bar{u}(r,s)=C_1I_0(p,r)+C_2K_0(p,r)+\phi_p\ , \tag{2.57}$$

where ϕ_p is the particular solution, $p=\sqrt{s/\upsilon}$, I_0 and K_0 are modified Bessel functions of the first and second kind respectively, C_1 and C_2 are arbitrary constants. By using boundary conditions (2.53) and (2.55), the authors of [79]

eventually obtained

$$\bar{u}(r,s)=\bar{u}_p(s).\bar{G}(r,s)\ , \tag{2.58}$$

where $\bar{G}(r,s)=\dfrac{\left[I_0(B\sqrt{s})-I_0(A\sqrt{s})\right]}{\left[I_0(B\sqrt{s})-\dfrac{2I_1(B\sqrt{s})}{B\sqrt{s}}\right]}$ and $\bar{u}_p(s)$ comes from Laplace transform

of $u_p(t)$. The velocity solution is then obtained using convolution theorem

$$u(r,t)=\frac{1}{2\pi i}\int_{\gamma-i\infty}^{\gamma+i\infty}\bar{u}_p(s).\bar{G}(r,s)e^{st}ds\ . \tag{2.59}$$

As examples, the solutions for various cases have been investigated, including the trapezoidal piston motion, constant acceleration case, impulsively started flow, impulsively blocked fully developed flow, oscillatory flow and flow in a two dimensional channel [79] .

2.4.2 Direct Solution

In [97], the pressure drop of the fully developed laminar flow in smooth arbitrary cross-section channels is studied. Consider the fully developed steady state, laminar flow in a channel with boundary Γ, constant cross sectional A and constant perimeter P. The flow is assumed to be incompressible and have constant properties. Moreover, body force such as gravity, centrifugal, coriolis, and electromagnetic do not exist. Also the rear faction and surface effects are assumed to be negligible and the fluid is considered to be a continuum. For such a flow, the Navier Stokes equations reduces to the Poison's equation with the source term representing the pressure gradient along the length of the duct, namely

$$\nabla^2 w = \frac{1}{\mu}\frac{dp}{dz} \text{ with } w = 0 \text{ on } \Gamma, \tag{2.60}$$

where w and z are the fluid velocity and the flow direction respectively. The boundary condition for the velocity is the no-slip condition on the wall. Since w does not vary with z, it follows from the z-momentum equation that the gradient $\frac{dp}{dz}$ must only be a constant. Equation (2.60) has been solved subject to no-slip condition for various cases of cross-sections [41, 72]. To examine the exact solutions, Bahrami et al. [97] compare the value of the Reynolds number Fanning friction factor product $f\,\mathrm{Re}_{\sqrt{A}}$ between the approximate model and the exact

solution for selected cross sections, where f is the Fanning friction factor and $\mathrm{Re}_{\sqrt{A}}$ is the Reynolds number, defined by

$$f\,\mathrm{Re}_{\sqrt{A}} = \frac{2\pi\sqrt{\pi}\left(1+\varepsilon^2\right)}{\sqrt{\varepsilon}E\left(\sqrt{1-\varepsilon^2}\right)}. \tag{2.61}$$

where $0 \le \varepsilon \le 1$ and $E(x) = \int_0^{\pi/2} \sqrt{1 - x^2 \sin^2 t}\, dt$.

A compact approximate model is proposed that predicts the pressure drop of the fully developed, laminar flow in channels of arbitrary cross section, i.e., arbitrary in area, perimeter, and polar moment of inertia. The proposed model is compared with analytical and numerical solutions for several shapes. Except for the equilateral triangular channel (with 14% difference), the present model successfully predicts the pressure drop for a wide variety of shapes with a maximum difference in the order 8%. Moreover, a compact model is developed using a mapping approach, which predicts the $f\,\mathrm{Re}_{\sqrt{A}}$ for isosceles triangular channels with a maximum difference of less than 3.5%. Comparison of $f\,\mathrm{Re}_{\sqrt{A}}$ for elliptical and rectangular micro-channels shows good agreement.

The proposed model is also validated with either experimental data or exact analytical solutions for rectangular, trapezoidal, triangular (isosceles), square, and circular cross sections collected by several researchers and shows good agreement [97].

2.4.3 Fourier Series Solution

In [98] the author conducted a theoretical and numerical study of the fully developed forced convection in various rectangular ducts. Each duct is filled with

porous materials and the Brinkman model describes the laminar fluid flow inside this fully saturated porous passage.

Modelling fluid flow in porous heterogeneous materials with more than one typical pore size (e.g., concrete, micro porous rocks and fractured materials) presents a challenge because it is difficult to simultaneously resolve all the microstructural features of the porous medium that are at different length scales. One possible approach is to divide the porous medium into two regions: the larger pores and homogeneous regions of smaller pores. In the larger pores, the Stokes' equation for incompressible flow is applicable.

Regions with the smaller pores are treated as a permeable medium and the flow is described by Darcy's law. The two boundary conditions to be satisfied on the pore/ permeable medium interface are continuity of the fluid velocity and the shear stress. Darcy's law alone is not sufficient to satisfy these boundary conditions. The Brinkman equation is a generalization of Darcy's law that facilitates the matching of boundary conditions on the interface between the larger pores and the permeable medium.

For a steady and hydrodynamically fully developed flow passing through an impermeable rectangular channel, the Brinkman momentum equation is

$$\mu_e\left(\frac{\partial^2 u}{\partial y^2}+\frac{\partial^2 u}{\partial z^2}\right)-\frac{\mu}{K}u-\frac{\partial p}{\partial x}=0\,, \tag{2.62}$$

with a constant pressure gradient $\Phi=-\frac{\partial p}{\partial x}$, the effective viscosity is μ_e, the fluid viscosity is μ , and the permeability is *K*.

The formulation of velocity distribution begins by selecting a functional relation in the form of Fourier series

$$\bar{u} = \sum_{n=1}^{\infty}\sum_{m=1}^{\infty} a_{mn} \cos\left(\beta_n \bar{y}\right)\cos\left(\gamma_m \bar{z}\right). \tag{2.63}$$

The boundary conditions are

$$\bar{u} = 0 \text{ on } \bar{y} = \pm 1 \text{ and } \bar{z} = \pm\bar{b} = \pm b/a,$$

$$\partial\bar{u}/\partial\bar{y} = 0 \text{ on } \bar{y} = 0 \text{ and}$$

$$\partial\bar{u}/\partial\bar{z} = 0 \text{ on } \bar{z} = 0.$$

The value of a_{mn} is found by applying the orthogonality condition [98, 75].

The average velocity is $\bar{U} = \frac{1}{ab}\int_{y=0}^{a}\int_{z=0}^{b} u\, dzdy = \sum_{n=1}^{\infty}\sum_{m=1}^{\infty} \frac{4}{\left(\bar{b}\beta_n\gamma_m\right)^2\left(\beta_n^2 + \gamma_m^2 + \frac{1}{MDa}\right)}$,

where $M = \frac{\mu_e}{\mu}$ and $Da = \frac{K}{a^2}$ is the Darcy number.

2.4.4 Infinite Series Form

In [75], Chakraborty discussed the methods for the analysis of flow through micro-channels. One of the methods is the infinite series solution method. The flow problem within a straight micro-channel of arbitrary cross section is analyzed. Based on exact analytical solutions for the flow profile for some simple geometries of channel section, a number of problems with relative more complicated geometries are solved either exactly or approximately in [75].

Consider incompressible flow within a straight micro-channel of uniform cross section. Following the Navier-Stokes equation (2.29), the steady flow velocity $u(y,z)$ along the axial direction is governed by the equation

$$\mu\left(\frac{\partial^2 u}{\partial y^2}+\frac{\partial^2 u}{\partial z^2}\right)=\frac{dp}{dx}, \tag{2.64}$$

where $\frac{dp}{dx}$ is the constant pressure gradient along the x- axis. The y and z axes are orthogonal to the x- axis and the x-y-z axes form a right handed co-ordinate system. The no-slip boundary condition on the boundary is given by

$$u(y,z)=0 \text{ on } \varphi(y,z)=0 \text{ or } \frac{\partial u}{\partial s}=0 \text{ on } \varphi(y,z)=0,$$

where s is the length measured along the boundary represented by $\varphi(y,z)=0$. The boundary curve is assumed to be rectifiable.

The solution in infinite series form is found by exploiting the analogy between the flow problem and the problem of vibration of a taut membrane where the equation of motion of the free transverse vibration of a membrane having uniform unit tension in all sides and unit thickness and material density is given by

$$\frac{\partial^2 w}{\partial t^2}-\left(\frac{\partial^2 w}{\partial y^2}+\frac{\partial^2 w}{\partial z^2}\right)=0, \tag{2.65}$$

where w is the transverse deflection of any point within the membrane. The deflection vanishes on the boundary.

The normal modes possess orthogonal property and form a complete set in the sense that any function $f(y,z)$ satisfying the boundary conditions can be expressed in terms of the normal modes as

$$f(y,z)=\sum_{n=1}^{\infty} a_n W_n(y,z). \tag{2.66}$$

The constants a_n can be obtained by using the orthogonality relation [75, 98], while the fluid flow profile can be obtained in two steps. In the first step, the eigen modes for the given cross section are calculated using the membrane analogy. In the second step, the true flow profile is calculated as summation of the normal modes whose contribution is obtained from the flow equation.

As an example, consider a rectangular channel with dimensions of *2a* and *2b* along the *y* and *z* axes, respectively. Taking the origin at the center of cross section, the normal modes of the rectangular can be easily shown as $W_{mn}(y,z)$ and the corresponding natural frequency is ω_{mn}. The flow profile in the rectangular channel can be written as $u(y,z)=\sum_{m,n=1}^{\infty} a_{mn} W_{mn}(y,z)$.

Substituting this equation into equation (2.64) and finding the unknown constants using orthogonality relation, we have

$$a_{mn} = -\frac{16}{(2m+1)(2n+1)\pi^2 \omega_{m,n}^2}\left(\frac{1}{\mu}\frac{dp}{dx}\right)(-1)^m(-1)^n ,$$

$$W_{mn}(y,z) = \cos\left(\frac{2m+1}{2a}\right)\pi y \cos\left(\frac{2n+1}{2b}\right)\pi z , \qquad (2.67)$$

$$\omega_{mn} = \sqrt{\left(\frac{2m+1}{2a}\right)^2 + \left(\frac{2n+1}{2b}\right)^2}\,\pi .$$

2.4.5 Variational Method

As shown in [75], solving a given flow problem in term of an infinite series may not be possible if the channel cross section is very complicated. In that case, approximate solutions are to be sought. A variational formulation of the flow

problem is given in [75] that can be used to obtain approximate flow profile for any channels, namely the velocity profile is obtained by minimizing the functional

$$J[u] = \iint \left\{ \frac{\mu}{2} \left[\left(\frac{\partial u}{\partial y} \right)^2 + \left(\frac{\partial u}{\partial z} \right)^2 \right] + u \left(\frac{dp}{dx} \right) \right\} dA \ , \tag{2.68}$$

where $u(y,z)$ is a function that satisfies the essential boundary condition. The functional attains the optimal value when the equation (2.64) is satisfied. As an example, consider the problem of flow through a channel of elliptical cross section whose boundary is given by $\varphi(y,z) = \frac{y^2}{a^2} + \frac{z^2}{b^2} - 1 = 0$. Let the trial function be $u(y,z) = m\left(\frac{y^2}{a^2} + \frac{z^2}{b^2} - 1 \right)$. The unknown quantity m can be obtained if

$$J[u] = \int \left[2\mu m^2 \left(\frac{y^2}{a^4} + \frac{z^2}{b^4} \right) + m \frac{dp}{dx} \left(\frac{y^2}{a^2} + \frac{z^2}{b^2} - 1 \right) \right] dydz \tag{2.69}$$

is minimized with respect to m. Hence the flow profile becomes

$$u(y,z) = \frac{a^2 b^2}{2\left(a^2 + b^2\right)} \left(\frac{1}{\mu} \frac{dp}{dx} \right) \left(\frac{y^2}{a^2} + \frac{z^2}{b^2} - 1 \right) \tag{2.70}$$

In this case, the result obtained by the approximate method is also exact because the trial function satisfies the boundary condition as well as the governing equation.

2.5 Existing Exact Solutions for Slip Boundary Conditions

The governing field equations for the flow of incompressible Newtonian fluids consist of the incompressible continuity equation, the Navier-Stokes equations, and a set of boundary conditions. Some methods have been utilized to solve the Navier- Stokes equation supplemented by slip boundary conditions, including the

Fourier Series Expansion method, the Direct Solution method and the Integral Transform Technique.

2.5.1 Fourier Series Expansion

Wu et al. [35] considered the transient flow of an incompressible Newtonian fluid through a circular micro-tube with the *z*-axis being in the axial direction. They formulate the field equation by assuming that the flow is axial symmetric so that there is no swirling flow in the channel and the velocity components in the radial and transverse directions vanish, namely $v_r = 0$, $v_\theta = 0$.

Substituting the above into the continuity equation yields

$$\frac{\partial u}{\partial z} = 0, \tag{2.71}$$

which gives rise to $u = u(r, \theta)$. Because the flow is horizontal, $g_z = 0$. By substituting these into equation (2.34), which $u = v_z$ yields

$$\frac{\mu}{\rho}\left(\frac{\partial^2 u}{\partial r^2} + \frac{1}{r}\frac{\partial u}{\partial r}\right) - \frac{\partial u}{\partial t} = \frac{1}{\rho}\frac{\partial p}{\partial z}. \tag{2.72}$$

The authors then consider the fluid flow driven by the pressure field with a pressure gradient $\overline{q}(t)$ in the form of the Fourier series, namely

$$\frac{\partial p}{\partial z} = \overline{q}(t) = a_0 + \sum_{n=1}^{\infty}\left[a_n \cos(n\omega t) + b_n \sin(n\omega t)\right]. \tag{2.73}$$

As a wide range of functions can be expressed in terms of Fourier series, the assumption of the form of pressure gradient above will not lose generality. However, it is noted that their work is limited to the cases where the pressure gradient varies with time only.

Flow of fluids driven by non-constant pressure gradient occurs in many natural and industrial processes. A typical example is the pulsatile blood flow through arteries in which the pressure gradient driving the flow of blood is in pulsatile form [3]. Various methods can also be used to generate pulsatile flows, such as those by using reciprocating pistons, servo valves or air pulsation [66, 67].

For convenient in deriving analytical solutions of the field equations, the complex number is used to express (2.73) by exponential functions, namely

$$\frac{\partial p}{\partial z} = \mathrm{Re}\left(\sum_{n=0}^{\infty} c_n e^{in\omega t} \right), \tag{2.74}$$

where

$$c_n = a_n - b_n i\,, \quad e^{in\omega t} = \cos\left(n\omega t\right) + i\sin\left(n\omega t\right). \tag{2.75}$$

Exact solutions for the velocity field and stress field have been derived. The authors also show that boundary slip on the flow behaviour is qualitatively different for different types of pressure fields driving the flow. For pressure fields with a constant pressure gradient, the boundary slip does not alter the interior material deformation and stress field. But for pressure fields with a wave form pressure gradient, the boundary slip is found to cause the change of interior material deformation and consequently the velocity profile and stress field. The asymptotic expressions for the exact solutions are also derived through a parameter $\overline{\beta}$ which is identified to dominate the behaviour of the flow driven by the wave form pressure gradient, establishing an explicit formulae for the critical slip parameter leading to the maximum transient flow rate.

Wiwatanapataphe et al. [4] considered the transient flow of an incompressible Newtonian liquid through a circular annual of inner radius a and outer radius R with the z-axis being in the axial direction. The field equations governing the flow

include the continuity equation and the Navier–Stokes equations where u satisfying equation (2.72), derived by similar ways, but supplemented by different boundary conditions. Their analysis is limited to the fully developed flow and to the case that the slip length does not change along the flow direction.

The analytical solutions in [4] show that the influences of boundary slip on the flow behaviour are qualitatively different for different types of pressure fields driving the flow. For pressure fields with a constant pressure gradient, the flow rate increases with the increase of the slip parameter ℓ almost linearly when ℓ is large; while, for pressure fields with a wave form pressure gradient within a certain frequency range, as the slip parameter ℓ increases, the amplitude of the flow rate increases first and then approaches a constant value when ℓ becomes sufficiently large. The authors also found that to achieve a given flow rate, one could have different designs.

Duan and Muzychka [36] studied the steady slip flow in elliptic micro-channels. They examined the momentum equations and considered the various force balances between the friction and pressure forces for a long micro-channel by using the method of scale analysis. In the elliptic cross-section, they compare the scale between friction and inertial forces to obtain

$$\frac{\mu\dfrac{\partial^2 u}{\partial y^2}}{\rho u\dfrac{\partial u}{\partial x}} \sim \frac{\mu\dfrac{U}{D_h^2}}{\dfrac{\rho U^2}{L}} = \frac{L}{D_h \operatorname{Re}_{D_h}} = L^+ . \tag{2.76}$$

The starting point of the analysis is the law of conservation of momentum. When $L^+ \gg 1$, the continuum flow momentum equation reduces to the form

$$\frac{\partial^2 u}{\partial x^2} + \frac{\partial^2 u}{\partial y^2} = \frac{1}{\mu}\frac{dp}{dz} . \tag{2.77}$$

In elliptic micro-channels, it is convenient to use elliptic cylinder coordinates to facilitate the solution process. Then, the momentum equation becomes

$$\frac{\partial^2 u}{\partial \eta^2}+\frac{\partial^2 u}{\partial \psi^2}=\frac{c^2}{\mu}\frac{dp}{dz}\left(\cosh^2\eta-\cos^2\psi\right). \tag{2.78}$$

This equation can be solved by using the separation of variables method. In order to overcome the difficulty caused by metric coefficient, a binomial series is used to approximate the metric coefficient. Some constants are found by applying the orthogonality principles.

After lengthy derivation, the velocity distribution is found. In the limit of $Kn \to 0$, the velocity distribution reduces to its continuum flow solution:

$$u=-\frac{c^2}{8\mu}\frac{dp}{dz}\left[\cosh 2\eta_o+\frac{1}{\cosh 2\eta_o}\cos(2\psi)\cosh(2\eta)-\cosh(2\eta)-\cos(2\psi)\right] \tag{2.79}$$

The mean velocity is then found by integration of the velocity on the cross-section. The Poiseuille number is then defined by $PoD_h=\frac{\tau D_h}{\mu\overline{u}}$ where D_h is the hydraulic diameter and $\overline{u}$ denotes the mean velocity. It can be demonstrated that the limit of PoD_h as $b/a \to 1$ corresponding to circular tubes is:

$$\lim_{b/a\to 1} PoD_h=\frac{8}{1+\frac{2-\sigma}{\sigma}8Kn}. \tag{2.80}$$

The accuracy of the proposed simple model was found to be within 3 % of the exact values.

In [52], Ebert and Sparrow analysed the velocity and pressure drop characteristics of the moderately rarefied gas flow in rectangular and annular ducts. The density level is such that a velocity slip may occur on the duct wall. For rectangular ducts, the momentum equation takes the form (2.77) where u is the axial velocity distribution, and p is the static pressure.

For annular ducts, the governing equations are similar to those in [35] but for steady case, the momentum equation reduces to

$$\frac{1}{r}\frac{\partial}{\partial r}\left(r\frac{\partial w}{\partial r}\right)=\frac{1}{\mu}\frac{dp}{dz}. \tag{2.81}$$

It is found that the effect of slip is to flatten the velocity distribution for a continuum flow. Furthermore, the axial pressure gradient is diminished under the slip flow conditions. The effect of compressibility on the axial pressure drop was also investigated. It was found that compressibility increases the pressure drop primarily through an increase in viscous shear rather than through an increase in momentum flux.

Ebert and Sparrow [52] also suggested a method of solution. In rectangular ducts, a solution for the velocity distribution may be proposed as

$$\frac{w}{\left(h^2/\mu\right)\left(dp/dz\right)}=\sum_{i=1}^{\infty}\psi_i\left(\xi\right)\cos\left(\alpha_i\eta\right), \tag{2.82}$$

in which the α_i are a set of eigenvalues, and the ψ_i are a set of ξ-dependent functions. This form of solution has to satisfy the boundary conditions. On the other hand, in annular ducts, a direct solution yields

$$\begin{aligned}\frac{w}{\left(r_0^2/4\mu\right)\left(-dp/dz\right)}&=1-\gamma_i^2+2\left(1-\gamma_i\right)Kn\\&+\left[\frac{\gamma_i\left(1-\gamma_i\right)^2\left(1+2Kn\right)\left[\left(1-\gamma_i\right)Kn-\ell n\left(\gamma_i\right)\right]}{\gamma_i\,\mathrm{Ln}\left(\gamma_i\right)-\left(1-\gamma_i^2\right)Kn}\right],\end{aligned} \tag{2.83}$$

where

$$\gamma = \frac{r}{r_0}, \quad \gamma_i = \frac{r_i}{r_0}, Kn = \frac{2-f}{f}\frac{\lambda}{r_0 - r_i}.$$

To solve the equation supplemented by boundary condition, single Fourier series proposed by Ebert and Sparrow does not converge with second-order boundary condition. Therefore, Aubert and Colin proposed a new form based on the double Fourier series, namely

$$W^*(x^*, y^*) = \sum_{i,j=1}^{\infty} A_{ij} N_{ij} \cos\left(\varphi_i \frac{x^*}{a}\right) \cos(\psi_j y^*) + \frac{9}{4} Kn^2 \ . \qquad (2.84)$$

2.5.2 Direct Solution

In [74], Arkilic et al. studied slip flow in micro-channels. The effect of the boundary slip on the velocity is investigated and compared with the measured flow results. It is found that the no-slip solution of the Navier-Stokes equations fails to adequately model the momentum transferred from the fluid to the channels wall and therefore under-estimates the mass flow for a given inlet and outlet pressures. However, by including a slip flow boundary condition on the wall, which is derived from a momentum balance, we can accurately model the mass flow pressure relationship.

They assumed that the flow is steady and isothermal, the pressure drop associated with the inlet and outlet contraction/expansion can be ignored, and that the fluid pressure is solely a function of z, *i*.e. $P = P(z)$. Based on the assumptions, the constant viscosity momentum equation (Navier-Stokes equation) in the z-direction is

$$\rho u \frac{\partial u}{\partial z} + \rho v \frac{\partial u}{\partial y} \frac{L}{H} = -\frac{1}{\gamma} \frac{\partial p}{\partial z} + \frac{Ma_0}{\mathrm{Re}} \frac{L}{H} \frac{\partial^2 u}{\partial y^2}. \tag{2.85}$$

The non-dimensional slip velocity boundary condition on the wall is

$$\frac{u_w}{c} = \frac{2-F}{F} K_n \left. \frac{du/c}{dy/H} \right|_w. \tag{2.86}$$

After integrating the momentum equation above, the result is obtained as follows

$$u = -\frac{Re\, H}{8\gamma Ma_0 L} \frac{dP}{dx} \left(1 - 4y^2 + 4 \frac{2-F}{F} Kn \right). \tag{2.87}$$

By comparing the analytical solution with experimental results, the authors of [74] concluded that although the outlet Knudsen number, *Kn,* is within the flow regime usually characterized as transitional flow, the results of the slip model with a specular reflection coefficient F=1, seem to fit the data nicely.

In [71], Aubert and Colin proposed an analytical model of steady gaseous flow through rectangular micro-ducts with second-order boundary conditions. The influence of the second-order terms and the geometric parameters is analysed. It is shown that the mass flow rate is underestimated when the second-order terms are not taken into account and these terms become more significant when the cross section of the micro-duct tends to a square cross section.

The field equations are formulated by the following assumptions:

i. The flow is steady, laminar, and isothermal, and the gas is ideal.

ii. The transverse velocities are negligible compared with the axial velocity *W*.

iii. The duct is long: $h << L$ and $b << L$.

iv. The flow is locally fully developed, i.e. the density ρ and the pressure P are constant within a cross section. The axial distribution of the velocity is due to the axial pressure and density gradients.

Under these assumptions, the steady compressible gaseous flow in a cross section of the rectangular micro-duct is governed by the conservation equations for mass and momentum, namely

$$\frac{\partial W^*}{\partial z} = 0 \text{ and } \frac{\partial^2 W^*}{\partial y^{*2}} + a^2 \frac{\partial^2 W^*}{\partial x^{*2}} = -1,$$

where $x^* = \frac{x}{b}$, $y^* = \frac{y}{b}$, $W^* = \frac{W}{W_0}$, $W_0 = \frac{-h^2}{\mu}\frac{dP}{dz}$, $P = \rho RT$.

The boundary conditions are as follows

$$W^*\Big|_{y^*=1} = -\frac{2-\sigma_v}{\sigma_v} 2Kn \frac{\partial W^*}{\partial y^*}\bigg|_{y^*=1} - \frac{9}{4} Kn^2 \left(\frac{\partial^2 W^*}{\partial y^{*2}}\bigg|_{y^*=1} - 1 \right), \tag{2.88}$$

$$W^*\Big|_{x^*=1} = -\frac{2-\sigma_v}{\sigma_v} 2aKn \frac{\partial W^*}{\partial x^*}\bigg|_{x^*=1} - \frac{9}{4} Kn^2 \left(a^2 \frac{\partial^2 W^*}{\partial x^{*2}}\bigg|_{x^*=1} - 1 \right). \tag{2.89}$$

The solution is found in the form

$$W^*(x^*, y^*) = \sum_{i,j=1}^{\infty} A_{ij} N_{ij} \cos\left(\varphi_i \frac{x^*}{a} \right) \cos\left(\psi_j y^* \right) + \frac{9}{4} Kn^2, \tag{2.90}$$

where φ_i and ψ_j are respectively the solution of

$$1 - 2Kn \frac{(2-\sigma_v)}{\sigma_v} \psi_j \tan\psi_j - \frac{9}{4} Kn^2 \psi_j^2 = 0 \text{ and} \tag{2.91}$$

$$1 - 2Kn \frac{(2-\sigma_v)}{\sigma_v} \varphi_i \tan\frac{\varphi_i}{a} - \frac{9}{4} Kn^2 \varphi_i^2 = 0. \tag{2.92}$$

In order to determine the terms A_{ij}, the solution (2.90) is substituted into the momentum equation and yields

$$A_{ij}N_{ij} = \frac{1}{\varphi_i^2 + \psi_j^2}\left\{\frac{4\sin(\varphi_i/a)\sin\psi_j}{\varphi_i\psi_j} + \frac{9}{2}\frac{\sigma_v}{(2-\sigma_v)}Kn \times\left[\frac{\sin(\varphi_i/a)\cos\psi_j}{\varphi_i} + \frac{\cos(\varphi_i/a)\sin\psi_j}{\psi_j}\right]\right\} \times\left(\left[\frac{1}{a} + \frac{\cos(\varphi_i/a)\sin(\varphi_i/a)}{\varphi_i}\right]\left(1 + \frac{\sin\psi_j\cos\psi_j}{\psi_j}\right) + \frac{9}{4}\frac{\sigma_v}{(2-\sigma_v)}Kn \times\left\{\cos^2\psi_j\left[\frac{1}{a} + \frac{\cos(\varphi_i/a)\sin(\varphi_i/a)}{\varphi_i}\right] + \cos^2(\varphi_i/a)\left[1 + \frac{\sin\psi_j\cos\psi_j}{\psi_j}\right]\right\}\right)^{-1}.$$

To show the existence of the exact solution in [71], mass flow rate simulations from the rectangular second order model are compared with experimental data. There are two types of inaccuracy in the experiments: the inaccuracies in the mass flow measurement and the inaccuracies in the measurement of the section dimensions (depth and wide). Considering only an inaccuracy in the depth, good agreement is found between the experimental data of Shih et al. [111] and this second order model with σ_υ=1, for a channel with 1.145 μm in depth, 4.8% lower than the 1.2 μm depth given by the authors. Concerning the data of Arkilic [74] the agreement is found if the depth is changed from 1.33 to 1.31 μm, which corresponds to a difference of 1.5%. So, a decrease of the depth of 0.02 μm has the same importance as an increase for σ_υ of 10%. Although there is a problem in comparing the different models with experimental data which lies in the difficulty in determining σ_υ independently from the model itself, a good correlation between a first order model or a second order model and experiments can be obtained by fitting the coefficient σ_υ.

In the existing exact solutions for Poiseuille flow through ducts, as Couette flow, the Poiseuille number makes a lot more sense in laminar tube flow, $P0 = C_f \,\mathrm{Re}_D = \dfrac{2\tau_w D}{\mu \bar{u}} = 16$. This classic laminar flow solution is in good agreement with experiment.

2.5.3 Integral Transform Technique

Morini and Spiga (1998) considered slip flow in Rectangular micro-channels. The Navier Stokes equations reduce to equation (2.77) with $\dfrac{\partial p}{\partial z} = -\mu$. This equation, combined with the boundary conditions, can be solved by the integral transform method, resorting to the following kernel:

$$Z_{n,m}(x,y) = N_{n,m}\left(\beta_m \cos\beta_m x + \frac{\sin\beta_m x}{Kn}\right)\left(\delta_n \cos\delta_n y + \frac{\sin\delta_m y}{Kn}\right), \qquad (2.93)$$

where the eigenvalues β_n and δ_n are obtained by the transcendental equation

$$\tan\beta_n L_x = \frac{2\beta_m Kn}{Kn^2\beta_m^2 - 1}, \quad \tan\delta_n L_y = \frac{2\delta_n Kn}{Kn^2\delta_n^2 - 1}.$$

The inversion formula provides the velocity distribution

$$v(x,y) = \sum_{n=1}^{\infty}\sum_{m=1}^{\infty}\frac{N_{n,n}^2 A_{n,m}}{\beta_m^2 + \delta_n^2}\left(\beta_m \cos\beta_m x + \frac{\sin\beta_m x}{Kn}\right)\left(\delta_n \cos\delta_n y + \frac{\sin\delta_n y}{Kn}\right) \qquad (2.94)$$

where

$$N_{n,m}(x,y) = 2\left(\frac{Kn^2\beta_m^2 + 1}{Kn^2}\left(L_x + 2Kn\right)\frac{Kn^2\delta_n^2 + 1}{Kn^2}\left(L_y + 2Kn\right)\right)^{-1/2}, \qquad (2.95)$$

$$A_{n,m} = \left(\sin\beta_m L_x + \frac{1-\cos\beta_m L_x}{Kn\beta_m}\right)\left(\sin\delta_n L_y + \frac{1-\cos\delta_n L_y}{Kn\delta_n}\right). \qquad (2.96)$$

The results show that for different aspect ratios ($\beta = 0.25$ and $\beta = 1$) and Kn=0.1, in square duct, the fluid velocity experiences a slow and gradual increase from the walls to the center; in slip conditions the jump at the wall is well evident and the velocity distribution is more uniform over the cross section. In rectangular duct, there is a strong increase near the walls and an extended central core with high velocity. As the Knudsen number increases, the velocity profile becomes more flattered. In circular duct, the shear stress decreases rapidly as the Knudsen number increases, as expected since the slug flow condition is well approximated when the Knudsen number is large. It is noted that the corner stress increases as the Knudsen number increases up to 0.1, then decreases.

2.6 Numerical Studies in the Field

In general, it is very difficult to solve a fluid dynamics problem analytically to yield exact solutions. Thus one usually need to solve a flow problem numerically. The subject which concerns the numerical solutions of fluid dynamics problems is computational fluid dynamics.

Various numerical methods such as the finite difference method, the finite element method and the boundary element method have been used for solving flow problems approximately. Among these methods, the finite element method is the most widely used method.

Solving a fluid dynamic problem using the finite element method usually involves the following steps [107]:

1. Variational formulation to transform the partial differential equations to integral equations;

2. Numerical approximation of the variational problem to transform the integral equations to algebraic or ordinary differential equations;

3. Solve the algebraic or ordinary differential equations by iterations and time stepping.

As an example, In [100], Arulanandam and Li studied the liquid transport in rectangular micro-channels by electro osmotic pumping. Consider a rectangular micro-channel of width $2W$, height $2H$ and length L. There are two models which can be applied, electrical double layer (EDL) and velocity distribution in rectangular micro-channels. The first model leads to the non-dimensional Poisson Boltzmann equation:

$$\frac{\partial^2 \psi^*}{\partial y^{*2}} + \frac{\partial^2 \psi^*}{\partial z^{*2}} = \left(\kappa D_h\right)^2 \sinh\left(\psi^*\right), \tag{2.97}$$

where κ is the Debye-Huckle parameter and D_h is the hydraulic diameter.

This equation is a non-linear two-dimensional partial differential equation that must be solved numerically subject to the non-dimensional boundary condition given by

$$\frac{\partial \psi^*}{\partial y^*} = 0 = \frac{\partial \psi^*}{\partial z^*} \text{ on } y^* = 0 = z^* , \tag{2.98}$$

$$\psi^* = \zeta^* \text{ on } y^* = \frac{W}{D_h} = z^* .$$

A numerical finite difference scheme is used in [100] to discretise the governing differential equation, and the resulting system of algebraic equations is solved using the Gauss Seidel iterative technique with successive over relaxation employed to improve the convergence time. Since the electrical potential field in the EDL varies greatly within a small distance of the channel walls, variable grid

spacing was employed to ensure that as the surface was approached, the grid spacing was refined enough to capture the sharp gradient. Once the electrical potential distribution $\psi^*(y^*, z^*)$ has been found, the net charge density at any point in the channel can be found by using $\rho_e = -2n_\infty ze \sinh\left(-\frac{ze}{k_b T}\psi\right)$.

For the second model, by assuming that the flow is steady, two dimensional and fully developed, the velocity components can be described by*:* $u = u(y,z)$, $\boldsymbol{v}$=0 and $\boldsymbol{w} = 0$. The Navier-Stokes equations in dimensionless form with electrical force per unit volume $F_x = \rho_e E_x$ reduce to

$$\frac{\partial^2 u^*}{\partial y^{*2}} + \frac{\partial^2 u^*}{\partial z^{*2}} = M E_x^* \sinh\left(\psi^*\right), \tag{2.99}$$

where $u^* = \frac{u}{U}$, $E_x^* = \frac{E_x L}{\zeta}$ and M is a new dimensionless group, which is a ratio of the electrical to frictional forces per unit volume, given by $M = \frac{2n_\infty ze\zeta D_h^2}{\mu UL}$.

This equation is a 2D linear partial differential equation that can be solved numerically using a finite difference scheme, once a solution for $\psi^*(y^*, z^*)$ has been obtained. The performance of an electro-osmotic pumping system can be characterized using the volumetric flow rate

$$Q_{vol} = 4\int_0^H \int_0^W u(y,z)\,dy\,dz\,, \tag{2.100}$$

and the average velocity

$$\overline{u} = \frac{Q_{vol}}{A} = \frac{Q_{vol}}{4HW}\,. \tag{2.101}$$

The results of the study show the significance of geometry effects on the electro-osmotic force, namely the EOF is enhanced as the aspect ratio of the channel varies away from 1:1. It was also found that the increase in D_h leads to the increase in the volumetric flow rate but has little impact on the average velocity. Variations in zeta potential and concentration affect the flow rates significantly due to their impact on the formation of the double layer. Finally, while the volumetric flow rate was shown to vary linearly with the applied voltage field, there are upper limits to the electrical field strength because of the potential increase in the temperature of the fluid which has not been included in this model.

Chapter 3

Unsteady Slip Flow in Rectangular Microchannels

3.1 General

In recent years, one of the important scientific research focuses worldwide has been on the study of behavior of materials at micro and nanoscales [22, 24]. Advancement from the research community in this area have led to the development of many biological and engineering devices and systems which involve fluid flow through micro-channels, referred to as microflows [1, 6, 5, 7, 22, 24]. Typical examples include fuel cell devices, drug delivery systems [16], biological sensing and energy conversion devices [11]. As the behavior of fluid flow in these systems determines the functional characteristics of the systems, the study of microflows is attracting more and more attention from the science and engineering communities in order to derive a better understanding of the mechanism of microflows and consequently better devices and systems [4, 22, 24].

The governing field equations for the flow of incompressible Newtonian fluids are the incompressible continuity equation, the Navier-Stokes equations, and a set of boundary conditions. Traditionally the no-slip boundary condition is used, namely the fluid velocity relative to the solid is assumed to be zero on the fluid-solid interface [29]. However, evidence of slip of a fluid on a solid surface have been reported [25].

Recent experiments in micrometer scale and molecular dynamic simulations have shown that the flow of fluids in microsystems is granular and slip can occur on the fluid-solid interface [3, 4, 31, 40, 45]. Hence for the study of microflow, it is important to take into account the boundary slip of fluids on the fluid solid interfaces.

Over the last couple of decades, many investigations have been made to study various flow problems of Newtonian and non-Newtonian fluids with the no slip boundary condition or a slip boundary condition [5, 8, 10, 20, 21, 24, 27, 28, 43, 44]. Exact and numerical solutions to many flow problems of Newtonian fluids under the no-slip assumption have been obtained and are available in the literature [29, 36-38], but very few exact solutions for the slip case are available in the literature. Steady-state slip solutions for the transient flow through circular microtubes and circular micro annuals have been derived and discussed in the papers [4, 35, 39].

For micro-channels with rectangular cross section, a no-slip solution has been obtained [52, 74, 75, 83, 97]. For the slip case steady state solution has also been obtained [37, 71, 77, 80, 82]. However, so far no exact solution has been derived for the transient flow of fluids through rectangular channel under pulsatile pressure. As many micro-systems and devices have mico-channels of rectangular cross section, it is important to derive exact solutions for the behavior of transient flow through rectangular micro channels with slip boundary.

Motivated by the previous work, we study the transient flow of an incompressible Newtonian liquid through a rectangular micro-channel with a slip boundary. The rest

of the study is organized as follows. In the following section, we first define the problem and then present its mathematical formulation. In section 3.3, we solve the underlying boundary value problem to derive the exact solution for the velocity field and show that the solution includes some existing known solutions as special cases. In section 3.4, we interpret the exact solutions for some special cases. In section 3.5, an analysis is carried out to study the influence of the slip parameter on the flow behavior. Finally, a conclusion is given in section 3.6

3.2 Problem Description and Mathematical Formulation

Consider the transient flow of incompressible Newtonian liquid through a rectangular channel of cross-section dimension $a \times b$ with the z-axes being in the axial direction as shown in figure 3.1. The field equations governing the flow include the continuity equation and the Navier–Stokes equations. As the flow is symmetric about the xz-plane and the yz-plane and fully developed, there is no cross-sectional flow and the velocity components in the x and y directions vanish, namely $\mathbf{v} = \left(v_x, v_y, v_z\right) = (0, 0, u)$

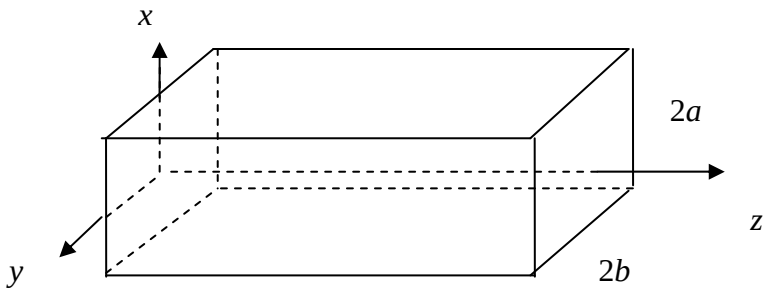

Figure 3.1: The flow channel and the coordinate system used

Thus, from the continuity equation (2.21) and the Navier-Stokes equation (2.31), u must satisfy the following equation:

$$\frac{\mu}{\rho}\left(\frac{\partial^2 u}{\partial x^2}+\frac{\partial^2 u}{\partial y^2}\right)-\frac{\partial u}{\partial t}=\frac{1}{\rho}\frac{\partial p}{\partial z}. \tag{3.1}$$

Since a wide range of functions can be expressed in terms of Fourier series, in this work, we consider the fluid flow driven by the pressure field with a pressure gradient $\frac{\partial p}{\partial z}$ that can be expressed by the Fourier series

$$\frac{\partial p}{\partial z}=a_0+\sum_{n=1}^{\infty}\left[a_n\cos\left(n\omega t\right)+b_n\sin\left(n\omega t\right)\right]. \tag{3.2}$$

To completely define the problem, the field equations must be supplemented by the boundary condition. In this work, we use the Navier slip boundary condition. That is, on the solid fluid interface $x=\pm a$ and $y=\pm b$, the axial fluid velocity, relative to the solid surface, is proportional to the shear stress on the interface. Let the unit outward normal vector of the surface S of the fluid be $\mathbf{n}=\left(n_1,n_2,n_3\right)$, and the positive tangential direction be $\mathbf{t}=\left(t_1,t_2,t_3\right)$. Also let the fluid velocity in the tangential direction be u_t, and the velocity of the solid surface in the tangential direction be u_{st}. As shown in [4], the Navier –type boundary condition for Newtonian fluids can be written as

$$\left(u_i-u_{st}\right)t_i=-\frac{\ell\left(\sigma_{ji}n_j t_i\right)}{\mu}. \tag{3.3}$$

The negative sign in the above equations is to indicate that the direction of the surface traction force exerted on the fluid by the solid surface is opposite to the tangential

velocity of fluid relative to the solid surface. Now for our problem in the (x, y, z) system, $\mathbf{v} = (0, 0, u)$, $\mathbf{v}_s = (0, 0, 0)$. For the surface $x = a$, $\mathbf{n} = (1, 0, 0)$ and $\mathbf{t} = (0, 0, 1)$, and so $u_t - u_{st} t_i = v_i \; t_i = u$ and $f_t = \sigma_{xz} = \mu \dfrac{\partial u}{\partial x}$ and consequently (3.3) for the surface $x = a$ takes the following form:

$$u(a, y, t) = -\ell \frac{\partial u}{\partial x}(a, y, t). \tag{3.4}$$

On the surface $x = -a$, $\mathbf{n} = (-1, 0, 0)$ and $\mathbf{t} = (0, 0, 1)$, and so $u_t - u_{st} t_i = v_i \; t_i = u$ and $f_t = -\sigma_{xz} = -\mu \dfrac{\partial u}{\partial x}$ and consequently (3.3) on the surface takes the following form:

$$u(-a, y, t) = \ell \frac{\partial u}{\partial x}(-a, y, t) \; . \tag{3.5}$$

Similarly, the boundary condition on the surface $y = \pm b$ are

$$u(x, \pm b, t) = \mp \ell \frac{\partial u}{\partial y}(x, \pm b, t). \tag{3.6}$$

It should be addressed here that for $\ell = 0$, conditions (3.4) – (3.6) reduces to the no-slip boundary condition; while, for $\ell \to \infty$, equations (3.4) and (3.5) give the surface traction conditions for perfectly smooth surfaces, i.e, $\sigma_{xz}(\pm a, y, t) = \sigma_{yz}(x, \pm b, t) = 0$.

3.3 Exact Solutions for the Transient Velocity and Stress Field

To solve equation (3.1), first we use complex number to express the above Fourier series by exponential functions, namely

$$\frac{\partial p}{\partial z} = \mathrm{Re}\left(\sum_{n=0}^{\infty} c_n e^{in\omega t} \right), \tag{3.7}$$

where $c_n = a_n - b_n i$ and $e^{in\omega t} = \cos(n\omega t) + i\sin(n\omega t)$.

From the linear property of equation (3.1), we have $u = \sum_{n=0}^{\infty} \mathrm{Re}(u_n)$, where u_n is defined by

$$\frac{\mu}{\rho}\left(\frac{\partial^2 u_n}{\partial x^2} + \frac{\partial^2 u_n}{\partial y^2} \right) - \frac{\partial u_n}{\partial t} = \frac{c_n}{\rho} e^{in\omega t}. \tag{3.8}$$

Let

$$u_n = f_n(x, y)\, e^{in\omega t}, \tag{3.9}$$

then we have

$$\frac{\mu}{\rho}\left(\frac{\partial^2 f_n}{\partial x^2} + \frac{\partial^2 f_n}{\partial y^2} \right) - in\omega f_n = \frac{c_n}{\rho} \quad . \tag{3.10}$$

For $n \geq 1$, it can be proved that the above governing equation for $f_n(x, y)$ admits solution of the form

$$f_n = U_n(x, y) + V_n(x, y) - \frac{c_n}{in\rho\omega}, \tag{3.11}$$

with $U_n(x,y)$ and $V_n(x,y)$ being defined respectively by the following two boundary value problems:

$$(BVP1)\begin{cases} \dfrac{\partial^2 U_n}{\partial x^2}+\dfrac{\partial^2 U_n}{\partial y^2}-i\dfrac{n\omega\rho}{\mu}U_n=0\,, & (3.12)\\ \dfrac{\partial U_n}{\partial x}(0,y)=0,\quad \dfrac{\partial U_n}{\partial y}(x,0)=0\,, & (3.13)\\ U_n(a,y)+\ell\dfrac{\partial U_n}{\partial x}(a,y)=\dfrac{c_n}{in\omega\rho},\quad U_n(x,b)+\ell\dfrac{\partial U_n}{\partial y}(x,b)=0, & (3.14)\end{cases}$$

$$(BVP2)\begin{cases} \dfrac{\partial^2 V_n}{\partial x^2}+\dfrac{\partial^2 V_n}{\partial y^2}-i\dfrac{n\omega\rho}{\mu}V_n=0\,, & (3.15)\\ \dfrac{\partial V_n}{\partial x}(0,y)=0,\quad \dfrac{\partial V_n}{\partial y}(x,0)=0, & (3.16)\\ V_n(a,y)+\ell\dfrac{\partial V_n}{\partial x}(a,y)=0,\quad V_n(x,b)+\ell\dfrac{\partial V_n}{\partial y}(x,b)=\dfrac{c_n}{in\omega\rho}. & (3.17)\end{cases}$$

Thus, the problem becomes simple and the remaining work for finding f_n is to solve the two BVPs.

We first solve (BVP1) to obtain $U_n(x,y)$ by the separation of variables. For this purpose, let

$$U_n = X(x)\,Y(y)\,. \tag{3.18}$$

Then from (3.12) and the homogeneous boundary conditions in (3.13) and (3.14), we have

$$Y''+\lambda Y=0,\quad Y'(0)=0,\quad Y(b)+\ell\,Y'(b)=0\,, \tag{3.19}$$

$$X''-\left(i\frac{n\rho\omega}{\mu}+\lambda\right)X=0,\quad X'(0)=0\,. \tag{3.20}$$

It can be proved that non-trivial solutions exist only for $\lambda = \upsilon^2 > 0$. From the ordinary differential equations, we have

$$Y = C_1 \cos\left(\sqrt{\lambda}\, y\right) + C_2 \sin\left(\sqrt{\lambda}\, y\right), \tag{3.21}$$

$$X = D_1 \cosh\left(\gamma x\right) + D_2 \sinh\left(\gamma x\right), \tag{3.22}$$

where $\gamma = \sqrt{\lambda + i\dfrac{n\rho\omega}{\mu}}$.

The boundary conditions $(3.19)_2$ and $(3.20)_2$ require that $C_2 = D_2 = 0$; while the boundary condition $(3.19)_3$ implies

$$\cot\left(\sqrt{\lambda}\, b\right) = \ell\sqrt{\lambda} \quad \text{or} \quad \cot\left(b\upsilon\right) = \ell\upsilon \ . \tag{3.23}$$

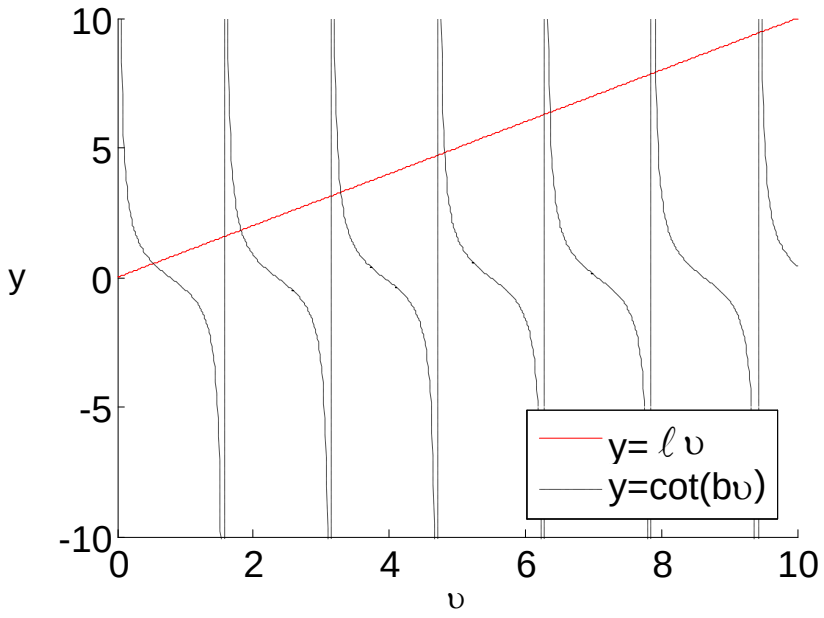

Figure 3.2: Diagram showing graphic solution of eq (3.23)

As shown graphically in figure 3.2, equation (3.23) has infinite number of solutions $\upsilon_1, \upsilon_2, \upsilon_3, \ldots$ being the value of the intersections of the graphs $y = \ell\upsilon$ and $y = \cot(b\upsilon)$. Consequently there exist an infinite number of corresponding eigenvalues and eigenfunctions as follows

$$\lambda_m = \upsilon_m^2, \quad \Phi_m = \cos\left(\sqrt{\lambda_m}\, y\right), \quad m = 1, 2, 3.\cdots. \tag{3.24}$$

Thus, the solution of (BVP1) can be written as

$$U_n = \sum_{m=1}^{\infty} A_{nm} \cosh\left(\gamma_{nm}\, x\right) \cos\left(\upsilon_m\, y\right), \tag{3.25}$$

where $\gamma_{nm} = \sqrt{\upsilon_m^2 + i\dfrac{n\rho\omega}{\mu}}$. (3.26)

To meet the nonhomogeneous boundary condition for U_n, i.e $(3.14)_1$, it requires

$$\sum_{m=1}^{\infty} \left[\cosh\left(\gamma_{nm}\, a\right) + \ell\, \gamma_{nm} \sinh\left(\gamma_{nm}\, a\right)\right] A_{nm} \cos\left(\upsilon_m\, y\right) = -i\frac{c_n}{n\rho\omega}\ . \tag{3.27}$$

The eigen functions $\Phi_m = \cos\left(\upsilon_m\, y\right), \quad (m = 1, 2, 3.\cdots)$ are orthogonal on [0,*b*] with

$$\begin{aligned} &\int_0^b \Phi_m \Phi_n\, dy = 0 \quad for \quad n \neq m \quad \text{and} \\ &M_{mm} = \int_0^b \Phi_m \Phi_m\, dy = \int_0^b \cos^2\left(\upsilon_m\, y\right) dy = \frac{2b\upsilon_m + \sin\left(2b\upsilon_m\right)}{4\upsilon_m}. \end{aligned} \tag{3.28}$$

To show $\{\Phi_n\}$ are orthogonal set, let $Y_n = \Phi_m = \cos\left(\upsilon_n y\right)$ and $Y_m = \Phi_m = \cos\left(\upsilon_m y\right)$.

As Y_m and Y_n are solutions of (3.19), we have

$$Y_n'' + \lambda Y_n = 0 \tag{3.29}$$

$$Y_m'' + \lambda Y_m = 0 \tag{3.30}$$

Multiplying (3.29) by Y_m and (3.30) by Y_n then adding them together yield

$$Y_m Y_n'' + \lambda_n Y_m Y_n - Y_n Y_m'' - \lambda_m Y_n Y_m = 0,$$

which gives

$$\begin{aligned}
(\lambda_n - \lambda_m)\int_0^b Y_n Y_m dy &= \int_0^b Y_n Y_m'' dy - \int_0^b Y_m Y_n'' dy \\
&= Y_n(b)Y_m'(b) - Y_n(0)Y_m'(0) - \int_0^b Y_m' dY_n \\
&\quad - Y_m(b)Y_n'(b) + Y_m(0)Y_n'(0) + \int_0^b Y_n' dY_m \\
&= Y_n(b)Y_m'(b) - Y_m(b)Y_n'(b) \\
&= Y_n(b)\left(-\frac{1}{\ell}Y_m(b)\right) - Y_m(b)\left(-\frac{1}{\ell}Y_n(b)\right) \\
&= -\frac{1}{\ell}\left[Y_n(b)Y_m(b) - Y_m(b)Y_n(b)\right] \\
&= 0.
\end{aligned}$$

Hence , for $\lambda_n \neq \lambda_m$, $\int_0^b Y_n Y_m dy = \int_0^b \Phi_n(y)\Phi_m(y)dy = 0$.

Thus, the coefficients of A_{nm} can be determined by

$$\begin{aligned}
A_{nm} &= -i\frac{c_n}{n\rho\omega M_{mm}\left[\cosh(\gamma_{nm}a) + \ell\gamma_{nm}\sinh(\gamma_{nm}a)\right]}\int_0^b \cos(\upsilon_m y)dy \\
&= -i\frac{4c_n\sin(b\upsilon_m)}{n\rho\omega\left[2b\upsilon_m + \sin(2b\upsilon_m)\right]\left[\cosh(a\gamma_{nm}) + \ell\gamma_{nm}\sinh(a\gamma_{nm})\right]}.
\end{aligned} \tag{3.31}$$

Similarly, the solution V_n of the (BVP2) is

$$V_n = \sum_{m=1}^{\infty} B_{nm}\cosh(\bar{\gamma}_{nm}y)\cos(\bar{\upsilon}_m x), \tag{3.32}$$

where $\bar{\upsilon}_m$ are the roots of the equation

$$\cot\left(a\bar{\upsilon}\right) = \ell\bar{\upsilon}, \tag{3.33}$$

and

$$\bar{\gamma}_{nm} = \sqrt{\bar{\upsilon}_m^2 + i\frac{n\rho\omega}{\mu}}, \tag{3.34}$$

$$\bar{M}_{mm} = \int_0^a \cos^2\left(\bar{\upsilon}_m\, x\right) dx = \frac{2a\bar{\upsilon}_m + \sin\left(2a\bar{\upsilon}_m\right)}{4\bar{\upsilon}_m}, \tag{3.35}$$

$$\begin{aligned} B_{nm} &= -i\frac{c_n}{n\rho\omega\bar{M}_{mm}\left[\cosh\left(\bar{\gamma}_{nm}b\right) + \ell\,\bar{\gamma}_{nm}\sinh\left(\bar{\gamma}_{nm}\,b\right)\right]}\int_0^a \cos\left(\bar{\upsilon}_m\, x\right) dx \\ &= -i\frac{4c_n\sin\left(a\,\bar{\upsilon}_m\right)}{n\rho\omega\left[2a\bar{\upsilon}_m + \sin\left(2a\bar{\upsilon}_m\right)\right]\left[\cosh\left(b\bar{\gamma}_{nm}\right) + \ell\,\bar{\gamma}_{nm}\sinh\left(b\bar{\gamma}_{nm}\right)\right]}. \end{aligned} \tag{3.36}$$

Substituting (3.25) and (3.32) into (3.11) yields the solution

$$\begin{aligned} u_n\left(x,y,t\right) = e^{in\omega t}\Bigg\{ & i\frac{c_n}{n\rho\omega} + \sum_{m=1}^{\infty}\Big[A_{nm}\cosh\left(\gamma_{nm}x\right)\cos\left(\upsilon_m\, y\right) \\ & + B_{nm}\cosh\left(\bar{\gamma}_{nm}\, y\right)\cos\left(\bar{\upsilon}_m\, x\right)\Big]\Bigg\}. \end{aligned} \tag{3.37}$$

For $n = 0$, proceeding as for finding $u_n\left(x,y,t\right)$, we obtain

$$\begin{aligned} u_0\left(x,y,t\right) = \frac{c_0}{4\mu}\left(x^2 + y^2\right) + \sum_{m=1}^{\alpha}\Big[& A_{0m}\cosh\left(\gamma_{0m}x\right)\cos\left(\upsilon_m\, y\right) \\ & + B_{0m}\cosh\left(\bar{\gamma}_{0m}\, y\right)\cos\left(\bar{\upsilon}_m\, x\right)\Big], \end{aligned} \tag{3.38}$$

where γ_{0m} and $\bar{\gamma}_{0m}$ are as defined in (3.28) and (3.34) with $n = 0$, i.e., $\gamma_{0m} = \upsilon_m$ and $\bar{\gamma}_{0m} = \bar{\upsilon}_m$; A_{0m} and B_{0m} are determined as follows.

$$A_{0m} = \frac{-c_0}{4\mu M_{mm}\left[\cosh\left(a\upsilon_m\right)+\ell\upsilon_m\sinh\left(a\upsilon_m\right)\right]}\int_0^b\left(a^2+y^2+2a\ell\right)\cos\left(\upsilon_m y\right)dy$$

$$= \frac{-c_0\left[\left(a^2+2a\ell\right)\sin\left(b\upsilon_m\right)+b^2\sin\left(b\upsilon_m\right)+\dfrac{2}{\upsilon_m}\left(b\cos\left(b\upsilon_m\right)-\dfrac{\sin\left(b\upsilon_m\right)}{\upsilon_m}\right)\right]}{\mu\left[2b\upsilon_m+\sin\left(2b\upsilon_m\right)\right]\left[\cosh\left(a\upsilon_m\right)+\ell\upsilon_m\sinh\left(a\upsilon_m\right)\right]}, \tag{3.39}$$

$$B_{0m} = \frac{-c_0}{4\mu \bar{M}_{mm}\left[\cosh\left(b\bar{\upsilon}_m\right)+\ell\bar{\upsilon}_m\sinh\left(b\bar{\upsilon}_m\right)\right]}\int_0^a\left(x^2+b^2+2b\ell\right)\cos\left(\bar{\upsilon}_m x\right)dx$$

$$= \frac{-c_0\left[\left(b^2+2b\ell\right)\sin\left(a\bar{\upsilon}_m\right)+a^2\sin\left(a\bar{\upsilon}_m\right)+\dfrac{2}{\bar{\upsilon}_m}\left(a\cos\left(a\bar{\upsilon}_m\right)-\dfrac{\sin\left(a\bar{\upsilon}_m\right)}{\bar{\upsilon}_m}\right)\right]}{\mu\left[2a\bar{\upsilon}_m+\sin\left(2a\bar{\upsilon}_m\right)\right]\left[\cosh\left(b\bar{\upsilon}_m\right)+\ell\bar{\upsilon}_m\sinh\left(b\bar{\upsilon}_m\right)\right]}. \tag{3.40}$$

Hence collecting all solutions of the subproblems, we have

$$u\left(x,y,t\right) = \frac{a_0}{4\mu}\left(x^2+y^2\right)+\sum_{n=1}^{\infty}\frac{-a_n\sin\left(n\omega t\right)+b_n\cos\left(n\omega t\right)}{n\omega\rho}$$
$$+\sum_{n=0}^{\infty}\mathrm{Re}\left\{e^{in\omega t}\sum_{m=1}^{\infty}\left[A_{nm}\cosh\left(\gamma_{nm}x\right)\cos\left(\upsilon_m y\right)+B_{nm}\cosh\left(\bar{\gamma}_{nm}y\right)\cos\left(\bar{\upsilon}_m x\right)\right]\right\}, \tag{3.41}$$

where υ_m and $\bar{\upsilon}_m$ are determined respectively by $(3.23)_2$ and (3.33); γ_{nm} and $\bar{\gamma}_{nm}$ are defined by (3.26) and (3.34) respectively, A_{0m} and B_{0m} are defined by (3.39) and (3.40), and A_{nm} and B_{nm} $\left(m,n\geq 1\right)$ are defined by (3.31) and (3.36) respectively.

Now we determine the exact solutions of the flow rate and the stress field. From the axial velocity solution (3.41), the flow rate can be determined by

$$Q(t) = 4\int_0^b\int_0^a u(x,y,t)\,dx\,dy = Q_0+\sum_{n=1}^{\infty}Q_n\ , \tag{3.42}$$

where Q_0 and Q_n are respectively, the flow rate corresponding to the constant component and the *n*th harmonic component of the pressure gradient and

$$Q_0 = \frac{a_0}{3\mu}\left[a^3 b + a b^3\right] + 4\,\mathrm{Re}\sum_{m=1}^{\infty}\left[\frac{A_{0m}}{\gamma_{0m}\upsilon_m}\sinh\left(a\gamma_{0m}\right)\sin\left(b\upsilon_m\right) + \frac{B_{0m}}{\overline{\gamma}_{0m}\overline{\upsilon}_m}\sinh\left(b\overline{\gamma}_{0m}\right)\sin\left(a\overline{\upsilon}_m\right)\right], \tag{3.43}$$

$$Q_n = \frac{4ab\left[-a_n\sin\left(n\omega t\right) + b_n\cos\left(n\omega t\right)\right]}{n\omega\rho} + 4\,\mathrm{Re}\left\{e^{in\omega t}\sum_{m=1}^{\infty}\left[\frac{A_{nm}}{\gamma_{nm}\upsilon_m}\sinh\left(a\gamma_{nm}\right)\sin\left(b\upsilon_m\right) + \frac{B_{nm}}{\overline{\gamma}_{nm}\overline{\upsilon}_m}\sinh\left(b\overline{\gamma}_{nm}\right)\sin\left(a\overline{\upsilon}_m\right)\right]\right\}. \tag{3.44}$$

The stress in the fluid is related to the velocity field by the following constitutive equations:

$$\sigma = -p\mathbf{I} + 2\mu\mathbf{d}\ , \tag{3.45}$$

while the rate of the deformation tensor is related to the velocity vector by

$$\mathbf{d} = \frac{1}{2}\left(\nabla v + \left(\nabla v\right)^T\right)\ , \tag{3.46}$$

where $\sigma \equiv \left(\sigma_{ij}\right)$ and $\mathbf{d} = \left(d_{ij}\right)$ denote respectively, the second order stress tensor and the rate of the deformation tensor, **I** is an identity matrix. As **v** = (0, 0, *u*(*x*,*y*,*t*)), we have

$$\mathbf{d} = \frac{1}{2}\begin{pmatrix} 0 & 0 & \partial u/\partial x \\ 0 & 0 & \partial u/\partial y \\ \partial u/\partial x & \partial u/\partial y & 0 \end{pmatrix}. \tag{3.47}$$

From the above formula and using (3.19), we obtain $d_{xx} = d_{yy} = d_{zz} = d_{xy} = 0$ and

$$d_{xz} = \frac{a_0}{2\mu} x + \frac{1}{2} \sum_{n=0}^{\infty} \mathrm{Re}\left\{ e^{in\omega t} \sum_{m=1}^{\infty} \left[A_{nm} \gamma_{nm} \sinh\left(\gamma_{nm} x \right) \cos\left(\upsilon_m y \right) \right.\right. \\ \left.\left. - B_{nm} \bar{\upsilon}_m \cosh\left(\bar{\gamma}_{nm} y \right) \sin\left(\bar{\upsilon}_m x \right) \right] \right\}, \tag{3.48}$$

$$d_{yz} = \frac{a_0}{2\mu} y + \frac{1}{2} \sum_{n=0}^{\infty} \mathrm{Re}\left\{ e^{in\omega t} \sum_{m=1}^{\infty} \left[-A_{nm} \upsilon_m \cosh\left(\gamma_{nm} x \right) \sin\left(\upsilon_m y \right) \right.\right. \\ \left.\left. + B_{nm} \bar{\gamma}_{nm} \sinh\left(\bar{\gamma}_{nm} y \right) \cos\left(\bar{\upsilon}_m x \right) \right] \right\}. \tag{3.49}$$

Hence from the constitutive equation (3.43), we obtain

$$\sigma_{xx} = \sigma_{yy} = \sigma_{zz} = -p = q(t)z + p_0(t),\ \sigma_{xy} = 0,\ \sigma_{xz} = 2\mu d_{xz},\ \sigma_{yz} = 2\mu d_{yz}, \tag{3.50}$$

where $q(t)$ is the pressure gradient $\frac{\partial p}{\partial z}$ while $p_0(t)$ is arbitrary and can be chosen to meet certain pressure condition.

3.4 Interpretation of Solutions for some Special Cases

With the exact solutions obtained in the previous sections, the solutions for a general pressure field given by (3.2) is the superposition of the solution due to the constant pressure gradient and the solutions due to the sine and cosine wave form pressure gradients. Without loss of generality, we consider here two different cases of driving pressure fields in this discussion. The first case is for a pressure field with a constant pressure gradient, while the second one is for pressure field with a sine wave form pressure gradient. For convenience in the discussion, we introduce the following dimensionless variables:

$$x^* = \frac{x}{a};\ y^* = \frac{y}{b},\ t^* = \frac{\omega t}{2\pi},\ \varepsilon = \frac{b}{a}. \tag{3.51}$$

3.4.1 Case 1: $\frac{\partial p}{\partial z} = a_0$

For this case, $c_0 = a_0$ and $c_n = 0$ for all $n \geq 1$. The constant pressure gradient means that the pressure gradient does not depend on time. The shear stress in the fluid is independent of the slip length ℓ. From (3.41), (3.43), (3.49) and (3.50), we obtain the following normalized velocity, normalized flow rate and shear stressed

$$u^*\left(x^*, y^*\right) = \frac{4\mu}{a_0 a^2} u = x^{*2} + \left(\varepsilon y^*\right)^2 + \frac{4\mu}{a_0 a^2} \operatorname{Re} \sum_{m=1}^{\infty} \left[A_{0m} \cosh\left(a \upsilon_m x^*\right) \cos\left(b \upsilon_m y^*\right) + B_{0m} \cosh\left(b \bar{\upsilon}_m y^*\right) \cos\left(a \bar{\upsilon}_m x^*\right) \right] \tag{3.52}$$

$$Q_0^* = \frac{3\mu}{a_0 \varepsilon a^4} Q_0 = 1 + \varepsilon^2 + \frac{12\mu}{a_0 \varepsilon a^4} \operatorname{Re} \sum_{m=1}^{\infty} \left[\frac{A_{0m}}{\upsilon_m^2} \sinh\left(a \upsilon_m\right) \sin\left(b \upsilon_m\right) + \frac{B_{0m}}{\bar{\upsilon}_m^2} \sinh\left(b \bar{\upsilon}_m\right) \sin\left(a \bar{\upsilon}_m\right) \right] \tag{3.53}$$

$$\sigma_{xz}^* = \frac{1}{a_0 a} \sigma_{xz} = x^* + \frac{\mu}{a_0 a} \operatorname{Re} \sum_{m=1}^{\infty} \left[A_{0m} \upsilon_m \sinh\left(\upsilon_m a x^*\right) \cos\left(b \upsilon_m y^*\right) - B_{0m} \bar{\upsilon}_m \cosh\left(\bar{\upsilon}_m b y^*\right) \sin\left(a \bar{\upsilon}_m x^*\right) \right] \tag{3.54}$$

$$\sigma_{yz}^* = \frac{1}{a_0 a} \sigma_{yz} = \varepsilon y^* + \frac{\mu}{a_0 a} \operatorname{Re} \sum_{m=1}^{\infty} \left[-A_{0m} \upsilon_m \cosh\left(\upsilon_m a x^*\right) \sin\left(b \upsilon_m y^*\right) + B_{0m} \bar{\upsilon}_m \sinh\left(b \bar{\upsilon}_m y^*\right) \cos\left(a \bar{\upsilon}_m x^*\right) \right] \tag{3.55}$$

As pressure gradient does not depend on time, the normalized velocity, normalized flow rate and shear stress are influenced by slip length ℓ only, which is implicitly contained in υ_m and $\bar{\upsilon}_m$.

3.4.2 Case 2: $\frac{\partial p}{\partial z} = b_1 \sin(\omega t)$

The pressure gradient is sinusoidal with amplitude b_1. For this case $a_0 = 0, c_1 = -b_1 i,$ $c_n = 0$ for $\forall n \geq 2$.

From (3.41), we have

$$u^*(x^*, y^*) = \frac{\rho\omega}{b_1} u = \cos(2\pi t^*) + \frac{\rho\omega}{b_1} \mathrm{Re} \sum_{m=1}^{\infty} e^{i2\pi t^*} \left[A_{1m} \cosh(a\gamma_{1m} x^*) \cos(b\upsilon_m y^*) + B_{1m} \cosh(b\overline{\gamma}_{1m} y^*) \cos(a\overline{\upsilon}_m x^*) \right] \tag{3.56}$$

Let

$$\gamma_{1m} = \left(\upsilon_m^2 + i \frac{\rho\omega}{\mu} \right)^{1/2} := \alpha_{1m} + i\beta_{1m},$$

where

$$\alpha_{1m} = \left[\upsilon_m^4 + \left(\frac{\rho\omega}{\mu} \right)^2 \right]^{1/4} \cos\left(\frac{\theta_m}{2} \right), \beta_{1m} = \left[\upsilon_m^4 + \left(\frac{\rho\omega}{\mu} \right)^2 \right]^{1/4} \sin\left(\frac{\theta_m}{2} \right)$$

$$\theta_m = arc \tan\left(\frac{\rho\omega}{\mu\upsilon_m^2} \right)$$

then

$$\cosh(a\gamma_{1m}) = \cosh(a\alpha_{1m}) \cos(a\beta_{1m}) + i \sinh(a\alpha_{1m}) \sin(a\beta_{1m}),$$

$$\sinh(a\gamma_{1m}) = \sinh(a\alpha_{1m}) \cos(a\beta_{1m}) + i \cosh(a\alpha_{1m}) \sin(a\beta_{1m}).$$

Using (3.31) and (3.36), through a lengthy derivation, we obtain

$$u^* = \cos\left(2\pi t^*\right) + \sum_{m=1}^{\infty}\left[d_{3m}\cos\left(2\pi t^*\right) - d_{4m}\sin\left(2\pi t^*\right)\right] \tag{3.57}$$

where

$$d_{1m} = \cosh\left(a\alpha_{1m}\right)\cos\left(a\beta_{1m}\right) + \ell\alpha_{1m}\sinh\left(a\alpha_{1m}\right)\cos\left(a\beta_{1m}\right) - \ell\beta_{1m}\cosh\left(a\alpha_{1m}\right)\sin\left(a\beta_{1m}\right),$$

$$d_{2m} = \sinh\left(a\alpha_{1m}\right)\sin\left(a\beta_{1m}\right) + \ell\alpha_{1m}\cosh\left(a\alpha_{1m}\right)\sin\left(a\beta_{1m}\right) + \ell\beta_{1m}\sinh\left(a\alpha_{1m}\right)\cos\left(a\beta_{1m}\right),$$

$$\begin{aligned} d_{3m} &= A_{1m}^*\cos\left(b\upsilon_m y^*\right)\left[d_{1m}\cosh\left(a\alpha_{1m}x^*\right)\cos\left(a\beta_{1m}x^*\right) + d_{2m}\sinh\left(a\alpha_{1m}x^*\right)\sin\left(a\beta_{1m}x^*\right)\right] \\ &\quad + B_{1m}^*\cos\left(a\bar{\upsilon}_m x^*\right)\left[\bar{d}_{1m}\cosh\left(b\bar{\alpha}_{1m}y^*\right)\cos\left(b\bar{\beta}_{1m}y^*\right) + \bar{d}_{2m}\sinh\left(b\bar{\alpha}_{1m}y^*\right)\sin\left(b\bar{\beta}_{1m}y^*\right)\right], \\ d_{4m} &= A_{1m}^*\cos\left(b\upsilon_m y^*\right)\left[d_{1m}\sinh\left(a\alpha_{1m}x^*\right)\sin\left(a\beta_{1m}x^*\right) - d_{2m}\cosh\left(a\alpha_{1m}x^*\right)\cos\left(a\beta_{1m}x^*\right)\right] \\ &\quad + B_{1m}^*\cos\left(a\,\bar{\upsilon}_m x^*\right)\left[\bar{d}_{1m}\sinh\left(b\bar{\alpha}_{1m}y^*\right)\sin\left(b\bar{\beta}_{1m}y^*\right) - \bar{d}_{2m}\cosh\left(b\bar{\alpha}_{1m}y^*\right)\cos\left(b\bar{\beta}_{1m}y^*\right)\right], \end{aligned}$$

$$A_{1m}^* = -\frac{4\sin\left(b\,\upsilon_m\right)}{\left[2b\upsilon_m + \sin\left(2b\upsilon_m\right)\right]\left(d_{1m}^2 + d_{2m}^2\right)};\quad A_{1m} = \frac{b_1}{\rho\omega}A_{1m}^*\left(d_{1m} - d_{2m}i\right),$$

$$B_{1m}^* = -\frac{4\sin\left(a\,\bar{\upsilon}_m\right)}{\left[2a\bar{\upsilon}_m + \sin\left(2a\bar{\upsilon}_m\right)\right]\left(\bar{d}_{1m}^2 + \bar{d}_{2m}^2\right)};\quad B_{1m} = \frac{b_1}{\rho\omega}B_{1m}^*\left(\bar{d}_{1m} - \bar{d}_{2m}i\right),$$

For convenience in discussion, transform (3.57) into the following form

$$u^* = \cos\left(2\pi t^*\right) + \sum_{m=1}^{\infty} u_m^*\cos\left(2\pi t^* + \phi_m\right), \tag{3.58}$$

where u_m^* and ϕ_m are respectively the amplitude and phase angles of the normalized velocity defined by

$$u_m^* = \left[d_{3m}^2 + d_{4m}^2\right]^{1/2},\quad \phi_m = \arctan\left(\frac{d_{4m}}{d_{3m}}\right). \tag{3.59}$$

The flow rate is

$$Q_1 = \frac{4abb_1 \cos\left(2\pi t^*\right)}{\rho\omega} + 4\sum_{m=1}^{\infty} \mathrm{Re}\, e^{i2\pi t^*} \left[\frac{A_{1m}}{\gamma_{1m}\upsilon_m} \sinh\left(a\gamma_{1m}\right) \sin\left(b\upsilon_m\right) + \frac{B_{1m}}{\overline{\gamma}_{1m}\overline{\upsilon}_m} \sinh\left(b\overline{\gamma}_{1m}\right) \sin\left(a\overline{\upsilon}_m\right) \right]. \tag{3.60}$$

Using real arithmetic, through lengthly calculation, we obtain the normalized flow rate

$$\begin{aligned} Q^* = \frac{\rho\omega}{b_1\left(4ab\right)} Q_1 &= \cos\left(2\pi t^*\right) + \frac{\rho\omega}{b_1\left(ab\right)} \sum_{m=1}^{\infty} \mathrm{Re}\left[e^{i2\pi t^*} \left(\frac{A_{1m}}{\gamma_{1m}\upsilon_m} \sinh\left(a\gamma_{1m}\right) \sin\left(b\upsilon_m\right) \right.\right. \\ &\left.\left. + \frac{B_{1m}}{\overline{\gamma}_{1m}\overline{\upsilon}_m} \sinh\left(b\overline{\gamma}_{1m}\right) \sin\left(a\overline{\upsilon}_m\right) \right) \right] \\ &= \cos\left(2\pi t^*\right) + \frac{\rho\omega}{abb_1} \sum_{m=1}^{\infty} \mathrm{Re}\left(Q_m\right), \end{aligned} \tag{3.61}$$

where

$$Q_m = e^{i2\pi t^*} \left(\frac{A_{1m}}{\gamma_{1m}\upsilon_m} \sinh\left(a\gamma_{1m}\right) \sin\left(b\upsilon_m\right) + \frac{B_{1m}}{\overline{\gamma}_{1m}\overline{\upsilon}_m} \sinh\left(b\overline{\gamma}_{1m}\right) \sin\left(a\overline{\upsilon}_m\right) \right),$$

$$A_{1m} = -i \frac{4c_1 \sin\left(b\upsilon_m\right)}{\rho\omega\left[2b\upsilon_m + \sin\left(2b\upsilon_m\right)\right]\left[\cosh\left(a\gamma_{1m}\right) + \ell\gamma_{1m} \sinh\left(a\gamma_{1m}\right)\right]},$$

and

$$B_{nm} = -i \frac{4c_1 \sin\left(a\overline{\upsilon}_m\right)}{\rho\omega\left[2a\overline{\upsilon}_m + \sin\left(2a\overline{\upsilon}_m\right)\right]\left[\cosh\left(b\overline{\gamma}_{1m}\right) + \ell\overline{\gamma}_{1m} \sinh\left(b\overline{\gamma}_{1m}\right)\right]}.$$

As

$$\cosh\left(a\gamma_{1m}\right) = \cosh\left(a\alpha_{1m}\right) \cos\left(a\beta_{1m}\right) + i \sinh\left(a\alpha_{1m}\right) \sin\left(a\beta_{1m}\right),$$

$$\sinh(a\gamma_{1m}) = \sinh(a\alpha_{1m})\cos(a\beta_{1m}) + i\cosh(a\alpha_{1m})\sin(a\beta_{1m}),$$

$$\text{where } \gamma_{1m} = \left(\upsilon_m^2 + i\frac{\rho\omega}{\mu}\right)^{1/2} := \alpha_{1m} + i\beta_{1m},$$

we have

$$\begin{aligned}\gamma_{1m}\sinh(a\gamma_{1m}) &= (\alpha_{1m} + i\beta_{1m})\left[\sinh(a\alpha_{1m})\cos(a\beta_{1m}) + i\cosh(a\alpha_{1m})\sin(a\beta_{1m})\right] \\ &= \left[\alpha_{1m}\sinh(a\alpha_{1m})\cos(a\beta_{1m}) - \beta_{1m}\cosh(a\alpha_{1m})\sin(a\beta_{1m})\right] \\ &\quad + i\left[\beta_{1m}\sinh(a\alpha_{1m})\cos(a\beta_{1m}) + \alpha_{1m}\cosh(a\alpha_{1m})\sin(a\beta_{1m})\right].\end{aligned}$$

Therefore

$$\begin{aligned}\cosh(a\gamma_{1m}) + \ell\gamma_{1m}\sinh(a\gamma_{1m}) &= \cosh(a\alpha_{1m})\cos(a\beta_{1m}) + i\sinh(a\alpha_{1m})\sin(a\beta_{1m}) \\ &\quad + \ell\left(\left[\alpha_{1m}\sinh(a\alpha_{1m})\cos(a\beta_{1m}) - \beta_{1m}\cosh(a\alpha_{1m})\sin(a\beta_{1m})\right]\right. \\ &\quad \left. + i\left[\beta_{1m}\sinh(a\alpha_{1m})\cos(a\beta_{1m}) + \alpha_{1m}\cosh(a\alpha_{1m})\sin(a\beta_{1m})\right]\right) \\ &= \left[\cosh(a\alpha_{1m})\cos(a\beta_{1m}) + \ell\left[\alpha_{1m}\sinh(a\alpha_{1m})\cos(a\beta_{1m}) - \right.\right. \\ &\quad \left.\left. \beta_{1m}\cosh(a\alpha_{1m})\sin(a\beta_{1m})\right]\right] \\ &\quad + i\left[\sinh(a\alpha_{1m})\sin(a\beta_{1m}) + \ell\left[\beta_{1m}\sinh(a\alpha_{1m})\cos(a\beta_{1m}) + \right.\right. \\ &\quad \left.\left. \alpha_{1m}\cosh(a\alpha_{1m})\sin(a\beta_{1m})\right]\right] \\ &= d_{1m} + i\,d_{2m}.\end{aligned}$$

On the other hand,

$$\begin{aligned}\frac{A_{1m}}{\gamma_{1m}\upsilon_m} &= -i\frac{4c_1\sin(b\upsilon_m)}{\rho\omega\left[2b\upsilon_m + \sin(2b\upsilon_m)\right]\left[d_{1m} + id_{2m}\right]}\frac{1}{(\alpha_{1m} + i\beta_{1m})\upsilon_m} \\ &= \frac{-4b_1\sin(b\upsilon_m)}{\rho\omega\left[2b\upsilon_m + \sin(2b\upsilon_m)\right]\left[d_{1m}\alpha_{1m} - d_{2m}\beta_{1m}\right] + i(\alpha_{1m}d_{2m} + \beta_{1m}d_{1m})} \\ &= \frac{-4b_1\sin(b\upsilon_m)}{\rho\omega\left[2b\upsilon_m + \sin(2b\upsilon_m)\right]\left[d_{3m} + id_{4m}\right]}, \quad c_1 = -b_1 i,\end{aligned}$$

and

$$\begin{aligned}\frac{A_{1m}}{\gamma_{1m}\upsilon_m}\sinh\left(a\gamma_{1m}\right) = & \frac{-4b_1\sin\left(b\upsilon_m\right)}{\rho\omega\upsilon_m\left[2b\upsilon_m+\sin\left(2b\upsilon_m\right)\right]\left[d_{3m}+id_{4m}\right]} \\ & \times\left[\sinh\left(a\alpha_{1m}\right)\cos\left(a\beta_{1m}\right)+i\cosh\left(a\alpha_{1m}\right)\sin\left(a\beta_{1m}\right)\right] \\ & = p\frac{\left(a_2+ib_2\right)}{\left[d_{3m}+id_{4m}\right]} \\ & = p\frac{\left(a_2+ib_2\right)}{\left[d_{3m}^2+d_{4m}^2\right]}\left[d_{3m}-id_{4m}\right] \\ & = \frac{p}{\left[d_{3m}^2+d_{4m}^2\right]}\left[\left(a_2d_{3m}+b_2d_{4m}\right)+i\left(b_2d_{3m}-a_2d_{4m}\right)\right] \\ & = \frac{p\left(d_{5m}+id_{6m}\right)}{\left[d_{3m}^2+d_{4m}^2\right]},\end{aligned}$$

where

$$\begin{aligned}p &= \frac{-4b_1\sin\left(b\upsilon_m\right)}{\rho\omega\upsilon_m\left[2b\upsilon_m+\sin\left(2b\upsilon_m\right)\right]}, \\ a_2 &= \sinh\left(a\alpha_{1m}\right)\cos\left(a\beta_{1m}\right), \\ b_2 &= \cosh\left(a\alpha_{1m}\right)\sin\left(a\beta_{1m}\right), \\ d_{5m} &= a_2d_{3m}+b_2d_{4m}, \\ d_{6m} &= b_2d_{3m}-a_2d_{4m}.\end{aligned}$$

Hence

$$\frac{A_{1m}}{\gamma_{1m}\upsilon_m}\sinh\left(a\,\gamma_{1m}\right)\sin\left(b\,\upsilon_m\right) = \frac{p\left(d_{5m}+i\,d_{6m}\right)}{\left[d_{3m}^2+d_{4m}^2\right]}\sin\left(b\,\upsilon_m\right)$$

and

$$\frac{B_{1m}}{\overline{\gamma}_{1m}\overline{\upsilon}_m}\sinh\left(b\overline{\gamma}_{1m}\right)\sin\left(a\overline{\upsilon}_m\right) = \frac{\overline{p}\left(\overline{d}_{5m}+i\overline{d}_{6m}\right)}{\left[\overline{d}_{3m}^2+\overline{d}_{4m}^2\right]}\sin\left(a\overline{\upsilon}_m\right).$$

Since $e^{i2\pi t^*} = \cos(2\pi t^*) + i\sin(2\pi t^*)$, then

$$\begin{aligned}
\mathrm{Re}(Q_m) &= \mathrm{Re}\left[e^{i2\pi t^*} \left(\frac{A_{1m}}{\gamma_{1m}\upsilon_m} \sinh(a\gamma_{1m}) \sin(b\upsilon_m) + \frac{B_{1m}}{\bar{\gamma}_{1m}\bar{\upsilon}_m} \sinh(b\bar{\gamma}_{1m}) \sin(a\bar{\upsilon}_m) \right) \right] \\
&= \mathrm{Re}\left[\left(\cos(2\pi t^*) + i\, \mathrm{s}in(2\pi t^*) \right) \left(p_1 (d_{5m} + i\, d_{6m}) + \bar{p}_1 (\bar{d}_{5m} + i\, \bar{d}_{6m}) \right) \right] \\
&= \mathrm{Re}\left[\left(\cos(2\pi t^*) + i\, \mathrm{s}in(2\pi t^*) \right) \left(\left(p_1 d_{5m} + \bar{p}_1 \bar{d}_{5m} \right) + i \left(p_1 d_{6m} + \bar{p}_1 \bar{d}_{6m} \right) \right) \right] \\
&= d_{7m} \cos(2\pi t^*) - d_{8m}\, \mathrm{s}in(2\pi t^*),
\end{aligned}$$

where

$$\begin{aligned}
d_{7m} &= p_1 d_{5m} + \bar{p}_1 \bar{d}_{5m}, \\
d_{8m} &= p_1 d_{6m} + \bar{p}_1 \bar{d}_{6m}.
\end{aligned}$$

Finally we have

$$\begin{aligned}
Q^* &= \cos(2\pi t^*) + \frac{\rho\omega}{abb_1} \sum_{m=1}^{\infty} \mathrm{Re}(Q_m) \\
&= \cos(2\pi t^*) + \frac{\rho\omega}{abb_1} \sum_{m=1}^{\infty} (d_{7m} \cos(2\pi t^*) - d_{8m} \sin(2\pi t^*)) \\
&= \left[1 + \frac{\rho\omega}{abb_1} \sum_{m=1}^{\infty} d_{7m} \right] \cos(2\pi t^*) - \left[\frac{\rho\omega}{abb_1} \sum_{m=1}^{\infty} d_{8m} \right] \sin(2\pi t^*) \\
&= Q_m^* \cos(2\pi t^*) \cos(\theta) - Q_m^* \sin(2\pi t^*) \sin(\theta) \\
&= Q_m^* \cos(2\pi t^* + \theta),
\end{aligned}$$

where

$$\begin{aligned}
Q_m^* \cos(\theta) &= \left[1 + \frac{\rho\omega}{abb_1} \sum_{m=1}^{\infty} d_{7m} \right], \\
Q_m^* \sin(\theta) &= \left[\frac{\rho\omega}{abb_1} \sum_{m=1}^{\infty} d_{8m} \right].
\end{aligned}$$

Thus we have

$$Q_m^* = \left(\left(1 + \frac{\rho\omega}{abb_1} \sum_{m=1}^{\infty} d_{7m} \right)^2 + \left(\frac{\rho\omega}{abb_1} \sum_{m=1}^{\infty} d_{8m} \right)^2 \right)^{\frac{1}{2}} \tag{3.62}$$

is the amplitude of the flow rate, and

$$\theta = \tan^{-1} \left(\left(\frac{\rho\omega}{abb_1} \sum_{m=1}^{\infty} d_{8m} \right) \Big/ \left(1 + \frac{\rho\omega}{abb_1} \sum_{m=1}^{\infty} d_{7m} \right) \right).$$

As the pressure gradient depends on time, the normalized velocity, normalized flow rate and shear stress are influenced by the slip length and time.

Figures 3.3 and 3.4 show the 3D and 2D velocity profiles on the cross-section at various instants of time.

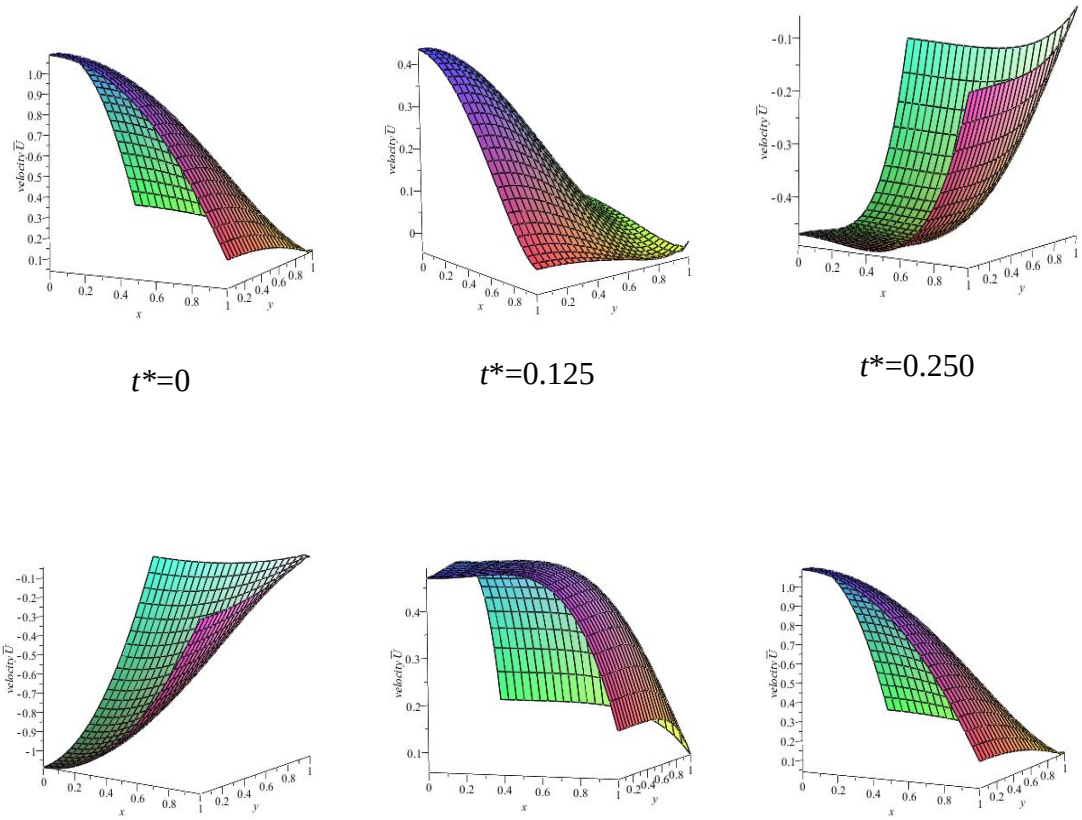

Figure 3.3: 3D graphs showing the axial velocity profiles on the cross-section of the channel at various instants of time: (a) $t^* = 0$, (b) $t^* = 0.125$, (c) $t^* = 0.25$, (d) $t^* = 0.5$, (e) $t^* = 0.75$, (f) $t^* = 1.0$.

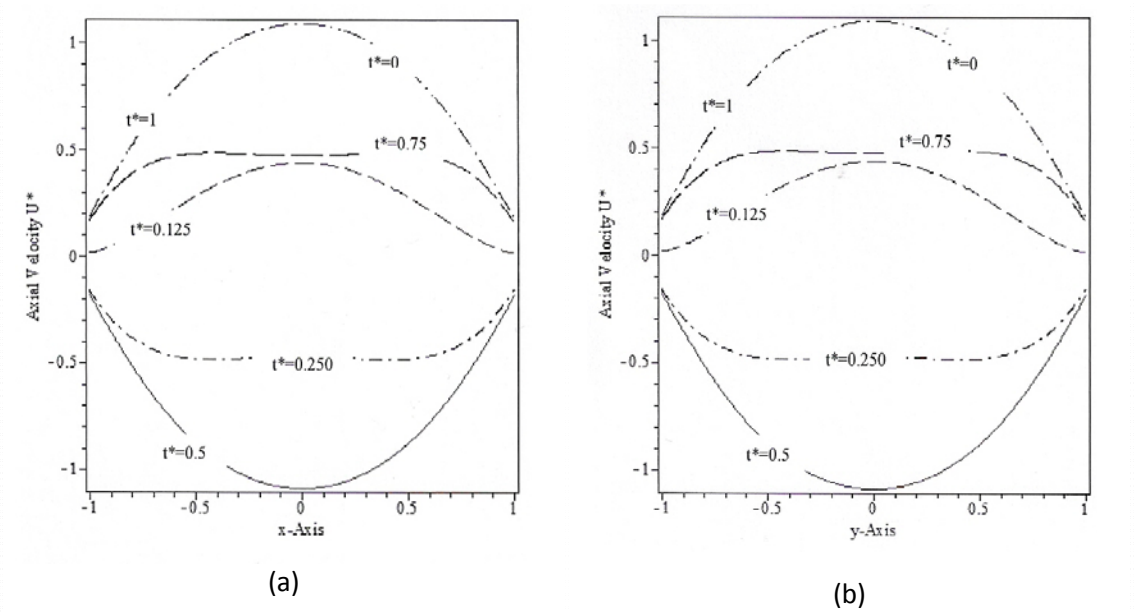

Figure 3.4: 2D graphs showing the axial velocity along the *x*-axis and *y*-axis at various instants of time: *dot line* t^* = 0; *dash line* t^* = 0.125, *dash dot line* t^*=0.250, *solid line* t^*=0.5, *long dash line* t^*=0.75, *long dash dot line* t^*=1.0.

Figures 3.3 and 3.4 show that the profiles along *x*-axis and *y*-axis are similar due to choosing $a = b = 1$. The profiles for $t^* = 0$ and $t^* = 1$ are similar. They are also similar to the profile for $t^* = 0.5$ with having opposite in sign. The axial velocity at $t^* = 0.75$ is similar to $t^* = 0.250$ with having opposite in sign.

3.5 Investigation of the Influence of Slip Parameter

In this section, we discuss the influences of the slip length on velocity, flow rate and stresses in the fluid.

Case 1: $\frac{\partial p}{\partial z} = a_0$. For this case, $c_0 = a_0$ and $c_n = 0$ for all $n \geq 1$.

To demonstrate the influence of the slip length in the flow behaviour, we analyze the solutions graphically in figures 3.5 – 3.6 which show the 3D and 2D velocity profiles on the cross-section of the channel for various different values of ℓ. Figure 3.7 shows the influence of the slip length ℓ on the flow rate Q^*

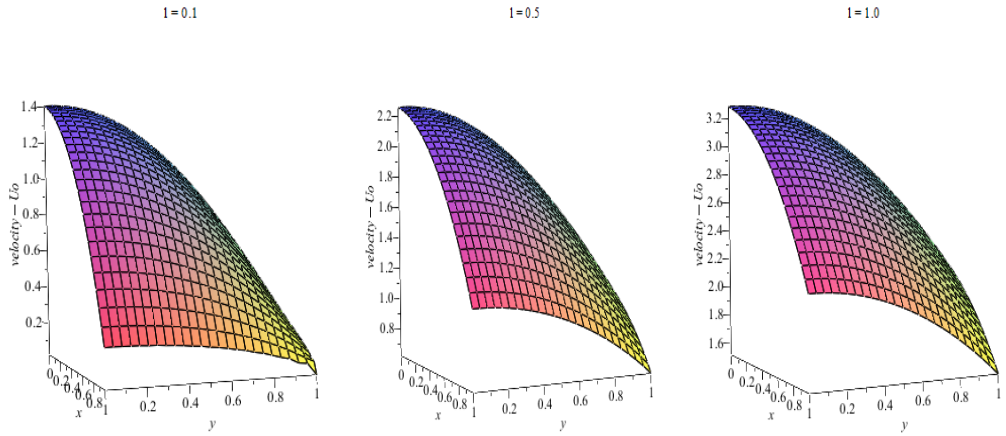

Figure 3.5: 3D graphs showing the axial velocity profiles on the cross-section of the channel for various different value of ℓ: (a) ℓ = 0.1; (b) ℓ = 0.5 ; (c) ℓ = 1.0

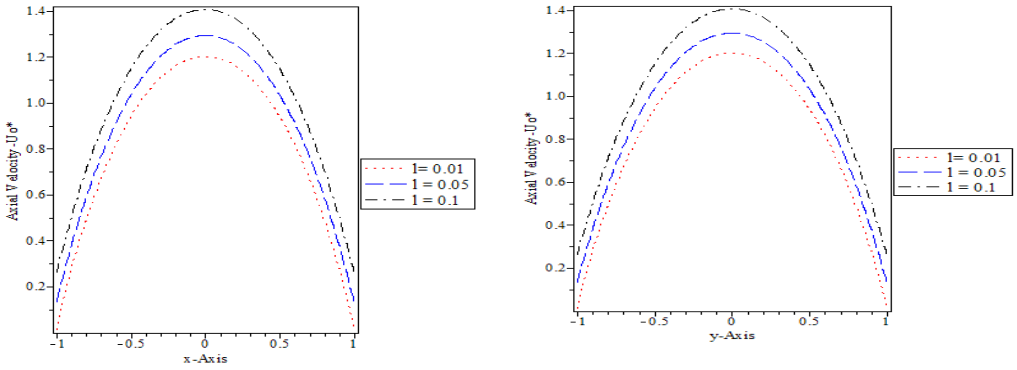

(a) (b)

Figure 3.6: 2D graphs showing the axial velocity profiles along the *x*- axis and *y*- axis for different ℓ values (a) along the *x* – axis; (b) along the *y* - axis.

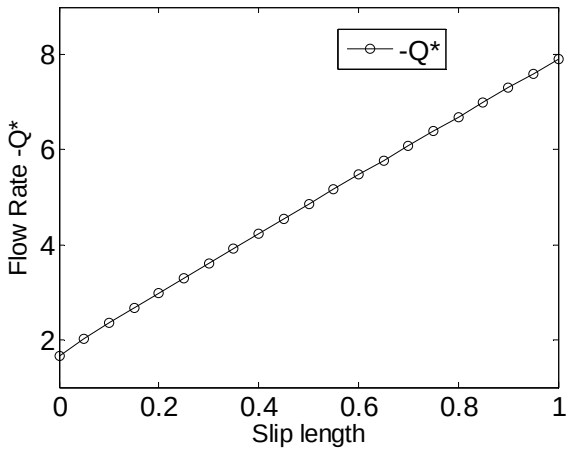

Figure 3.7: Variation of flow rate with slip length ℓ.

Figure 3.8 shows the influence of the geometry (*a* x *b*) of the cross-section on the flow rate for two different ℓ value.

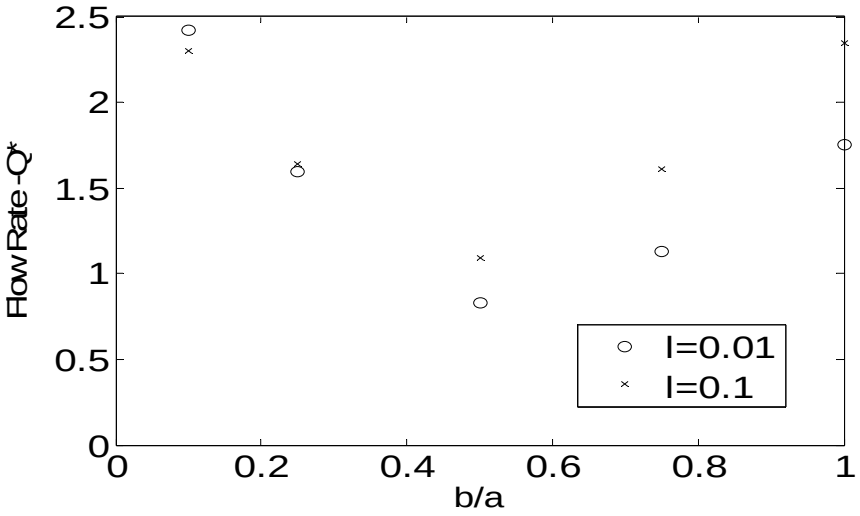

Figure 3.8: Flow rate of fluid through channel with the same cross-section area size but different ratios of width to depth (*a/b*) for two different slip length. In the diagram, $ab = a^2\varepsilon$ = constant but $\varepsilon = b/a$ take different values: ε = 1, 0.75, 0.5, 0.25, 0.1.

It can be concluded from figures 3.6 – 3.8 that the flow rate is linear in slip length and the axial velocity increases when the slip length increases. For constant (*ab*) and different fraction *b/a*, the flow rates have similar profile for different slip length ℓ.

Case 2: $\frac{\partial p}{\partial z} = b_1 \sin(\omega t)$. For this case $a_0 = 0, c_1 = -b_1 i, c_n = 0$ for $\forall n \geq 2$.

Figures 3.9 – 3.10 shows the influence of slip length ℓ on the velocity profile and flow rate.

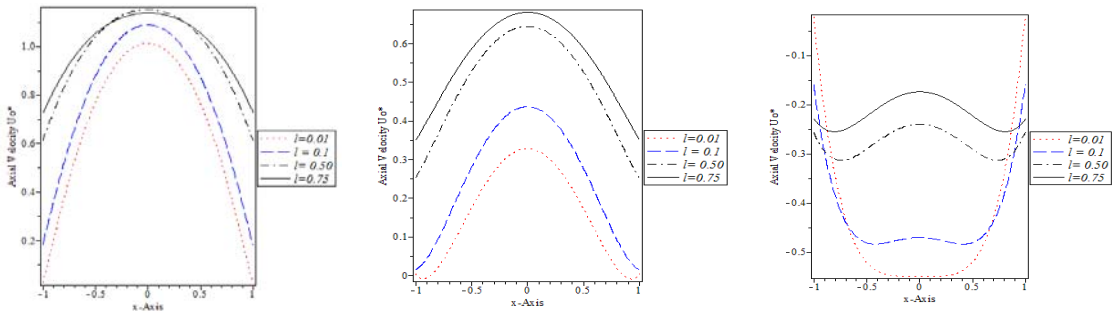

(a) (b) (c)

Figure 3.9: Influence of slip length on velocity profile at various instants of time (a) $t^* = 0$, (b) $t^* = 0.125$, (c) $t^* = 0.25$, _____ ℓ = 0.01; ------- ℓ = 0.1 ; __.__.__ ℓ = 0.50 ; _._._ ℓ = 0.75.

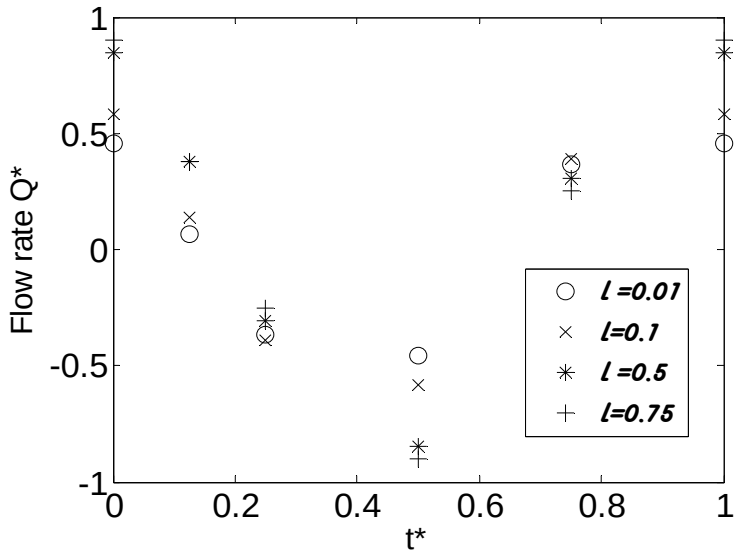

Figure 3.10: Influence of slip length on flow rate at various instants of time (a) t^* = 0, (b) t^* = 0.125, (c) t^* = 0.25, (d) t^* = 0.5, (e) t^* = 0.75, (f) t^*=1.0

Figure 3.11 shows the influence of ℓ on the transient solution Q_m^* under different frequencies $\omega = \alpha\,\mu/\rho\,a^2$ with five different α values: α = 0.005 , α = 0.025 , α =0.06 , α = 0.08 , α = 0.10.

Figure 3.12 shows the influence of the geometry $(a \times b)$ of the cross-section on the flow rate for different slip length ℓ under the same cross-sectional area size.

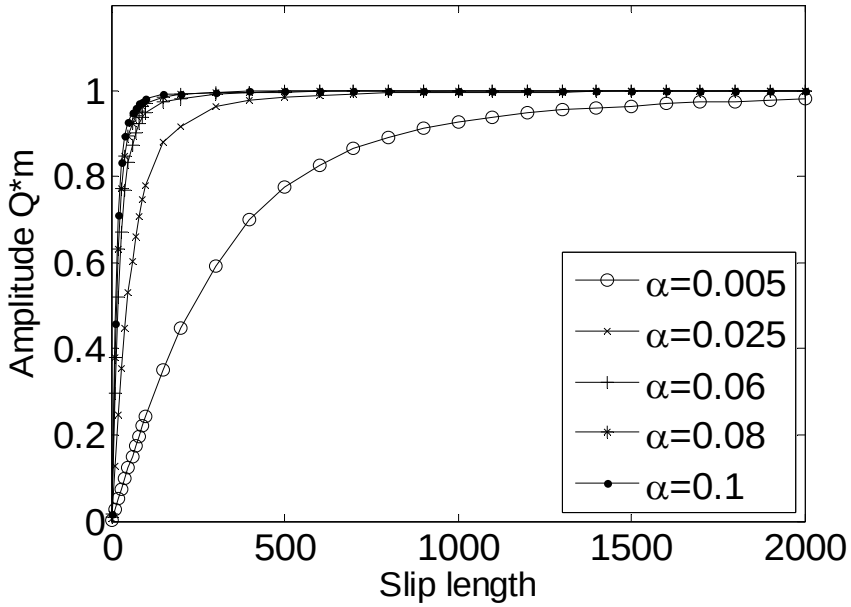

Figure 3.11: Influence of ℓ on the transient solution Q_m^* under different frequencies $\omega = \alpha \mu / \rho a^2$ with five different α values: -o- α =0.005, -x- α = 0.025, -+-α = 0.06, -*-α = 0.08 , -.- α= 0.1.

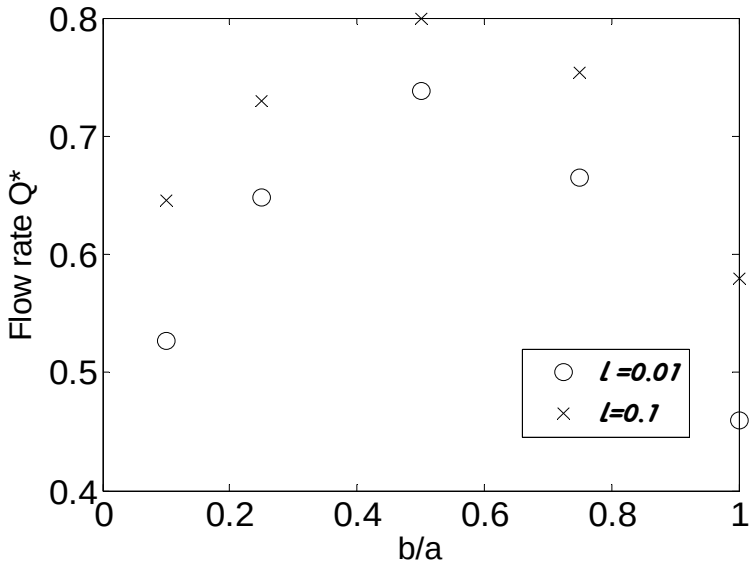

Figure 3.12: Flow rate of fluid through channel with the same cross-sectional area size but different ratios of width to depth (*a/b*) for two different slip lengths (a) ℓ = 0.01, (b) ℓ = 0.1.

Remark 3.1. For *t** = 0, the axial velocity has similar profile with *t** = 1, as $e^{i2\pi t^*} = 1$ is constant on the velocity equation (3.54) so that the curves coincide (figure 3.4). The profiles are similar on figure 3.4 (a) and (b) as the width (*a*) is the same as the depth (*b*). When (*ab*) is constant but with different width shown by the fraction $\varepsilon = b/a$, the flow rates appear like parabolic (figure 3.10 and 3.12). It shows that the flow rates are influenced not only by the slip length, but also by the fraction $\varepsilon = b/a$. The figure 3.10 shows that for similar width and depth, the flow rates seem to be parabolic for different ℓ and *t**. For *t**=0 and *t**=1, the flow rates are similar. The axial velocity also changes significantly when *t** and ℓ change (figure 3.9). The amplitudes of the flow rate initially increase significantly as the slip length ℓ increases but tend to a constant when ℓ becomes sufficiently large for various α values (figure 3.11).

3. 6 Concluding Remarks

In this chapter, we derive exact solutions for the transient flow of an incompressible Newtonian fluid through a rectangular micro-channel with a Navier slip boundary. From the analytical expressions of the velocity and flow rate solutions, we investigate the influence of the slip parameter ℓ and the geometry of the cross-section on the flow rate of fluid through the channel. The investigation shows that

(i) For flow through rectangular micro-channels with constant pressure gradient, the axial velocity increases faster in the center of the cross section than other area as the slip length increases; while for the flows driven by the wave form pressure gradient, the velocity changes significantly as the slip length increases.

(ii) For flow driven by a constant pressure gradient, the flow rate is linear, and for different values of $\varepsilon = b/a$ with constant ab, the flow rate is parabolic. While for the flows driven by the wave form pressure gradient, the flow rates are parabolic for different slip length.

(iii) The amplitudes of flow rate initially increase significantly as the slip length ℓ increases but tend to a constant when ℓ becomes sufficiently large for various α values. This profile is similar to the case shown in [4]

Chapter 4

Unsteady Slip Flow in Elliptic Microchannels

4.1 General

Micro-channels are the fundamental part of microfluidic systems. In addition to connecting different devices, micro-channels are also utilized as biochemical reaction chambers, in infrared detectors, in diode lasers, in miniature gas chromatographs, or as heat exchangers for cooling computer chips. Understanding the flow characteristics of micro-channel flows is very important in determining pressure distribution, heat transfer, and transport properties of the flow.

The elliptic cross-section is one useful channel shape that may be produced by micro-fabrication. Elliptic micro-channels have potential practical application in Micro-Electro-Mechanical Systems (MEMS). Ghosh et al. [104] studied an unsteady flow of an incompressible viscous fluid with embedded small inert spherical particles contained in a tube of elliptic cross-section due to a periodic pressure gradient acting along the length of the tube. Haslam & Zamir [103] considered a long tube of elliptic cross section as an idealization of the geometry of a compressed blood vessel. An exact solution of the governing equations for the pulsatile flow in a tube of elliptic cross section involves Mathieu functions which are considerably more difficult to evaluate than the Bessel functions in the case of a circular cross section. Hsu et al. [102] studied theoretically the electrokinetic flow of an electrolyte solution through an elliptical micro-channel and simulate the flow of fluid in veins. Hsu et al. [102] described the electrokinetic flow of an electrolyte solution in an elliptical micro-channel

covered by an ion-penetrable and charged membrane layer theoretically. Steady slip flow in elliptic micro-channels has been examined and a detailed theoretical analysis has been performed. A solution is obtained in elliptic cylindrical coordinates by using the method of separation of variables [36]. For the non-slip case, Bahrami et al. [97] investigated analytical solutions for various types of cross-sections and compared $f\,\mathrm{Re}_{\sqrt{A}}$ for selected cross sections. Chakraborty [75] studied some methods for the analysis of fluid flows through micro-channels. A variational method is applied to solve the problem of flow through a channel of elliptical cross section.

As pressure gradient is defined in the form of (3.7), if $n = 0$ then $\frac{\partial p}{\partial z} = c_0 = a_0$. For this case, the solution has been found by Duan & Muzychka [36]. Therefore, in this chapter, we will focus only on unsteady slip flows for the wave pressure gradient, namely $n \neq 0$.

The major aim of this chapter is to develop and study analytical solutions for the unsteady slip flows in elliptic micro-channels. The rest of this chapter is organized as follows. In the following section, we first review the Mathieu equation, the modified Mathieu equations and their solution. In section 4.3, we formulate the underlying boundary value problem in elliptic cylindrical coordinates. Then in section 4.4, we derive the exact solutions for the velocity and stress fields. It will be shown that the solution processes involve the solution of the modified Mathieu equation and that the solution obtained includes some existing known solutions as special cases. In section 4.5, we carry out some numerical investigations to study the velocity profile and the flow behavior. Finally, a conclusion is given in section 4.6.

4.2 The Mathieu Equations and Solution

Solving field problems in domain with elliptical geometries requires the computation of Mathieu and modified Mathieu functions. These are the eigensolutions of the wave equation in elliptical coordinates. Mathieu functions were introduced in 1868 when Mathieu determined the vibrational modes of a stretched membrane having an elliptical boundary [110]. The two dimensional wave equation

$$\frac{\partial^2 V}{\partial x^2} + \frac{\partial^2 V}{\partial y^2} + k_1^2 V = 0 \tag{4.1}$$

was transformed to the elliptic cylindrical coordinates and then split up into two ordinary differential equations. If $q^{\frac{1}{2}} = \frac{1}{2} k_1 h$ with h being the semi interfocal distance, and a being an arbitrary separation constant, the split equations take the form

$$\frac{d^2 u}{dz^2} + \left(a - 2q\cos 2z\right)u = 0 \tag{4.2}$$

$$\frac{d^2 u}{dz^2} - \left(a - 2q\cosh 2z\right)u = 0\,, \tag{4.3}$$

where the parameters a and q are real with $q > 0$.

Eq. (4.2) is called the Mathieu equation and Eq. (4.3) is termed the modified Mathieu equation. The appropriate solutions of equation (4.2) are called (ordinary) Mathieu functions, being periodic in z with period π or 2π. For periodicity, a must take special values called characteristic numbers. The corresponding solutions of (4.3) for the same value of a as in (4.2) are called modified Mathieu functions.

This Mathieu equation (4.2) has periodic solution of the first kind in the form

$$u = C_1\, ce_{2n}(z,q) + C_2\, se_{2n}(z,q) \tag{4.4}$$

where $ce_{2n}(z,q)$ and $se_{2n}(z,q)$ are Mathieu functions with period π, defined by

$$ce_{2n}(z,q) = \sum_{r=0}^{\infty} A_{2r}^{(2n)} \cos(2rz)\ , \tag{4.5}$$

$$se_{2n}(z,q) = \sum_{r=0}^{\infty} B_{2r}^{(2n)} \sin(2rz), \tag{4.6}$$

corresponding to characteristic numbers $a = a_{2n}$ and $a = b_{2n}$ respectively for n =0, 1, 2, …. The a_{2n} and b_{2n} are respectively characteristic numbers of the Mathieu functions $ce_{2n}(z,q)$ and $se_{2n}(z,q)$, and depend on q; while $A_{2r}^{(2n)}$ and $B_{2r}^{(2n)}$ are functions of q. Since $ce_{2n}(z,q)$ and $se_{2n}(z,q)$ do not correspond to the same value of a, their linear combination (4.4) does not express the general solution of the Mathieu equation. Either $ce_{2n}(z,q)$ or $se_{2n}(z,q)$ may be used if a series of such terms satisfies the boundary conditions. If neither satisfy the boundary conditions, one must introduce Mathieu functions of the second kind which are non-periodic [105].

The other Mathieu functions are

$$ce_{2n+1}(z,q) = \sum_{r=0}^{\infty} A_{2r+1}^{(2n+1)} \cos(2r+1)z\ , \tag{4.7}$$

$$se_{2n+1}(z,q) = \sum_{r=0}^{\infty} B_{2r+1}^{(2n+1)} \sin(2r+1)z\,, \tag{4.8}$$

which correspond to characteristic number $a = a_{2n+1}$, $a = b_{2n+1}$ respectively, n = 0, 1, 2, … and have period 2π.

Obviously, the Mathieu functions are given in series form. For example, for n = 0, the Mathieu function corresponding to characteristic number a_0 is given by

$$ce_0(z,q) = A_0 + A_2 \cos 2z + A_4 \cos 4z + \ldots \ . \tag{4.9}$$

Writing Mathieu function in the series form is to calculate the function approximately or numerically. Thus formula for finding characteristic numbers a_{2n} and b_{2n}, and the coefficients *A* and *B* are required, which are available in [110] and one also given in appendix. A numerical procedure based on the formula has been established for the solution of our problems.

The functions $ce_m(z,q)$ and $se_m(z,q)$ are orthogonal, namely

$$\int_0^{2\pi} ce_m(z,q)\, se_p(z,q)\, dz = 0 \text{, } m \text{ and } p \text{ positive integers.}$$

$$\int_0^{2\pi} ce_m(z,q)\, ce_p(z,q)\, dz = 0, \quad (m \neq p), \text{ and} \tag{4.10}$$

$$\int_0^{2\pi} se_m(z,q)\, se_p(z,q)\, dz = 0, \quad (m \neq p).$$

If we write *iz* for *z* on the Mathieu equation (4.2), it becomes

$$\frac{d^2u}{dz^2} - (a - 2q\cosh 2z)\, u = 0, \tag{4.11}$$

which is called the Modified Mathieu equation. For the values of *a* corresponding to $ce_m(z,q)$ and $se_m(z,q)$, the solution of (4.11) are derived by substituting *iz* for *z* in the solution of the Mathieu equations [110], namely

$$Ce_{2n}(z,q) = ce_{2n}(iz,q) = \sum_{r=0}^{\infty} A_{2r}^{(2n)} \cosh(2rz) \ ; \tag{4.12}$$

$$Se_{2n+2}(z,q) = -i\, se_{2n+2}(iz,q) = \sum_{r=0}^{\infty} B_{2r}^{(2n+2)} \sinh(2r+2)z \tag{4.13}$$

which have characteristic numbers $a = a_{2n}$, $b = b_{2n+2}$ and period πi. *A* and *B* are functions of *q*.

The other modified Mathieu functions are

$$Ce_{2n+1}(z,q) = ce_{2n+1}(iz,q) = \sum_{r=0}^{\infty} A_{2r+1}^{(2n+1)} \cosh(2r+1)z \tag{4.14}$$

$$Se_{2n+1}(z,q) = -i\, se_{2n+1}(iz,q) = \sum_{r=0}^{\infty} B_{2r+1}^{(2n+1)} \sin(2r+1)z \tag{4.15}$$

which have characteristic numbers $a = a_{2n+1}$, $a = b_{2n+1}$ and period $2\pi i$. These are defined to be modified Mathieu functions of the first kind of integral order for $q > 0$. Similar procedures are used to calculate the coefficients of A and B on the modified Mathieu functions.

4.3 Formulation of Governing Equations in Elliptic Cylindrical Coordinates

Consider the unsteady Navier-Stokes equation (3.8) in rectangular coordinates derived in section 3.3:

$$\begin{aligned} &\frac{\mu}{\rho}\left(\frac{\partial^2 u_n}{\partial x^2} + \frac{\partial^2 u_n}{\partial y^2}\right) - \frac{\partial u_n}{\partial t} = \frac{c_n}{\rho} e^{in\omega t} \\ &c_n = a_n - b_n i,\ n \neq 0. \end{aligned} \tag{4.16}$$

In elliptic micro-channels, it is convenient to use elliptic cylindrical coordinates (Moon & Spencer, 1971).

We let the orthogonal coordinates be (u^1, u^2, u^3), rectangular coordinates be $(x^1, x^2, x^3) = (x, y, z)$, and elliptic cylindrical coordinates be (η, ψ, z). Then we have the following coordinate transformation

$$\begin{aligned} &x = c \cosh\eta \cos\psi \\ &y = c \sinh\eta \sin\psi;\ \ 0 \le \eta < \infty,\ 0 \le \psi < 2\pi \\ &z = z;\quad -\infty < z < +\infty. \end{aligned} \tag{4.17}$$

To understand the elliptic coordinate system, we get from the coordinate transformation (4.17) that

$$\begin{aligned} \frac{x^2}{c^2\cosh^2\eta}+\frac{y^2}{c^2\sinh^2\eta}&=1, \\ \frac{x^2}{c^2\cos^2\psi}-\frac{y^2}{c^2\sin^2\psi}&=1. \end{aligned} \tag{4.18}$$

Thus $\eta=\eta_i$ gives a family of confocal ellipses for different η_i values; while $\psi=\psi_i$ gives a family of confocal hyperbolas with the same foci, as shown in figure 4.1. The two families of curves intersect orthogonally, and each intersection defines a point with coordinates $x=c\cosh\eta\cos\psi$ and $y=c\sinh\eta\sin\psi$.

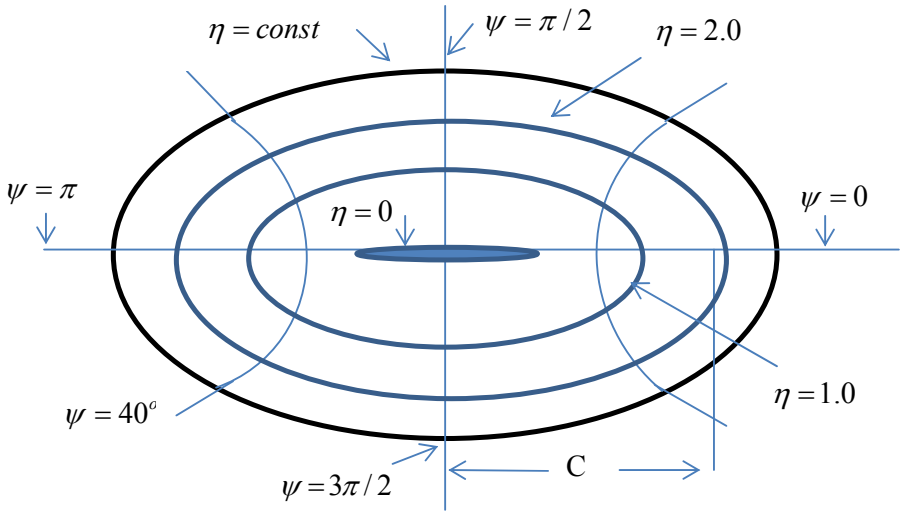

Figure 4.1: Elliptic cylindrical coordinate system

From (4.17), we have

$$\begin{aligned} \frac{\partial x}{\partial\eta}&=c\sinh\eta\cos\psi; \quad \frac{\partial y}{\partial\eta}=c\cosh\eta\sin\psi; \\ \frac{\partial x}{\partial\psi}&=-c\cosh\eta\sin\psi; \quad \frac{\partial y}{\partial\psi}=c\sinh\eta\cos\psi. \end{aligned} \tag{4.19}$$

The metric coefficients are defined by [36]

$$g_{ii} = \left(\frac{\partial x^1}{\partial u^i}\right)^2 + \left(\frac{\partial x^2}{\partial u^i}\right)^2 + \left(\frac{\partial x^3}{\partial u^i}\right)^2 \tag{4.20}$$

and the distance is

$$(ds)^2 = g_{11}\left(du^1\right)^2 + g_{22}\left(du^2\right)^2 + g_{33}\left(du^3\right)^2. \tag{4.21}$$

Therefore we have

$$\begin{aligned} g_{11} &= c^2 \sinh^2\eta \cos^2\psi + c^2 \cosh^2\eta \sin^2\psi \\ &= c^2 \sinh^2\eta\left(1-\sin^2\psi\right) + c^2\left(1+\sinh^2\eta\right)\sin^2\psi \\ &= c^2\left(\sinh^2\eta + \sin^2\psi\right) \\ &= c^2\left(\cosh^2\eta - 1 + 1 - \cos^2\psi\right) \\ &= c^2\left(\cosh^2\eta - \cos^2\psi\right), \end{aligned} \tag{4.22}$$

$$\begin{aligned} g_{22} &= \left(-c\,\cosh\eta\sin\psi\right)^2 + \left(c\sinh\eta\cos\psi\right)^2 \\ &= c^2\cosh^2\eta\sin^2\psi + c^2\sinh^2\eta\cos^2\psi \\ &= c^2\cosh^2\eta\sin^2\psi + c^2\left(\cosh^2\eta - 1\right)\cos^2\psi \\ &= c^2\cosh^2\eta\ \left(\sin^2\psi + \cos^2\psi\right) - c^2\cos^2\psi \\ &= c^2\left(\cosh^2\eta - \cos^2\psi\right) \\ &= g_{11}, \end{aligned} \tag{4.23}$$

$$g_{33} = 0 + 0^2 + \left(\frac{\partial z}{\partial z}\right) = 1, \tag{4.24}$$

so that

$$g = \left(g_{11}.g_{22}.g_{33}\right) = c^4\left(\cosh^2\eta - \cos^2\psi\right)^2, \tag{4.25}$$

$$g^{1/2} = c^2\left(\cosh^2\eta - \cos^2\psi\right). \tag{4.26}$$

The Laplacian of v in elliptic cylinder coordinates is defined by [36]

$$\nabla^2 v = g^{1/2}\sum_{i=1}^{3}\frac{\partial}{\partial u^i}\left(\frac{g^{1/2}}{g_{ii}}\frac{\partial v}{\partial u^i}\right); \quad \left(u^1,u^2,u^3\right) = \left(\eta,\psi,z\right). \tag{4.27}$$

Thus

$$\begin{aligned}\nabla^2 v &= \frac{1}{c^2\left(\cosh^2\eta-\cos^2\psi\right)}\left(\frac{\partial}{\partial\eta}\left(\frac{g^{1/2}}{g_{11}}\frac{\partial v}{\partial\eta}\right)+\frac{\partial}{\partial\psi}\left(\frac{g^{1/2}}{g_{22}}\frac{\partial v}{\partial\psi}\right)+\frac{\partial}{\partial z}\left(\frac{g^{1/2}}{g_{33}}\frac{\partial v}{\partial z}\right)\right)\\ &= \frac{1}{c^2\left(\cosh^2\eta-\cos^2\psi\right)}\left(\frac{\partial}{\partial\eta}\left(1.\frac{\partial v}{\partial\eta}\right)+\frac{\partial}{\partial\psi}\left(1.\frac{\partial v}{\partial\psi}\right)\right.\\ &\quad\left.+\frac{\partial}{\partial z}\left(c^2\left(\cosh^2\eta-\cos^2\psi\right)\frac{\partial v}{\partial z}\right)\right)\\ &= \frac{1}{c^2\left(\cosh^2\eta-\cos^2\psi\right)}\left(\frac{\partial^2 v}{\partial\eta^2}+\frac{\partial^2 v}{\partial\psi^2}\right)+\frac{\partial^2 v}{\partial z^2}.\end{aligned} \tag{4.28}$$

In rectangular coordinates, as there is no swirling flow, we have $\frac{\partial v}{\partial z}=0$. Thus the momentum equation (4.16) written in elliptic cylindrical coordinates is

$$\frac{1}{c^2\left(\cosh^2\eta-\cos^2\psi\right)}\left(\frac{\partial^2 v}{\partial\eta^2}+\frac{\partial^2 v}{\partial\psi^2}\right)-\frac{\rho}{\mu}\frac{\partial v_n}{\partial t}=\frac{c_n}{\mu}e^{in\omega t}. \tag{4.29}$$

The velocity distribution must satisfy the slip boundary condition on the walls. The local slip velocity is proportional to the local velocity gradient normal to the wall. In elliptic cylindrical coordinates, the boundary conditions (Duan and Muzychka, 2007), assuming a one quarter basic cell, are

$$\text{(i)}\ \frac{1}{\sqrt{g_{22}}}\frac{\partial v}{\partial\psi}(\eta,0)=0\ , \tag{4.30}$$

$$\text{(ii)}\ \frac{1}{\sqrt{g_{22}}}\frac{\partial v}{\partial\psi}\left(\eta,\frac{\pi}{2}\right)=0\,,$$

$$\text{(iii)}\ \frac{1}{\sqrt{g_{11}}}\frac{\partial v}{\partial\eta}(0,\psi)=0\,,$$

$$\text{(iv)}\quad v+\frac{\ell}{\sqrt{g_{11}}}\frac{\partial v}{\partial\eta}(\eta_0,\psi)=0;\quad \eta_0=\ln\frac{1+b/a}{\sqrt{1-(b/a)^2}};$$

$$c=\frac{a}{\cosh\eta_0}=\frac{b}{\sinh\eta_0},$$

where ℓ is slip length. The slip length is defined by $\ell = \lambda \dfrac{2-\sigma}{\sigma}$ in [36], where λ is the molecular mean free path and σ denotes the tangential momentum accommodation coefficient, which has values that typically lie between 0.87 and 1 [101]. It should be addressed here that for $\ell = 0$, conditions (4.32) reduces to the no-slip boundary condition.

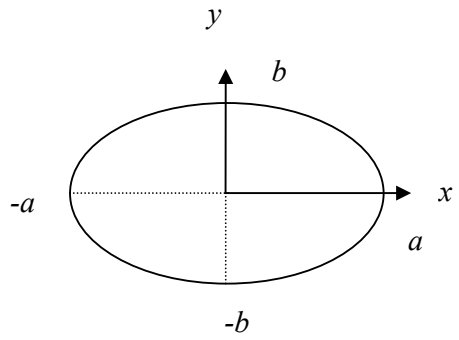

Figure 4.2: An elliptic duct

4.4 Solution of Velocity and Stress Fields

We let $v_n = f_n e^{in\omega t}$; $\quad f_n = f_n(\eta, \psi)$, so that

$$\frac{\partial^2 v_n}{\partial \eta^2} = \frac{\partial^2 f_n}{\partial \eta^2} e^{in\omega t},$$

$$\frac{\partial^2 v_n}{\partial \psi^2} = \frac{\partial^2 f_n}{\partial \psi^2} e^{in\omega t}, \tag{4.31}$$

$$\frac{\partial v_n}{\partial t} = in\omega f_n \, e^{in\omega t}.$$

Substituting (4.31) into the momentum equation (4.29) yields

$$\frac{e^{in\omega t}}{c^2\left(\cosh^2\eta-\cos^2\psi\right)}\left(\frac{\partial^2 f_n}{\partial\eta^2}+\frac{\partial^2 f_n}{\partial\psi^2}\right)-\frac{in\omega\rho}{\mu}f_n\,e^{in\omega t}=\frac{c_n}{\mu}e^{in\omega t}, \tag{4.32}$$

which gives

$$\frac{1}{c^2\left(\cosh^2\eta-\cos^2\psi\right)}\left(\frac{\partial^2 f_n}{\partial\eta^2}+\frac{\partial^2 f_n}{\partial\psi^2}\right)-\frac{in\omega\rho}{\mu}f_n=\frac{c_n}{\mu}\ . \tag{4.33}$$

For $n\neq 0$, let $f_n=W_n\left(\eta,\psi\right)-\dfrac{c_n}{in\omega\rho}$, then we have

$$\frac{\partial^2 f_n}{\partial\eta^2}=\frac{\partial^2 W_n}{\partial\eta^2},\quad \frac{\partial^2 f_n}{\partial\psi^2}=\frac{\partial^2 W_n}{\partial\psi^2}\,. \tag{4.34}$$

The momentum equation now becomes

$$\frac{1}{c^2\left(\cosh^2\eta-\cos^2\psi\right)}\left(\frac{\partial^2 W_n}{\partial\eta^2}+\frac{\partial^2 W_n}{\partial\psi^2}\right)-\frac{in\omega\rho}{\mu}\left(W_n-\frac{c_n}{in\omega\rho}\right)=\frac{c_n}{\mu}, \tag{4.35}$$

or

$$\frac{1}{c^2\left(\cosh^2\eta-\cos^2\psi\right)}\left(\frac{\partial^2 W_n}{\partial\eta^2}+\frac{\partial^2 W_n}{\partial\psi^2}\right)-\frac{in\omega\rho}{\mu}W_n=0\,. \tag{4.36}$$

To solve this equation, we let $W_n\left(\eta,\psi\right)=F_n\left(\eta\right)G_n\left(\psi\right)$, then

$$\frac{\partial^2 W_n}{\partial\eta^2}=\frac{\partial^2 F_n}{\partial\eta^2}G_n;\quad \frac{\partial^2 W_n}{\partial\psi^2}=F_n\frac{\partial^2 G_n}{\partial\psi^2}\,. \tag{4.37}$$

Because $\cosh^2\eta=\dfrac{1}{2}\left(1+\cosh 2\eta\right);\quad \cos^2\psi=\dfrac{1}{2}\left(1+\cos 2\psi\right)$, we have from (4.36)

that

$$\frac{2}{c^2\left(\cosh 2\eta-\cos 2\psi\right)}\left(G_n\frac{\partial^2 F_n}{\partial\eta^2}+F_n\frac{\partial^2 G_n}{\partial\psi^2}\right)-\frac{in\omega\rho}{\mu}\,F_n\,G_n=0\,, \tag{4.38}$$

or

$$\left(G_n\frac{\partial^2 F_n}{\partial\eta^2}+F_n\frac{\partial^2 G_n}{\partial\psi^2}\right)-\frac{in\omega\rho c^2}{2\mu}\left(\cosh 2\eta-\cos 2\psi\right)F_n\,G_n=0\,. \tag{4.39}$$

Dividing both sides of the above equation by $F_n\,G_n$, we have

$$\frac{\left(\frac{\partial^2 F_n}{\partial \eta^2}\right)}{F_n}+\frac{\left(\frac{\partial^2 G_n}{\partial \psi^2}\right)}{G_n}-\frac{in\omega\rho c^2}{2\mu}\left(\cosh 2\eta-\cos 2\psi\right)=0\,, \tag{4.40}$$

which gives

$$\frac{\left(\frac{\partial^2 F_n}{\partial \eta^2}\right)}{F_n}+\frac{\left(\frac{\partial^2 G_n}{\partial \psi^2}\right)}{G_n}=\frac{in\omega\rho c^2}{2\mu}\cosh 2\eta-\frac{in\omega\rho c^2}{2\mu}\cos 2\psi \tag{4.41}$$

or

$$\frac{\left(\frac{\partial^2 F_n}{\partial \eta^2}\right)}{F_n}-iq_n\cosh 2\eta=-\frac{\left(\frac{\partial^2 G_n}{\partial \psi^2}\right)}{G_n}-iq_n\cos 2\psi=k, \tag{4.42}$$

where $q_n=\dfrac{n\omega\rho c^2}{2\mu}$. Hence we obtain

$$\frac{\partial^2 F_n}{\partial \eta^2}-\left(k+iq_n\cosh 2\eta\right)F_n=0\ , \tag{4.43}$$

$$\frac{\partial^2 G_n}{\partial \psi^2}+\left(k+iq_n\cos 2\psi\right)G_n=0\ , \tag{4.44}$$

where k is separator constant.

Remark 4.1. The number k refers to the characteristic number as derived in (4.42) and can be chosen as a function of q_n.

Let $-2p=iq_n$, then equations (4.43) and (4.44) become

$$\frac{\partial^2 F_n}{\partial \eta^2}-\left(k-2p\cosh 2\eta\right)F_n=0\ , \tag{4.45}$$

$$\frac{\partial^2 G_n}{\partial \psi^2}+\left(k-2p\cos 2\psi\right)G_n=0\ , \tag{4.46}$$

which admit solutions

$$F_n\left(\eta\right)=A_1\ ce_{2n}\left(i\eta,p\right)+B_1\ se_{2n}\left(i\eta,p\right) \tag{4.47}$$

$$G_n(\psi) = A_2\, ce_{2n}(\psi, p) + B_2\, se_{2n}(\psi, p) \tag{4.48}$$

where $ce_{2n}(i\eta, p)$, $se_{2n}(\psi, p)$, $se_{2n}(i\eta, p)$ and $ce_{2n}(\psi, p)$ are Mathieu functions of the first kind.

By using boundary conditions 4.30(i) and 4.30(iii), we get $B_1 = 0$ and $B_2 = 0$.

As the characteristic number *k* is a function of q_n, there exist an infinite number of *k*, so that the solution has the following general form

$$W_n(\eta, \psi) = \sum_{m=0}^{\infty} A_{mn}\, ce_{2m}(i\eta, p)\, ce_{2m}(\psi, p) \tag{4.49}$$

where

$$ce_{2m}(\psi, p) = \sum_{r=0}^{\infty} A_{2r}^{(2m)} \cos(2r\psi) \text{ and} \tag{4.50}$$

$$ce_{2m}(i\eta, p) = \sum_{r=0}^{\infty} A_{2r}^{(2m)} \cosh(2r\eta). \tag{4.51}$$

The coefficients $A_{2r}^{(2m)}$ are found through a recurrence relation which depend on the order of the function, *2m*, and on the parameter *p*.

Now from (4.51), we have

$$\begin{aligned} \frac{\partial}{\partial \eta}\left(ce_{2m}(i\eta, p)\right) &= \frac{\partial}{\partial \eta}\left(\sum_{r=0}^{\infty} A_{2r}^{(2m)} \cosh(2r\eta)\right) \\ &= \sum_{r=1}^{\infty} 2r\, A_{2r}^{(2m)} \sinh(2r\eta). \end{aligned} \tag{4.52}$$

In order to overcome the difficulty in calculating the metric coefficient, we use a binomial series to approximate the metric coefficient and take the first three terms:

$$(1+x)^{\alpha} = 1 + \sum_{n=0}^{\infty} \frac{\alpha(\alpha-1)(\alpha-2)\ldots(\alpha-n+1)}{n!} x^n; \quad -1 < x < 1. \tag{4.53}$$

The metric coefficient at $\eta = \eta_0$ may now be written as:

$$\begin{aligned}\frac{1}{\sqrt{g_{22}}} &= \frac{1}{c\left(\cosh^2\eta_0-\cos^2\psi\right)^{1/2}}\\ &= \frac{1}{c\cosh\eta_0\left(1-\dfrac{\cos^2\psi}{\cosh^2\eta_0}\right)^{1/2}}\\ &\approx \frac{1+\dfrac{1}{2}\dfrac{\cos^2\psi}{\cosh^2\eta_0}+\dfrac{3}{8}\dfrac{\cos^4\psi}{\cosh^4\eta_0}}{c\cosh\eta_0}.\end{aligned} \tag{4.54}$$

$$\begin{aligned}\frac{\ell}{\sqrt{g_{22}}} &= \ell\left(\frac{1+\dfrac{1}{2}\dfrac{\cos^2\psi}{\cosh^2\eta_0}+\dfrac{3}{8}\dfrac{\cos^4\psi}{\cosh^4\eta_0}}{c\cosh\eta_0}\right)\\ &= \ell\left(\frac{1+\dfrac{1}{2}\dfrac{\cos^2\psi}{\cosh^2\eta_0}+\dfrac{3}{8}\dfrac{\cos^4\psi}{\cosh^4\eta_0}}{a}\right)\\ &= \frac{\ell}{a}g(\psi),\end{aligned} \tag{4.55}$$

where $g(\psi)=1+\dfrac{1}{2}\dfrac{\cos^2\psi}{\cosh^2\eta_0}+\dfrac{3}{8}\dfrac{\cos^4\psi}{\cosh^4\eta_0}$, $c=\dfrac{a}{\cosh\eta_0}$.

By differentiating (4.49) with respect to η, we have

$$\frac{\partial W_n}{\partial\eta}(\eta_0,\psi)=A_{mn}ce_{2m}(\psi,p)\sum_{r=1}^{\infty}2r(-1)^r A_{2r}^{(2m)}\sinh(2r\eta_0).$$

Because $f_n=W_n(\eta,\psi)-\dfrac{c_n}{in\omega\rho}$, and $v_n=f_n\,e^{in\omega t}$, we have

$$\begin{aligned}v_n &= \left(W_n-\frac{c_n}{in\omega\rho}\right)e^{in\omega t}\\ &= \left(\sum_{m=0}^{\infty}A_{mn}\,ce_{2m}(i\eta,p)\,ce_{2m}(\psi,p)-\frac{c_n}{in\omega\rho}\right)e^{in\omega t}\end{aligned} \tag{4.56}$$

Thus, from the superposition principle, we have

$$\begin{aligned} v(\eta,\psi) &= \sum_{n=1}^{\infty} \mathrm{Re}(v_n) \\ &= \sum_{n=1}^{\infty}\sum_{m=0}^{\infty} \mathrm{Re}\left[\left(A_{mn}\, ce_{2m}(i\eta, p)\, ce_{2m}(\psi, p) - \frac{c_n}{in\omega\rho}\right) e^{in\omega t}\right]. \end{aligned} \tag{4.57}$$

By differentiating v with respect to η, we have

$$\begin{aligned} \frac{\partial v}{\partial \eta} &= \sum_{n=1}^{\infty}\sum_{m=0}^{\infty} \mathrm{Re}\left[\left(A_{mn} ce_{2m}(\psi, p) \sum_{r=1}^{\infty} 2r\, A_{2r}^{(2m)} \sinh(2r\eta)\right) e^{in\omega t}\right] \\ &= \sum_{n=1}^{\infty}\sum_{m=0}^{\infty} \mathrm{Re}\left[\left(A_{mn} ce_{2m}(\psi, p) f(\eta)\right) e^{in\omega t}\right] \end{aligned} \tag{4.58}$$

where $f(\eta) = \sum_{r=1}^{\infty} 2r\, A_{2r}^{(2m)} \sinh(2r\eta)$.

Applying boundary condition 4.30(iv), namely

$$v(\eta_0,\psi,t) + \frac{\ell}{\sqrt{g_{11}}} \frac{\partial v}{\partial \eta}(\eta_0,\psi,t) = 0; \quad \eta_0 = \ln \frac{1 + b/a}{\sqrt{1-(b/a)^2}}; \tag{4.59}$$

we have

$$\begin{aligned} &\sum_{n=1}^{\infty}\sum_{m=0}^{\infty} \mathrm{Re}\left[\left(A_{mn}\, ce_{2m}(i\eta_0, p)\, ce_{2m}(\psi, p) - \frac{c_n}{in\omega\rho}\right) e^{in\omega t}\right] \\ &\qquad + \frac{\ell}{a} g(\psi) \sum_{n=1}^{\infty}\sum_{m=0}^{\infty} \mathrm{Re}\left[\left(A_{mn} ce_{2m}(\psi, p) f(\eta_0)\right) e^{in\omega t}\right] = 0, \end{aligned} \tag{4.60}$$

that is

$$\begin{aligned} &\sum_{n=1}^{\infty}\sum_{m=0}^{\infty} \mathrm{Re}\left[\left(A_{mn}\, ce_{2m}(\psi, p)\left[ce_{2m}(i\eta_0, p) \right.\right.\right. \\ &\qquad \left.\left.\left. + \frac{\ell}{a} g(\psi) f(\eta_0)\right] - \frac{c_n}{in\omega\rho}\right) e^{in\omega t}\right] = 0. \end{aligned} \tag{4.61}$$

For the above equation, to hold for any instant of time t, we require that

$$\sum_{n=1}^{\infty}\sum_{m=0}^{\infty}\mathrm{Re}\left[\left(A_{mn}\,ce_{2m}(\psi,p)\left[ce_{2m}(i\eta_0,p)+\frac{\ell}{a}g(\psi)f(\eta_0)\right]\right)\right] = \sum_{n=1}^{\infty}\mathrm{Re}\left[\frac{c_n}{in\omega\rho}\right] \tag{4.62}$$

A solution for A_{mn} may be obtained by means of a Fourier Expansion.

Multiplying both sides with $ce_{2m}(\psi,p)$, by orthogonality properties, we have

$$A_{mn}=\frac{\int_0^{2\pi}\mathrm{Re}\left[\frac{c_n}{in\omega\rho}\,ce_{2m}(\psi,p)\right]d\psi}{\int_0^{2\pi}\mathrm{Re}\left[ce_{2m}{}^2(\psi,p)\left[ce_{2m}(i\eta_0,p)+\frac{\ell}{a}g(\psi)f(\eta_0)\right]\right]d\psi}. \tag{4.63}$$

Obviously, the boundary condition 4.30(ii) is automatically satisfied.

The mean velocity is found by integration of Eq. (4.54) across the cross-section of the duct, namely

$$\bar{v}=\frac{1}{A}\int v\,dA=\frac{\int_0^{2\pi}\int_0^{\eta_0} v\,c^2\left(\cosh^2\eta-\cos^2\psi\right)d\eta d\psi}{\int_0^{2\pi}\int_0^{\eta_0} c^2\left(\cosh^2\eta-\cos^2\psi\right)d\eta d\psi} = \frac{1}{\pi ab}\int_0^{2\pi}\int_0^{\eta_0} v\,c^2\left(\cosh^2\eta-\cos^2\psi\right)d\eta d\psi \tag{4.64}$$

Now we determine the exact solutions of the stress field. The stress in the field is related to the velocity field by the constitutive equations (3.43). The rate of deformation tensor related to the velocity vector is shown by formula (3.45). As

$\boldsymbol{v} = (0, 0, v(\eta, \psi, t))$, we obtain

$$\mathbf{d} = \frac{1}{2}\begin{pmatrix} 0 & 0 & \dfrac{\partial u}{\partial \eta} \\ 0 & 0 & \dfrac{\partial u}{\partial \psi} \\ \dfrac{\partial u}{\partial \eta} & \dfrac{\partial u}{\partial \psi} & 0 \end{pmatrix} \tag{4.65}$$

From the above formula and using (3.43), (3.44) and (4.53), we have

$$d_{\eta\eta} = d_{\psi\psi} = d_{zz} = d_{\eta\psi} = d_{\psi\eta} = 0\,. \tag{4.66}$$

Hence

$$\sigma_{\eta\eta} = d_{\psi\psi} = d_{zz} = -p = q(t)z + p_0(t),\ \sigma_{\eta\psi} = \sigma_{\psi\eta} = 0 \tag{4.67}$$

where $q(t)$ is the pressure gradient, while $p_0(t)$ is arbitrary and can be chosen to meet certain pressure condition, and

$$\sigma_{\eta z} = 2\mu d_{\eta z} = \mu\frac{\partial v}{\partial \eta} = \mu\sum_{n=1}^{\infty}\sum_{m=0}^{\infty}\mathrm{Re}\left[\left(A_{mn}ce_{2m}\left(\psi, p\right)f\left(\eta\right)\right)e^{in\omega t}\right], \tag{4.68}$$

$$\sigma_{\psi z} = 2\mu d_{\psi z} = \mu\frac{\partial v}{\partial \psi} = \mu\sum_{n=1}^{\infty}\sum_{m=0}^{\infty}\mathrm{Re}\left[\left(A_{n}ce_{2n}\left(i\eta, p\right)h\left(\psi\right)\right)e^{in\omega t}\right], \tag{4.69}$$

where

$$f\left(\eta\right) = \sum_{r=1}^{\infty} 2r\ A_{2r}^{(2m)}\sinh\left(2r\eta\right),\quad h\left(\psi\right) = \sum_{r=1}^{\infty} -2r\ A_{2r}^{(2m)}\sinh\left(2r\psi\right) \tag{4.70}$$

4.5 Numerical Investigations

We have already shown the analytical solutions for $n \neq 0$ which correspond to wave form pressure gradient. We choose $c_1 = a_1 - b_1 i = -5i$, and $c_n = 0$ for $n > 1$, then

$$\frac{dp}{dz} = \mathrm{Re}\left(c_1 e^{i\omega t}\right) = 5\sin\left(4t\right).$$

For the case of wave pressure gradient, the velocity depends on time t and the slip length ℓ. The solution has been derived from the Navier-Stokes equations in elliptic cylindrical coordinates. The velocity solution has to be arranged into series in q in order to present the profile. As consequence, a smooth velocity profile is not visible.

To demonstrate the velocity profile of the wave pressure gradient, we take

$$a = 0.1, b = 0.05, \rho = 21, \omega = 4, \mu = 10, \ell = 0.1,$$

so that we have

$$\eta_0 = \ln \frac{1 + b/a}{\sqrt{1 - \left(b/a\right)^2}} = 0.549306446$$

and

$$q = \text{-}0.066\ \mathrm{I}.$$

We calculate the velocity profiles at various instants of time in the range of $0 \le \psi \le 2\pi$, $0 \le \eta \le 0.549$ for the elliptic cylindrical coordinates. Using Maple v.10 , the results are displayed in figures 4.4.

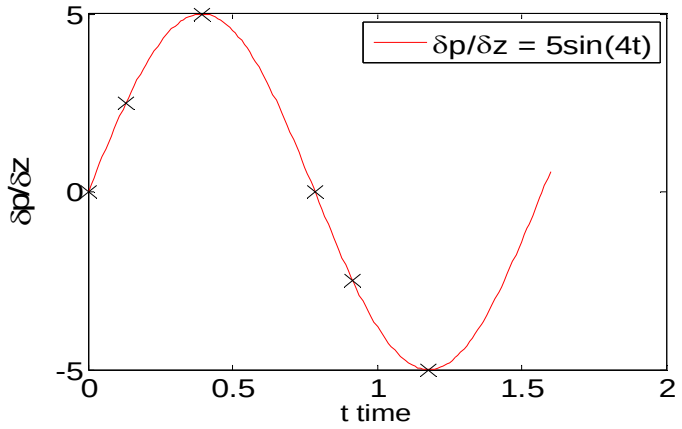

Figure 4.3: Pressure gradient driving the flow of the fluid

Calculation of the Mathieu equation and the modified Mathieu equation were based on the formula explained in section 4.2. We apply q = -0.066 i as small as required, fluid density $\rho = 21$, slip length $\ell = 0.1$, fluid viscosity $\mu = 10$, frequency $\omega = 4$, and ellipticity of the tube $\varepsilon = 0.5$. The velocity profiles at the instants of times t = 0, 0.131, 0.393, 0.785, 0.92, 1.178 corresponding to $\omega t = 0^o, 45^0, 90^0, 180^0, 225^0, 270^0$ during a full wave cycle are displayed in figure 4.4. When $\frac{dp}{dz} \geq 0$ and increases, the velocity decreases (decelerated flow) as t increases; while when $\frac{dp}{dz} \leq 0$, the velocity increases (accelerated flow) as t increases. For t = 0 and t = 0.785, $\frac{dp}{dz} = 0$ so that they have similar profile.

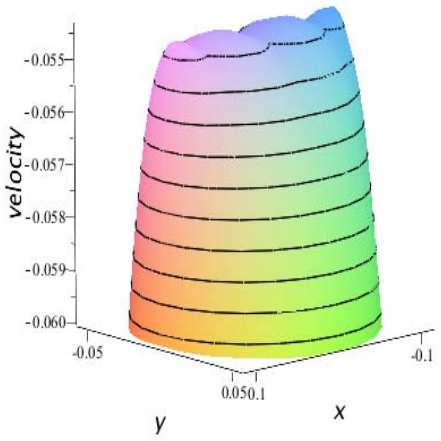

t = 0

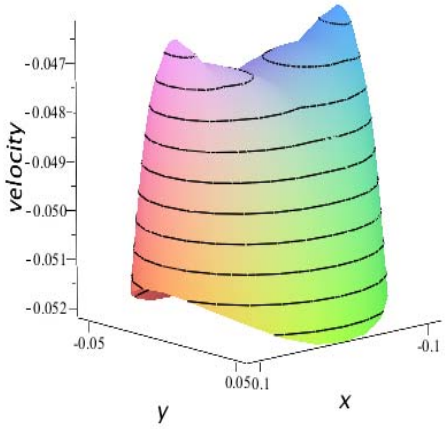

t = 0.131

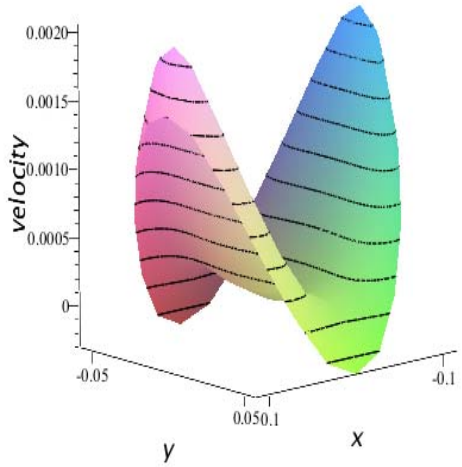

t = 0.393

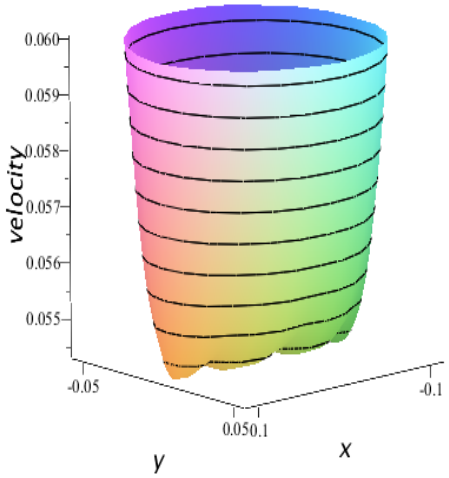

t = 0.785

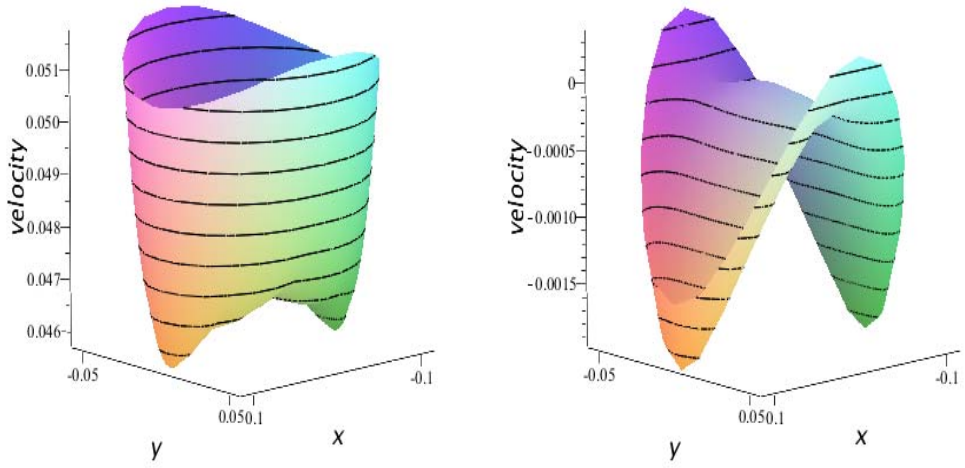

t = 0.92 t = 1.178

Figure 4.4: Velocity profiles at various instants of times during a full wave cycle (a) t=0, (b) t = 0.131, (c) t = 0.393, (d) t = 0.785, (e) t = 0.92, (f) t = 1. 178.

To demonstrate the influence of the slip on length in the flow behaviour, we analyze the solutions graphically in figures 4.5 which show the 3D velocity profiles on the cross-section of the channel for various different values of ℓ and t.

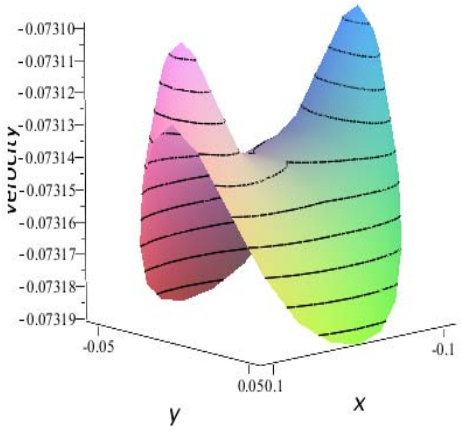

(a) ℓ = 10, t = 0

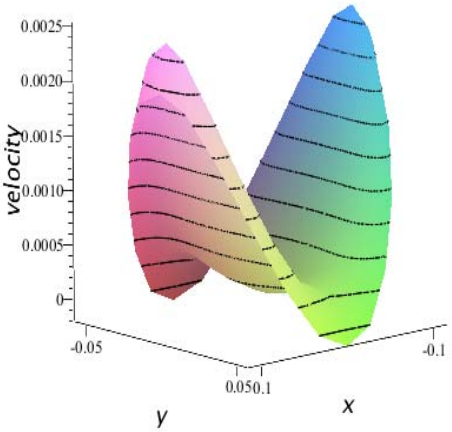

(b) ℓ = 10, t = 0.393

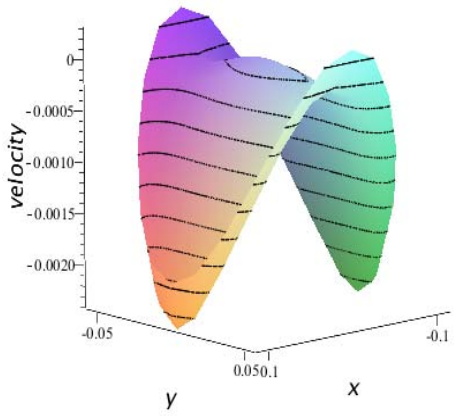

(c) ℓ = 10, t = 1.178

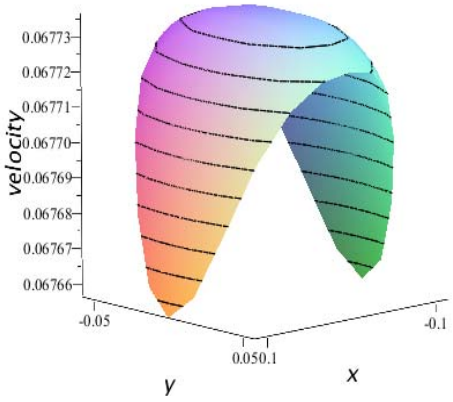

(d) ℓ = 100, t = 0

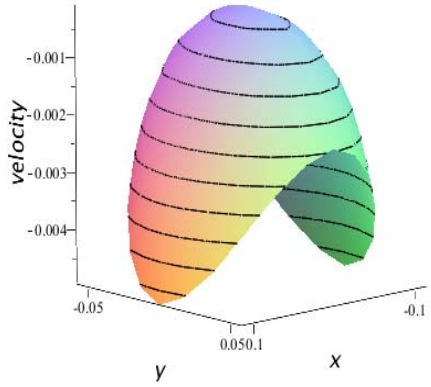

(e) ℓ = 100, t = 0.393

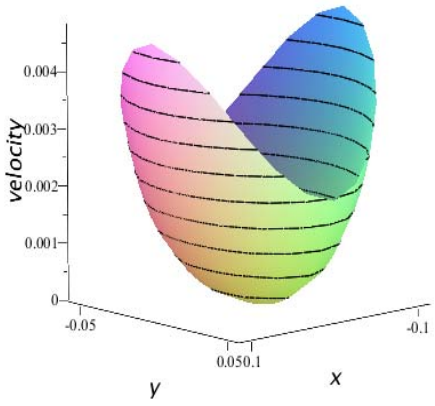

(f) ℓ = 100, t = 1.178

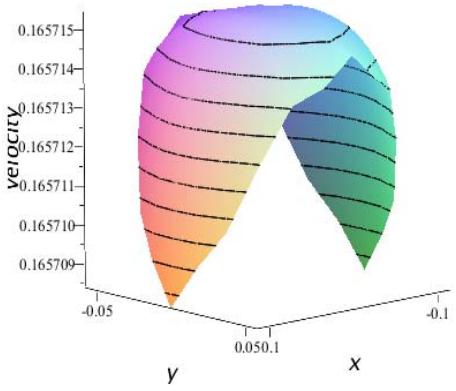

(g) ℓ = 1000, t = 0

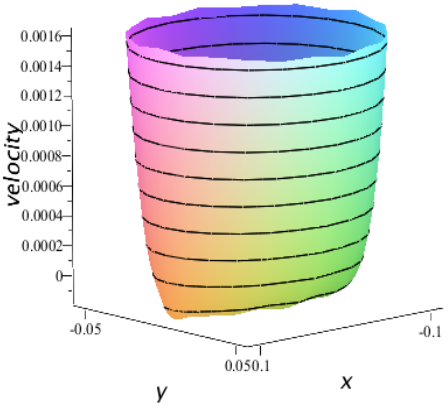

(h) ℓ = 1000, t = 0.393

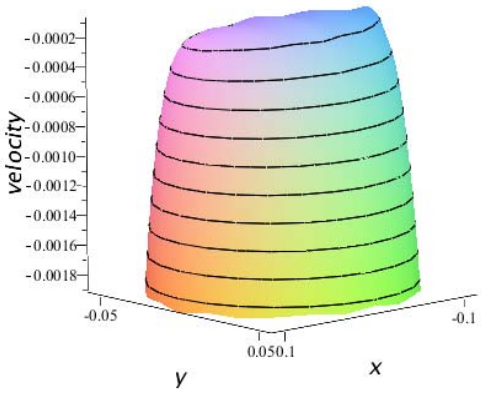

(i) ℓ = 1000, t = 1.178

Figure 4.5: 3D graphs showing the axial velocity profiles on the cross-section of the channel for various different value of ℓ and *t:* (a) ℓ = 10, t = 0; (b) ℓ = 10, t = 0.393 ; (c) ℓ = 10, t = 1.178; (d) ℓ = 100, t = 0; (e) ℓ = 100, t = 0.393; (f) ℓ = 100, t = 1.178; (g) ℓ = 1000, t = 0; (h) ℓ = 1000, t = 0.393; (i) ℓ = 1000, t = 1.178.

The velocity profiles show that for t = 0, the velocity increases when the slip length increases. For t = 0.393 and t = 1.178, the axial velocity changes significantly. As $\left.\frac{dp}{dz}\right|_{t=1.178} = -\left.\frac{dp}{dz}\right|_{t=0.393}$, the profiles are similar but in the opposite directions.

To demonstrate the influence of pressure gradient on the flow and the stress behaviour, we show the solutions graphically in figures 4.6 which show the 3D stress field profiles on the cross-section of the channel for various instants of time *t*.

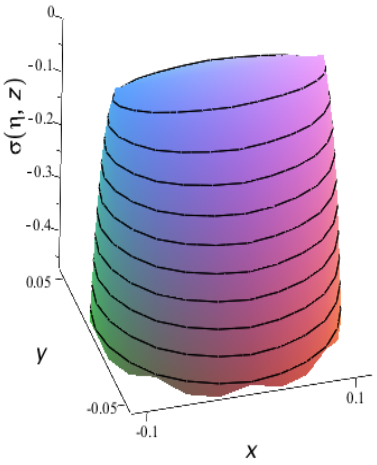

(a) t = 0

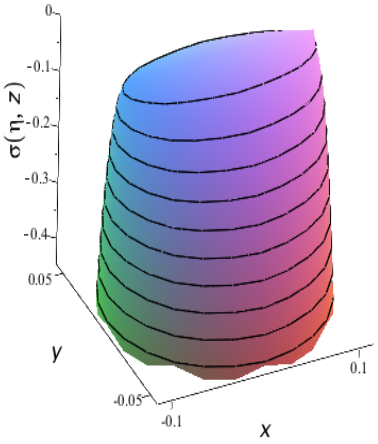

(b) t = 0.131

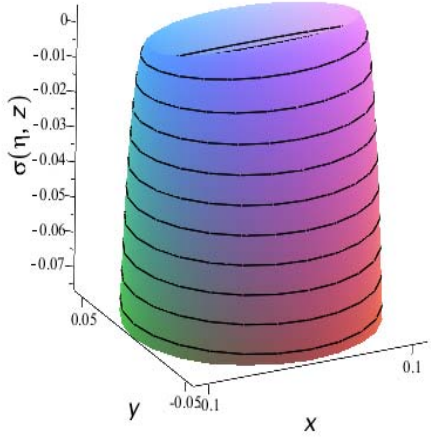

(c) t = 0.393

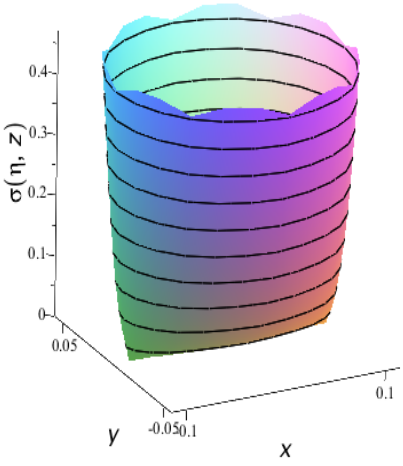

(d) t = 0.785

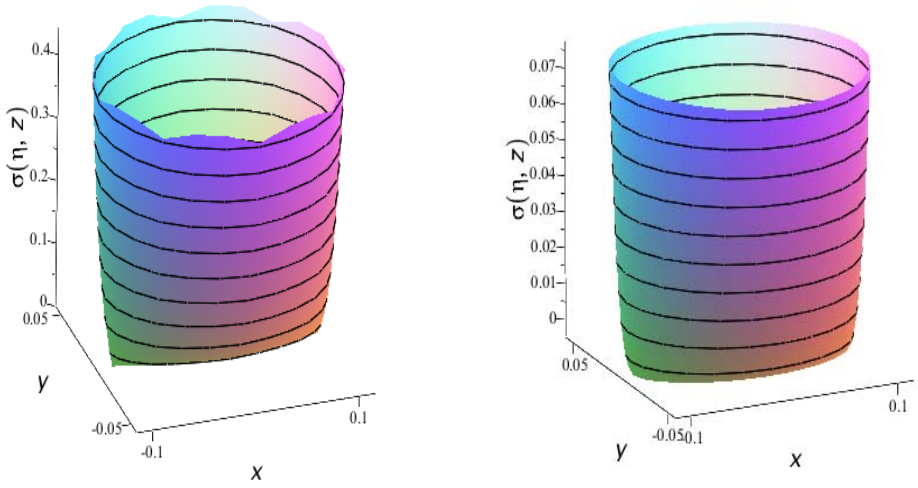

(e) t = 0.92 (f) t = 1.178

Figure 4.6: 3D graphs showing the stress field $\sigma_{\eta z}$ profiles on the cross-section of the channel for various instants of time *t:* (a) $t = 0$; (b) t = 0.131 ; (c) $t = 0.393$; (d) $t = 0.785$; (e) $t = 0.92$; (f) $t = 1.178$.

4.6 Concluding Remarks

This chapter expressed analytical solutions of unsteady fluid flow through elliptic micro-channels with boundary slip. The Navier-Stokes equation in rectangular coordinates is converted to the equation in elliptic cylindrical coordinates. The boundary conditions are formulated as in [36] but with simplifying $\lambda \frac{2-\sigma}{\sigma} = \ell$. For $n \neq 0$, the analytical solution is derived in this chapter by using Fourier series expansion. To demonstrate the analytical solution for the case of wave form pressure gradient, we convert the Mathieu and the modified Mathieu function into series of q. The velocity profile is determined for full wave cycle for $\ell = 0.1$ in

figure 4.4. When the pressure gradient increases, the velocity increases (accelerated flow); while when the pressure gradient decreases, the velocity decreases (decelerated flow). For t = 0 and t = 0.785, $\frac{dp}{dz} = 0$ so that they have similar profile but with the opposite direction. For t = 0, the axial velocity increases when the slip length increases. For t = 0.393 and t = 1.178, the profiles are similar but in the opposite directions. The stresses on the η-plane along the z direction show that the profiles are similar for $\frac{dp}{dz} \geq 0$ and $\frac{dp}{dz} \leq 0$ but in the opposite directions.

Chapter 5

Summary and Further Research

5.1 Summary

In this thesis, we study the analytical solutions of unsteady slip flows in rectangular and elliptical micro-channels. Based on previous work in the field, we have derived some important results. The main results achieved are in two aspects which are summarized below.

(1) Analytical results for unsteady slip flow in rectangular micro-channels

(i) The governing equations for the problem have been formulated and established based on the Navier-Stokes equations and the continuity equation in rectangular coordinates. By assuming that the flow is symmetric about the *xz*-plane and the *yz*- plane and is fully developed, the field equations for velocity field have reduced to a second order time-dependent partial differential equations in rectangular coordinates. The complete set of boundary conditions based on the Navier slip model has also been developed.

(ii) The governing partial differential equations subject to the slip boundary conditions have been solved successfully to yield the velocity field solutions. The basic method is to express the pressure gradient by the Fourier series and obtain the solution by using the superposition principle, that is, if u_n is the solution for $\partial p/\partial z = c_n e^{in\omega t}$, then the complete solution for $\partial p/\partial z = \mathrm{Re}\left(\sum_{n=0}^{\infty} c_n e^{in\omega t}\right)$ is

$u = \sum_{n=0}^{\infty} \mathrm{Re}(u_n)$. Then the solution is found by the separation of variables. Based on the velocity solutions, the complete set of solutions for the flow rate and the stress fields have also been obtained.

(iii) Based on the mathematical model constructed and the solutions obtained, a number of investigations have been carried out to study the dynamic flow phenomena and the influence of the slip parameter on the flow behaviour. It has been found that:

a. For the flow through rectangular micro-channels with constant pressure gradient, the axial velocity increases faster in the center of the cross section than other area when the slip length increases; while for the flows driven by the wave pressure gradient, the velocity changes significantly when the slip length increases.

b. For the flow driven by a constant pressure gradient, the flow rate is linear, and for different values of $\varepsilon=b/a$, the flow rate is parabolic. While for the flows driven by the wave form pressure gradient, the flow rates are parabolic for different slip length.

c. The amplitudes of flow rate initially increase significantly as the slip length increases but tend to a constant when the slip length becomes sufficiently large for various α values.

(2) Analytical results for unsteady slip flow in elliptical micro-channels

(i) The governing equations for the problem, including the Navier-Stokes equations and the continuity equation, have been formulated in elliptic cylindrical coordinates. The complete set of boundary conditions based on the Navier slip model in elliptical cross section has also been developed. In order to calculate the Mathieu and the modified Mathieu functions as a part of solution and to display the solutions, these functions are converted to the series of a and q.

(ii) Using methods similar to that used for the study of rectangular micro-channels, the complete set of solutions for the velocity and the stress fields have been derived. The solution process involves splitting of the partial differential equation into the Mathieu equation and the modified Mathieu equation, and part of the solutions are expressed in terms of the Mathieu functions and the modified Mathieu functions. To demonstrate the results, the coefficients of the Mathieu functions and the modified Mathieu functions have been converted to the series of the function parameters a and q, and a numerical procedure is applied to determine the coefficients.

(iii) Based on the mathematical model constructed and the solutions obtained, an investigation has been carried out to study the influence of the slip parameter on the flow behavior in elliptic micro-channels. It has been found that, as the pressure gradient increases, the velocity increases (accelerated flow); while as the pressure gradient decreases, the velocity decreases (decelerated flow). The profiles are similar for $t = 0$ and $t = 0.785$, as $\frac{dp}{dz} = 0$ but in the opposite directions. For $t = 0$, the axial velocity increases when the slip length increases. For $t = 0.393$ and $t = 1.178$, the profiles are similar but in the opposite directions. The stresses on the η-plane along the z direction show that the profiles are similar for $\frac{dp}{dz} \geq 0$ and $\frac{dp}{dz} \leq 0$ but in the opposite directions.

5.2 Further Research

In this project, we use Fourier series expansion to develop and investigate analytical solutions for unsteady slip flows in rectangular and elliptical micro-channels. Although some important results have been obtained, there are still problems for further research. In elliptic micro-channels, the form of the solution obtained is complicated and thus it is useful to search for solutions of simpler

form. Further work is still needed to study the influence of boundary slip on the velocity profile, the flow rate and the stress field. Analytical solution of unsteady slip flows for non-Newtonian fluids in elliptic micro-channels is still a challenge. Study of unsteady slip flows for Newtonian or non-Newtonian fluids in other cross sections such as triangular, trapezoidal, semi-circle, circular sector is another challenge.

References

[1] B. Bourlon, J. Wong, C. Miko, Nanoscale probe for fluidic and ionic transport, Nature Nanotechnology 2 (2) (2007) 104.

[2] B. Wiwatanapataphee, Y.H. Wu, J. Archapitak, P.F. Siew, B. Unyong, A numerical study of the turbulent flow of molten steel in a domain with a phasechange boundary, Journal of Computational and Applied Mathematics 166 (2004) 307.

[3] B. Wiwatanapataphee, D. Poltem, Y.H. Wu, Y. Lenbury, Simulation of pulsatile flow of blood in stenosed coronary artery bypass with graft, Mathematical Biosciences and Engineering 3 (2) (2006) 371.

[4] B. Wiwatanapataphee, Yong Hong Wu, Maobin Hu and K Chayantrakom, A study of transient flows of Newtonian fluids through micro-annuals with a slip boundary, J. Phys. A: Math. Theor. 42 (2009) 065206 (14pp)

[5] C.M. Ho, Y.C. Tai, Micro-electro-mechanical systems (MEMS) and fluid flows, Annual Review of Fluid Mechanics 30 (1998) 579.

[6] E.J. O'Donovan, R.I. Tanner, Numerical study of the Bingham squeeze film problem, J. Non-Newton. Fluid Mech. 15 (1984) 75.

[7] F. Saidi, Non-Newtonian flow in a thin film with boundary conditions of Coulomb's type, Zamm-Zeitschrift Fur Angewandte Mathematik Und Mechanik 86 (9) (2006) 702.

[8] G.H. Tang, X.F. Li, Y.L. He,W.Q. Tao, Electro-osmotic flow of non-Newtonian fluid in micro-channels, J. Non-Newtonian Fluid Mech. 157 (2009) 133–137

[9] H.A. Yousif, R. Melka, Bessel function of the first kind with complex argument, Computer Physics Communications 106 (1997) 199.

[10] H.B. Lee, I.W. Yeo, K.K. Lee, Water flow and slip on NAPL-wetted surfaces of a parallel-walled fracture - art. no. L19401, Geophysical Research Letters 34 (19) (2007) 19401.

[11] H. Herwig, O. Hausner, Critical view on new results in micro-fluid mechanics: An example, International Journal of Heat and Mass Transfer 46 (5) (2003) 935.

[12] H. Huang, T.S. Lee, C. Shu, Lattice Boltzmann method simulation gas slip flow in long microtubes, International Journal of Numerical Methods for Heat & Fluid Flow 17 (5–6) (2007) 587.

[13] H. Xu, Shi-Jun Liao, Ioan Pop, Series solution of unsteady boundary layer flows of non-Newtonian fluids near a forward stagnation point, J. Non-Newtonian Fluid Mech. 139 (2006) 31–43

[14] H. Zhu, D. De Kee, A numerical study for the cessation of Couette flow of on-Newtonian fluids with a yield stress, J. Non-Newtonian Fluid Mech, 143 (2007) 64–70

[15] J.J. Nakane, M. Akeson, A. Marziali, Nanopores sensors for nucleic acid analysis, Journal of Physics Condensed Matter 15 (2005) R1365.

[16] J.P. Pascal, Instability of power-law fluid flow down a porous incline, Journal of Non-Newtonian Fluid Mechanics 133 (2–3) (2006) 109.

[17] K.C. Sahu, P. Valluri, P.D.M. Spelt, O.K. Matar, Linear instability of pressure-driven channel flow of a Newtonian and a Herschel–Bulkley fluid, Physics of Fluids 19 (2007) 122101.

[18] M. Chatzimina, G.C. Georgiou, I. Argyropaidas, E. Mitsoulis, R.R. Huilgol, Cessation of Couette and Poiseuille flows of a Bingham plastic and finite stopping times, J. Non-Newton. Fluid Mech. 129 (2005) 117.

[19] M. Gad-el-Hak, The fluid mechanics of microdevices—The Freeman scholar lecture, Journal of Fluids Engineering-Transactions of the ASME 121 (1) (1999) 5.

[20] M.T. Matthews, J.M. Hill, Newtonian flow with nonlinear Navier boundary condition, Acta Mechanica 191 (3–4) (2007) 195.

[21] P.A. Thompson, S.M. Troian, A general boundary condition for liquid flow at solid surfaces, Nature 389 (1997) 360.

[22] P. Huang, Kenneth S. Breuer, Direct measurement of slip length in electrolyte solutions, Physics of Fluids 19 (2007) 028104.

[23] R. Pit, H. Hervet, L. Leger, Direct experimental evidence of slip in hexadecane: Solid interfaces, Physical Review Letters 85 (2000) 980.

[24] R. B. Bird, W. E. Stewart, E. N. Lightfoot, Transport Phenomena, John Wiley & Sons, 2007.

[25] S.J. Liao, Beyond Perturbation: Introduction to Homotopy Analysis Method, Chapman & Hall/ CRC Press, Boca Raton, 2003.

[26] S.P. Yang, K.Q. Zhu, Analytical solutions for squeeze flow of Bingham fluid with Navier slip condition, Journal of Non-Newtonian Fluid Mechanics 138 (2–3) (2006) 173.

[27] S.R. Deshmukh, D.G. Vlachos, CFD simulations of coupled, countercurrent combustor/reformer microdevices for hydrogen production, Industrial & Engineering Chemistry Research 44 (14) (2005) 4982.

[28] T.C. Kuo, D.M. Cannon, M.A. Shannon, P.W. Bohn, J.V. Sweedler, Hybrid three-dimensional nanofluidic/microfluidic devices using molecular gates, Sensors and Actuators, A 102 (2003) 223.

[29] T.C. Papanastasiou, Flows of materials with yield, J. Rheol. 31 (1987) 385.

[30] Unal Akdag, Mustafa Ozdemir, A. Feridun Ozgu, Heat removal from oscillating flow in a vertical annular channel, Heat Mass Transfer (2008) 44:393–400

[31] Y. Christophe, B. Catherine, Cottin-Bizonne Ccile, Joseph Pierre, Bocquet Lyd´ ric, Achieving large slip with superhydrophobic surfaces: Scaling laws for generic geometries, Physics of Fluids 19 (2007) 123601.

[32] Y.C. Su, L.W. Lin, A water-powered micro drug delivery system, Journal of Microelectromechanical Systems 13 (1) (2004) 75.

[33] Y. Donghyun, M. Parviz, Effects of hydrophobic surfaces on the drag and lift of a circular cylinder, Physics of Fluids 19 (2007) 081701.

[34] Y. H. Wu, B. Wiwatanapataphee, Modelling of turbulent flow and multi-phase heat transfer under electromagnetic force, Discrete and Continuous Dynamical Systems-Series B 8 (3) (2007) 695.

[35] Y. H. Wu, B. Wiwatanapataphee, Maobin Hu, Pressure-driven transient flows of Newtonian fluids through microtubes with slip boundary, Physica A 387 (2008) 5979–5990

[36] Z. Duan, Y.S. Muzychka, Slip flow in elliptic micro-channels, Int.Journal of Thermal Sciences 46 (2007) 1104–1111

[37] Z. Duan, Y.S. Muzychka, Slip flow in non-circular micro-channels, Microfluid Nanofluid, 3 (2007) 473 – 484.

[38] S. C. Hunter, 1983, *Mechanics of Continuous Media* (New York: Wiley)

[39] M.T. Mathews, J.M. Hill, Newtonian flow with nonlinear Navier boundary condition, Acta Mechanica 191 (3–4) (2007) 195.

[40] P.A. Thompson, S.M. Troian, A general boundary condition for liquid flow at solid surfaces, Nature 389 (1997) 360.

[41] R. Berker, 1963. Integration des equations du mouvement d'un fluide visqueux incompressible.In Handbuch der Physik, ed.S. FIiigge, VIII/2: 1-384. Berlin: SpringerVerlag.

[42] H. Schlichting,1968. Boundary-Layer Theory. New York: McGraw-HilI. 6th ed. 747

[45] C. Y. Wang, 1989. Exact solutions of the unsteady Navier-Stokes equations. Appl. Mech. Rev. 42: S269-82.

[46] C. Y. Wang, 1991. Exact solutions of the steady-state Navier-Stokes equations. Annu. Rev. Fluid.Mech. 23: 159 - 77.

[47] G. B. Whitham,1963. The Navier-Stokes equations of motion. In Laminar Boundary Layers, ed. 1. Rosenhead, pp. 114-62. Oxford: Clarendon

[48] Chun-I Chen, Cha'o-Kuang Chen and Heng-Ju Lin, 2008. Analysis of Unsteady Flow Through a Microtube With Wall Slip and Given Inlet Volume Flow Rate Variation, Journal of App. Mech. Vol 75, 014506-1, 7.

[49] S. Yu and T.A. Ameel, 2001, Slip Flow heat transfer in rectangular microchannels, International Journal of Heat and Mass transfer, 44, 4225 – 4234.

[50] J. B. Aparecido, R. M. Cotta, 1990, Thermally developing Laminar flow inside rectangular ducts, Int. J. heat Transfer 33. 341 – 347.

[51] R. M. Cotta, 1993, in : Integral Transforms in Coumputational Heat and Fluid Flow, CRC Press, Boca Raton, Florida, 180 – 188

[52] W.A. Ebert, E. M. Sparrow,1965. Slip flow in rectangular and annular ducts, Trans ASME, 1018 – 1024

[53] B. Y. Cao, M. Chen and Z. Y. Guo, 2006, Velocity Slip of liquid flow in nanochannels, *Acta Phys. Sin.* 55 5305

[54] B. Y. Cao, M. Chen and Z. Y. Guo**,** 2006**,** Liquid flow in surface-nanostructured channels studied by molecular dynamics simulation**,** *Phys. Rev.* E 74 066311

[55] P. Huang and K. S. Breuer, 2007 . Direct measurement of slip length in electrolyte solutions**.** *Phys. Fluids* 19 028104

[56] E. Lauga and T. M. Squires, 2005. Brownian motion near a partial-slip boundary: A local probe of the no-slip condition. *Phys. Fluids* 17 103102

[57] Pit R, Hervet H and L. Leger, 2000. Direct Experimental Evidence of Slip in Hexadecane: Solid Interfaces**.** *Phys. Rev. letter* 85 980

[58] J. C. Slattery, 1999 Advanced transport phenomena (Cambridge: Cambridge University Press)

[59] **L.** Szalmas, 2006 **,** Slip-flow boundary condition for straight walls in the lattice Boltzmann model **,** *Phys. Rev.* E 73 066710

[60] P. A. Thompson and S. M. Troian, 1997**.** Ceramics: Tough cookery**.** Nature 389-360

[61] D. C. Tretheway and C. D. Meinhart, 2002, Apparent fluid slip at hydrophobic microchannel walls. *Phys. Fluids* 14 L9

[62] K. Yanuar, Watanabe and H. Mizunuma, 1998, Slip of Newtonian fluids at slid boundary, *JSME Int. Journal Ser.* B 41 525

[63] J. L. Xu and Y. X. Li, 2007, Boundary conditions at the solid–liquid surface over the multiscale channel size from nanometer to micron, *Int. J. Heat Mass Transfer* **50** 2571–258

[64] C. Ybert, C. Barentin, C. Cottin-Bizonne, P. Joseph and L. Bocquet, 2007, Achieving large slip with superhydrophobic surfaces: Scaling laws for generic geometries**,** *Phys. Fluids* 19 123601

[65] Y. X. Zhu and S. Granick, 2001, Superlubricity: A Paradox about Confined Fluids Resolved, *Phys. Rev. Lett.* 87 096105

[66] M. Carpinlioglu, M. Gundogdu, 2001. A critical review on pulsatile pipe flow studies directing towards future research topics, Flow Measurement and Instrumentation 12 163.

[67] S. Ray, B. Unsal, F. Durst, O. Ertunc, O.A. Bayoumi,2005, Mass flow rate controlled fully developed laminar pulsating pipe flows, Journal of Fluids Engineering, 127, 405.

[68] J. Liu, Y.C. Tai, C.M. Ho, 1995. MEMS for pressure distribution studies of gaseous flows in micro-channels, in: Proceedings of IEEE International Conference on Micro Electro Mechanical Systems, Amsterdam, Netherlands, pp. 209–215.

[69] E. H. Kennard, 1938. Kinetic Theory of Gases. Mc. Graw-Hill, new York.

[70] N. M. Lebedev, I. P. Skalskaya, Y. S. Uflyand. 1965. Worked Problems in Applied Mathematics. Courier Dover Puvblications.

[71] C. Aubert & S. Colin, High order Boundary Conditions for Gaseous Flows in Rectangular Microducts, Microscale Thermophysical Engineering, 5: 41 – 54, 2001.

[72] F. M. White, Viscous Fluid Flow, Mc Graw Hill, 1974.

[73] R. M. Terrill, An Exact Solution for flow in a porous pipe, Jurnal of App. Math. Phys. (ZAMP), 33, 1982

[74] E. B. Arkilic, Slip Flow in MicroChannels, Proceeding of Rarefied Gas Dynamic Symposium, Oxford, UK, July, 1994.

[75] G. Chakraborty, A Note on Methods for Analysis of flow through Micro-channels. Int. Jurnal Of Heat and Mass transfer, 51, 4583-4588, 2008.

[76] G. Tunc, Y. Bayazitoglu, Heat Transfer for gaseous flow in microtubes with viscous heating. Proc. ASME. Heat Transfer Div. HTD 366-2, 299-306, 2000.

[77] G. Tunc, Y. Bayazitoglu, Heat Transfer in Rectangular Microchannels, Int. Jurnal of Heat and Mass transfer 45, 765-773, 2002.

[78] F. V. Castelloes, C. R. Cardoso, P. Couto & R. M. Cotta, Transient Analysis of Slip Flow and Heat Transfer in Microchannels, Heat ransfer Engineering, 28:6, 549-558, 2007.

[79] D. Das, J. H. Arakeri, Unsteady Laminar Duct Flow With a Given Volume Flow Rate Variation, Transaction of the ASME, 67, 274-281. 2000.

[80] G. L. Morini and M. Spiga, Slip Flow in Rectangular Microtubes. Microscale Thermophysical Engineering, 2: 4, 273-282, 1998.

[81] M. Spiga and G. L. Morini, A Symmetric Solution for Velocity Profile in Laminar Flow through Rectangular Ducts, *Int. Comm u n . Heat Mass Transfer*, vol. 21, pp. 469] 475,1994.

[82]. M. Spiga and G. L. Morini, Laminar Heat Transfer in Re ctangular Ducts, *Trend s in Heat, Mass* & *Mom entum Tran sfer*, vol. 3, pp. 19] 30, 1997.

[83] V. O'Brien, Pulsatile Fully Developed Flow in Rectangular Channels, Journal of the Franklin Institute, 800: 3, 1975.

[84] R. Berker, "Integration des Equations du Mouvement d'un Fluide Visqueux Incompressible", Handbuch der Physik, Vol. VIII/B, p. 70, Springer, Berlin, 1963.

[85] L. S. Han, "Hydrodynamic entrance lengths for incompressible laminar flow in rectangular ducts", Trans. *ASME*, Vol. 82, Series E, p. 403, 1960.

[86] N. Rott, "Theory of time-dependent laminar flows", in: "Theory of Laminar Flows" (ed. by F. K. Moore), Section D, p. 401, Princeton University Press, Princeton, 1964.

[87] S. Richardson, On the No-slip Boundary Condition, J. Fluid Mech. 59: 4, 707-719, 1973.

[88] E. M. Sparrow, S. H. Lin, Laminar Heat Transfer in Tubes under Sip Flow Conditions, J. heat Transfer 84, 363-369, 1962.

[89] T. A. Amel, R.F. Baron, X. Wang, R. O. Warrington, Laminar forced convection in a circular tube with constant heat flux and slip flow, Microscale Thermophys. Eng 1 (4), 303 – 320, 1997.

[90] S. Uchida, The Pulsating Viscous Flow Superposed on the Steady Laminar Motion of Incompressible Fluids in a Circular Pipe, Z. Angew. Math. Phys., **7**, pp. 403–422, 1956.

[91] J. R. Wemersley, ''Method for the Calculation of Velocity, Rate of Flow and Viscous Drag in Arteries When the Pressure Gradient is Known,'' J. Physiol., 127, pp. 553–563,1955.

[92] Y. Zhu and S. Granick, "The No-Slip Boundary Condition Switches to Partial Slip When Fluid Contains Surfactant," Langmuir 18, 10058 (2002).

[93] J. R. A. Pearson, & Petrie, C. J. S. On melt flow instability of extruded polymers, Polymer systems: Deformation and Flow. Proc. 1966 Ann. Conf. Brit. Soc. Rheol, (ed. R. E. Wetton & R. W. Whorlow), p.163. Macmillan, 1968.

[94] S. Goldstein. Modern Developments in Fluid Dynamics, Oxford University Press, 1938.

[95] M. J. Lighthill, In laminar Boundary layers (ed. L. Rosenhead) Chap. I. Oxford University Press, 1963.

[96] R. S. Brodkey , The Phenomena of Fluid Motions, Addison Wesley Pub Co, 1967

[97] M. Bahrami, M. Yavanovich, M., Culham J R, Pressure drop of fully developed Laminar flow in microchannels of arbitrary cross section, Journal of Fluid Engineering, vol 128. Sept 2006.

[98] Sheikh A Haji, Fully developed heat transfer of fluid flowin rectangular passages filled with porous materials, Journal of Heat ransfer, Transaction of the ASME vol 128, June 2006.

[99] B. M. Johnston, P. R. Johnston, S. Corney, and D. Kilpatrick. Non-newtonian blood flow in human right coronary arteries: steady state simulations, Journal of Biomechanics, 37: 709- 720, 2004.

[100] S. Arulanandam and D. Li, Liquid transport in rectangular micro-channels by electroosmotic pumping, Colloids and Surfaces A: Physicochem, Eng. Aspects 161 (2000) 89 – 102.

[101] W.M. Robsenow, H.Y. Choi. Heat, Mass and Momentum Transfer, Prentice Hall Inc, New York. 1961

[102] Jyh-Ping Hsu, Chen-Yuan Kao, Shiojenn Tseng, and Chur-Jen Chen, Electrokinetic Flow through an Elliptical Microchannel: Effects of Aspect Ratio and Electrical Boundary Conditions, Journal of Colloid and Interface Science 248, 176–184 (2002)

[103] H. M., Zamir, M. Pulsatile Flow in tubes of elliptic cross sections, Annals of Biomedical Eng. Vol. 26, pp. 780 – 787, 1998.

[104] A.K. Ghosh, A. R. Khan, L. Debnath, On a Pulsatile flow of a two Phase viscous fluid in a tube of elliptic cross section, Internat. J. Math. & Math. Sci.Vol. 13 No. 4 (1990) 669-676.

[105] P. Moon & D.E. Spencer, Field theory Handbook , 1971.

[106] E. H. Kennard, Kinetic Theory of Gases, McGraw-Hill, New York, 1938.

[107] Y. H. Wu., Applied Mathematical Modelling, Lecture Notes, Curtin University of Technology, 2009.

[108] B. M. Johnston, P. R. Johnston, S. Corney, and D. Kilpatrick. Non-Newtonian blood flow in human right coronary arteries: steady state simulations. Journal of Biomechanics, 37: 709 – 720, 2004.

[109] J. Koplik and J. R. Banavar, No-Slip Condition for a Mixture of Two Liquids, Phys. Rev. Lett. 80, 5125–5128.1998.

[110] N. W. McLachlan, Theory and Application of Mathieu Functions. Oxford University Press. 1947.

[111] J. C. Shih, C. M. Ho, J. liu, and Y. C. Tai, monoatomic and Poliatomic Gas Flow through Uniform Microchannels. DSC- Vol. 59. Pp. 197-203, ASME. New York, 1996.

[112] Navier, C. L. M. H., Mémoire sur les lois du mouvement des fluides. Mém. Acad. R. Sci. Inst. France 6,389-440(1823).

Appendix

To demonstrate the solutions which have been found in chapter 4, we require some formulas to calculate the Mathieu functions and the modified Mathieu functions as in Ref [110].

A.1 Formula for *a*

We designate the characteristic numbers for $ce_m(z,q)$ and $se_m(z,q)$ by a_m and b_m r espectively. Following the results in [110], we have

$$a_0 = -\frac{1}{2}q^2 + \frac{7}{128}q^4 - \frac{29}{2304}q^6 + \frac{68687}{18874368}q^8 + O\left(q^9\right). \tag{A.1}$$

$$b_1 = 1 - q - \frac{1}{8}q^2 + \frac{1}{64}q^3 - \frac{1}{1536}q^4 - \frac{11}{36864}q^5 + \frac{49}{589824}q^6 - \frac{55}{9437184}q^7 - \frac{265}{113246208}q^8 + O\left(q^9\right). \tag{A.2}$$

The characteristic number a_1 can be found by replacing –q for q in b_1.

$$b_2 = 4 - \frac{1}{12}q^2 + \frac{5}{13824}q^4 - \frac{289}{79626240}q^6 + \frac{21391}{458647142400}q^8 + O\left(q^{10}\right). \tag{A.3}$$

$$a_2 = 4 + \frac{5}{12}q^2 - \frac{763}{13824}q^4 + \frac{1002401}{79626240}q^6 - \frac{1669068401}{458647142400}q^8 + O\left(q^{10}\right). \tag{A.4}$$

$$b_3 = 9 + \frac{1}{16}q^2 - \frac{1}{64}q^3 + \frac{13}{20480}q^4 + \frac{5}{16384}q^5 - \frac{1961}{23592960}q^6 + \frac{1109}{104857600}q^7 + O\left(q^8\right). \tag{6.5}$$

The characteristic number a_3 can be found by replacing –q for q in b_3.

$$b_4 = 16 + \frac{1}{30}q^2 + \frac{317}{864000}q^4 + \frac{10049}{1728000}q^6 + O\left(q^8\right). \tag{A.6}$$

$$a_4 = 16 + \frac{1}{30}q^2 + \frac{433}{864000}q^4 - \frac{5701}{1728000}q^6 + O\left(q^8\right). \tag{A.7}$$

$$b_5 = 25 + \frac{1}{48}q^2 + \frac{11}{774144}q^4 - \frac{1}{147456}q^5 + \frac{37}{891813888}q^6 + O\left(q^7\right). \tag{A.8}$$

The characteristic number a_5 can be found by replacing –q for q in b_5.

$$b_6 = 36 + \frac{1}{70}q^2 + \frac{187}{43904000}q^4 - \frac{5861633}{92935987200000}q^6 + O\left(q^8\right). \tag{A.9}$$

$$a_6 = 36 + \frac{1}{70}q^2 + \frac{187}{43904000}q^4 + \frac{6743617}{92935987200000}q^6 + O\left(q^8\right). \tag{A.10}$$

When $m \geq 7$, the following formula is used.

$$a_m, b_m = m^2 + \frac{1}{2\left(m^2-1\right)}q^2 + \frac{5m^2+7}{32\left(m^2-1\right)^3\left(m^2-4\right)}q^4 + \frac{9m^4+58m^2+29}{64\left(m^2-1\right)^5\left(m^2-4\right)\left(m^2-9\right)}q^6 + \ldots \tag{A.11}$$

These formula may be used to calculate *a* when *q* is sufficiently small and of either sign. For equal accuracy, *q* may increase as *m* increases. For $m \geq 7$, it must not be inferred that $a_m = b_m$. As $|q| \to 0, a_m \to b_m$, but for $|q| > 0, \left(a_m - b_m\right) \neq 0$, although it is very small near *q = 0*.

A.2 Coefficients Formula

In the equation (4.2), if *y* is substituted by each series (4.5) – (4.8) in turn, and the coefficients for $\cos 2rz$, $\cos\left(2r+1\right)z$, $\sin\left(2r+1\right)z$, $\sin\left(2r+2\right)z$ are equated to zero for *r* = 0, 1, 2,…, the following recurrence relations are obtained [110]:

$$\text{for } ce_{2n}(z,q) \begin{cases} aA_0 - qA_2 = 0 \\ (a-4)A_2 - q(A_4 + 2A_0) = 0 \\ (a-4r^2)A_{2r} - q(A_{2r+2} + 2A_{2r-2}) = 0;\ r \geq 2 \end{cases} \tag{A.12}$$

$$\text{for } ce_{2n+1}(z,q) \begin{cases} (a-1-q)A_1 - qA_3 = 0 \\ \left[a-(2r+1)^2\right]A_{2r+1} - q(A_{2r+3} + 2A_{2r-1}) = 0;\ r \geq 1 \end{cases} \tag{A.13}$$

$$\text{for } se_{2n+1}(z,q) \begin{cases} (a-1+q)B_1 - qB_3 = 0 \\ \left[a-(2r+1)^2\right]B_{2r+1} - q(B_{2r+3} + B_{2r-1}) = 0;\ r \geq 1 \end{cases} \tag{A.14}$$

$$\text{for } se_{2n+2}(z,q) \begin{cases} (a-4)B_2 - qB_4 = 0 \\ (a-4r^2)B_{2r} - q(B_{2r+2} + B_{2r-2}) = 0;\ r \geq 2 \end{cases} \tag{A.15}$$

For simplicity the superscripts *2n, 2n+1, 2n+2* for *A* and *B* have been omitted.

Normalization of $ce_m(z,q)$ and $se_m(z,q)$ are:

$$2\left[A_0^{(2n)}\right]^2 + \sum_{r=1}^{\infty}\left[A_{2r}^{(2n)}\right]^2 = 1 \text{ for } m = 2n \text{ , and} \tag{A.16}$$

$$1 = \sum_{r=0}^{\infty}\left[A_{2r+1}^{(2n+1)}\right]^2 = \sum_{r=0}^{\infty}\left[B_{2r+1}^{(2n+1)}\right]^2 = \sum_{r=0}^{\infty}\left[B_{2r+2}^{(2n+1)}\right]^2 \text{ for } m = 2n+1 \tag{A.17}$$

A.3 Calculation of *A*

If *q* is sufficiently small, the formula for *a* given in (A.1) – (A.10) may be used.

Suppose we have to find the coefficients of the series for the function $ce_{2n}(z,q)$.

We commence with finding $a_{2n}, n = 0, 1, 2, \ldots$ by using the formula of *a*.

Writing $v_0 = A_2 / A_0, v_2 = A_4 / A_2, v_4 = A_6 / A_4, \ldots, v_{2r-2} = A_{2r} / A_{2r-2}, v_{2r} = A_{2r+2} / A_{2r}$

$v_0 v_2 = A_4 / A_0, v_0 v_2 v_4 = A_6 / A_0, \ldots$ and $v_0 = A_2 / A_0 = a / q$ from the first formula.

Dividing the second formula by A_0 and making these substitutions, gives

$$(4-a)v_0 + q(v_0 v_2 + 2) = 0 \tag{A.18}$$

so $$-v_0 = \frac{1}{2}q \Big/ \left[1 - \frac{1}{4}\left(a - qv_2\right)\right].$$

(A.19)

In the same way, from the equation $(A.12)_3$, we get

$$\left(4r^2 - a\right)v_{2r-2} + q\left(v_{2r}v_{2r-2} + 1\right) = 0\,, \tag{A.20}$$

$$-v_{2r-2} = \left(q/4r^2\right) \Big/ \left[1 - \left(1/4r^2\right)\left(a - qv_{2r}\right)\right]; r \geq 2. \tag{A.21}$$

which may be regarded as an alternative form of the recurrence relation.

To simplify calculation, we use a reasonable approximation and neglect $qv_{2r}/4r^2$ due to the term $|qv_{2r}|/4r^2 \ll 1$, and thus we have

$$-v_{2r-2} \simeq \left(q/4r^2\right) \Big/ \left[1 - a/4r^2\right]; r \geq 2\,, \tag{A.22}$$

provided *r* is large enough. Otherwise we use formula (A.21).

Since the values of v_m have been found, we may calculate A_{2n} after finding A_0 using the Normalization formula:

$$1 = 2A_0^2 + A_2^2 + A_4^2 + A_6^2 + \ldots. \tag{A.23}$$

Dividing by A_0^2 on both sides, we have

$$1/A_0^2 = 2 + A_2^2/A_0^2 + A_4^2/A_0^2 + A_6^2/A_0^2 + \ldots \tag{A.24}$$

so $$1/A_0^2 = 2 + \left(A_2/A_0\right)^2 + \left(A_4/A_0\right)^2 + \left(A_6/A_0\right)^2 + \ldots \tag{A.25}$$

To have positive root, we use formula

$$1/A_0 = \sqrt{2 + \left(A_2/A_0\right)^2 + \left(A_4/A_0\right)^2 + \left(A_6/A_0\right)^2 + \ldots}\,, \tag{A.26}$$

where

$$A_2/A_0 = v_0,\ A_4/A_0 = v_2v_0,\ A_6/A_0 = v_4v_2v_0, \ldots \tag{A.27}$$

Finally, putting all A_{2n} on the series of function $ce_{2n}\left(z,q\right)$, we have

$$ce_{2n}\left(z,q\right) = A_0 + A_2^{(2n)}\cos 2z + A_4^{(2n)}\cos 4z + A_6^{(2n)}\cos 6z + \ldots \tag{A.28}$$

A.4 Solution of the Mathieu Equation when *q* is negative imaginary

In the condition that *q* takes the form *–is* where *s* being real and positive, in numerical work, it is preferable to work with *q=+is* and then obtain the solution for *q=-is* by writing $\left(\frac{1}{2}\pi - z\right)$ for *z*. The value of *a* is real or complex depending on conditions. For *q* moderate, the series for a_m, b_m in (A1.1) are convergent, and may be used for computation. The series for a_{2n}, b_{2n} are proceeded in powers of q^2, while those for a_{2n+1}, b_{2n+1} are proceeded in power of *q*. Hence a_{2n}, b_{2n} are real, but a_{2n+1}, b_{2n+1} are complex. When $s > s_0$, with s_0 depending upon *n* and the function, a_{2n}, b_{2n} are complex.